

**A NEW FEATURE-BASED WAVELET
COMPLETED LOCAL TERNARY PATTERN
(FEAT-WCLTP) FOR TEXTURE AND
MEDICAL IMAGE CLASSIFICATION**

ABEER MOH'D SALEM SHAMAILEH

UMP

MASTER OF SCIENCE

UNIVERSITI MALAYSIA PAHANG

UNIVERSITI MALAYSIA PAHANG

DECLARATION OF THESIS AND COPYRIGHT

Author's Full Name : ABEER MOH'D SALEM SHAMAILEH

Date of Birth : 2 OCTOBER 1988

Title : A NEW FEATURE-BASED WAVELET COMPLETED LOCAL
TERNARY PATTERN (FEAT-WCLTP) FOR TEXTURE AND
MEDICAL IMAGE CLASSIFICATION

Academic Session : SEM 2 2018/2019

I declare that this thesis is classified as:

- CONFIDENTIAL (Contains confidential information under the Official Secret Act 1997)*
- RESTRICTED (Contains restricted information as specified by the organization where research was done)*
- OPEN ACCESS I agree that my thesis to be published as online open access (Full Text)

I acknowledge that Universiti Malaysia Pahang reserves the following rights:

1. The Thesis is the Property of Universiti Malaysia Pahang
2. The Library of Universiti Malaysia Pahang has the right to make copies of the thesis for the purpose of research only.
3. The Library has the right to make copies of the thesis for academic exchange.

Certified by:

(Student's Signature)

(Supervisor's Signature)

New IC/Passport Number
Date:

Name of Supervisor
Date:

NOTE : * If the thesis is CONFIDENTIAL or RESTRICTED, please attach a thesis declaration letter.

MAKLUMAT PANEL PEMERIKSA PEPERIKSAAN LISAN

Tesis ini telah diperiksa dan diakui oleh : Dr. Tuty Asmawaty Binti Abdul Kadir
This thesis has been checked and verified by Faculty of Computer Systems & Software Engineering, Universiti Malaysia Pahang

Nama dan Alamat Pemeriksa Dalam : Assoc. Prof. Dr. Shahrel Azmin Suandi
Name and Address Internal Examiner School of Electrical and Electronic Engineering, Engineering Campus Universiti Sains Malaysia

Nama dan Alamat Pemeriksa Luar :
Name and Address External Examiner

Nama dan Alamat Pemeriksa Luar :
Name and Address External Examiner

Disahkan oleh Timbalan Pendaftar di IPS
Verified by Deputy Registrar IPS

Tandatangan :
Signature

Tarikh:
Date

Nama :
Name

UMP

SUPERVISOR'S DECLARATION

We hereby declare that We have checked this thesis and, in our opinion, this thesis is adequate in terms of scope and quality for the award of the degree of Master of Science.

(Supervisor's Signature)

Full Name : TAHA HUSSEIN RASSEM

Position : SENIOR LECTURER

Date :

(Co-supervisor's Signature)

Full Name : LIEW SIAU CHUIN

Position : SENIOR LECTURER

Date :

STUDENT'S DECLARATION

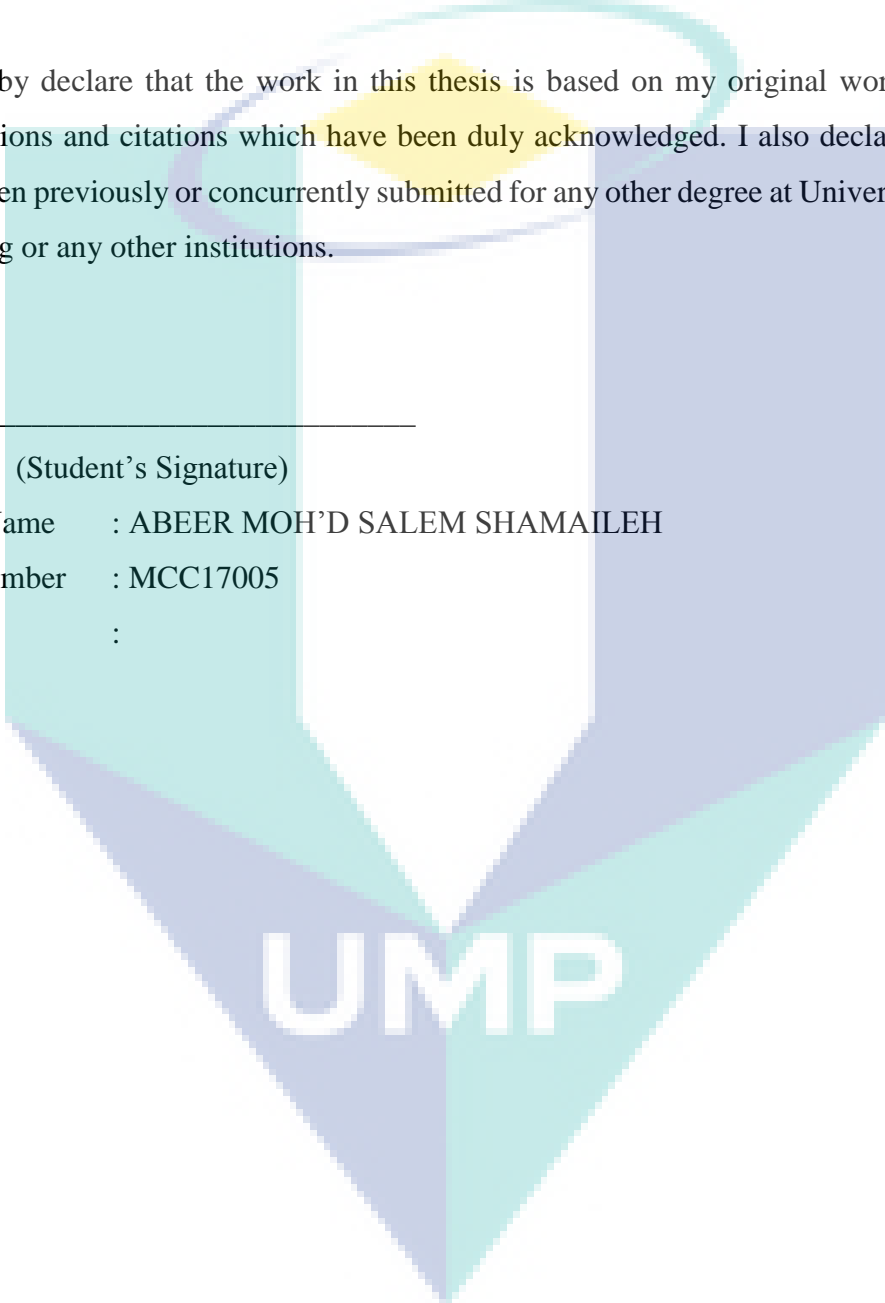
I hereby declare that the work in this thesis is based on my original work except for quotations and citations which have been duly acknowledged. I also declare that it has not been previously or concurrently submitted for any other degree at Universiti Malaysia Pahang or any other institutions.

(Student's Signature)

Full Name : ABEER MOH'D SALEM SHAMAILEH

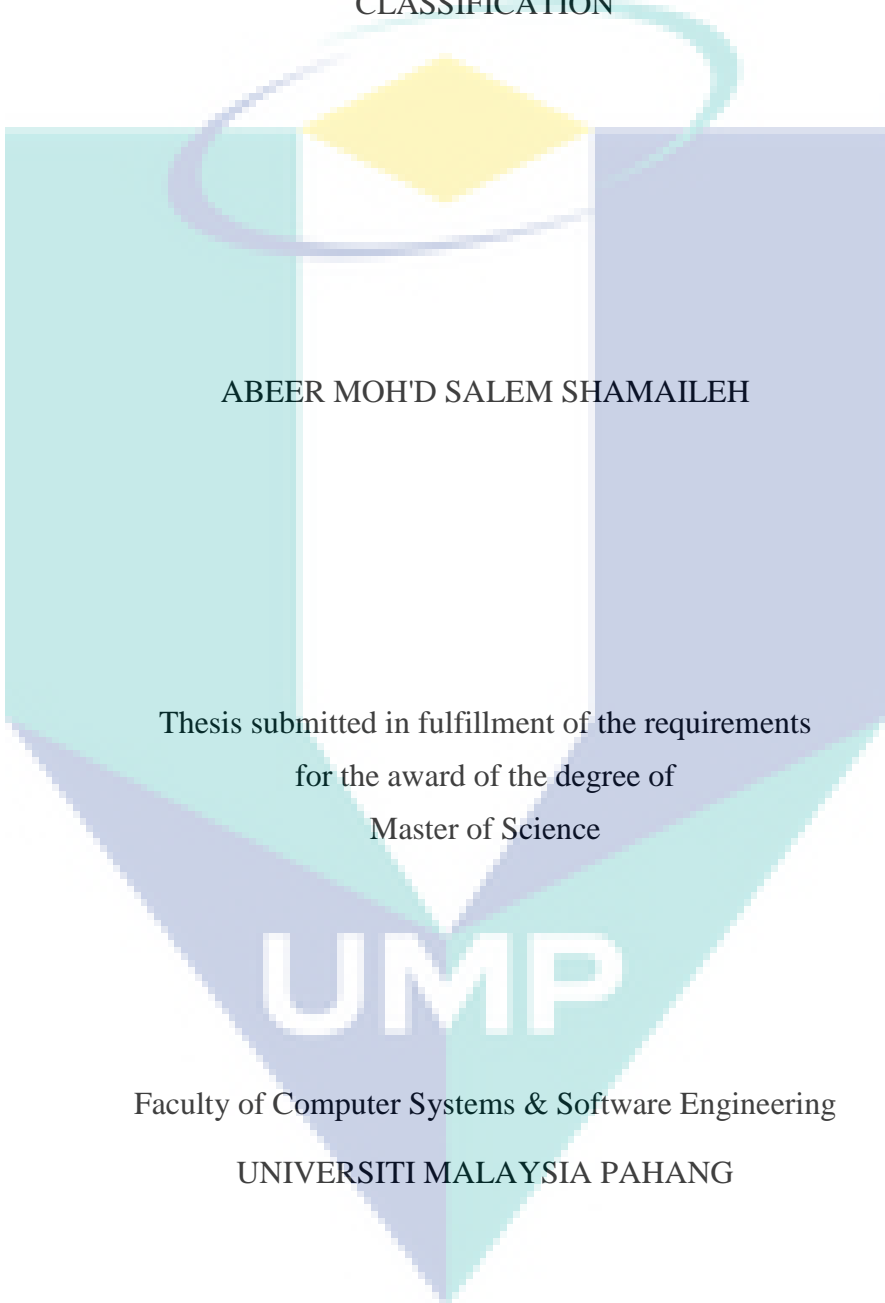
ID Number : MCC17005

Date :



UMP

A NEW FEATURE-BASED WAVELET COMPLETED LOCAL TERNARY
PATTERN (FEAT-WCLTP) FOR TEXTURE AND MEDICAL IMAGE
CLASSIFICATION

The logo of the University of Malaysia Pahang (UMP) is a shield-shaped emblem. It features a central white vertical band with a yellow diamond at the top. The shield is divided into four quadrants: top-left is light blue, top-right is light purple, bottom-left is light blue, and bottom-right is light purple. A stylized, glowing blue and yellow ring orbits the central diamond.

ABEER MOH'D SALEM SHAMAILEH

Thesis submitted in fulfillment of the requirements
for the award of the degree of
Master of Science

UMP

Faculty of Computer Systems & Software Engineering

UNIVERSITI MALAYSIA PAHANG

AUGUST 2019

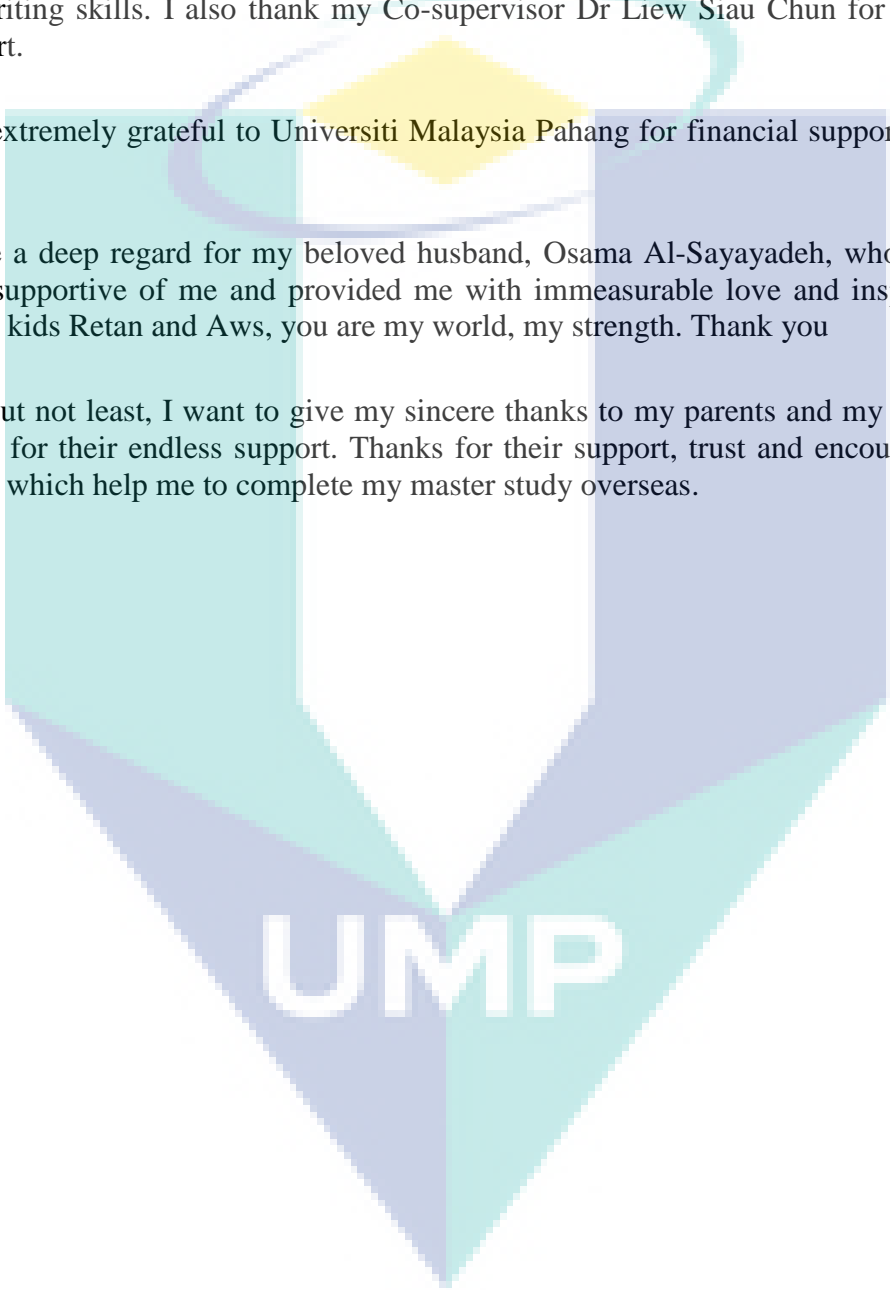
ACKNOWLEDGEMENTS

First of all, I would like to express my deepest gratitude to my supervisor, Dr Taha Hussein Rassem for his support, encouragement, patience, and immense knowledge guidance during my study journey. His technical and editorial advice was essential to the completion of this thesis. His invaluable guidance inspires me to see problems from different perspectives. In addition, I would like to thank him for improving and polishing my writing skills. I also thank my Co-supervisor Dr Liew Siau Chun for his advising support.

I am extremely grateful to Universiti Malaysia Pahang for financial support during this study.

I have a deep regard for my beloved husband, Osama Al-Sayayadeh, who has always been supportive of me and provided me with immeasurable love and inspiration. My lovely kids Retan and Aws, you are my world, my strength. Thank you

Last but not least, I want to give my sincere thanks to my parents and my brothers and sisters for their endless support. Thanks for their support, trust and encouragement all along, which help me to complete my master study overseas.



UMP

ABSTRAK

Pada masa kini, pemerihal imej berdasarkan tekstur diguna pakai dalam pelbagai aplikasi nyata yang penting. Penggunaan analisis tekstur dalam pengelasan imej perubatan dan tekstur telah menarik perhatian ramai pihak. Corak Perduaan Tempatan (LBP) salah satu yang paling mudah namun berkesan tekstur pemerihal. Tetapi ia mempunyai beberapa batasan yang boleh menjejaskan ketepatannya. Oleh itu, kebanyakan pemerihal berasaskan LBP telah dicadangkan untuk menangani kekurangan ini dan meningkatkan ketepatan mereka. Corak Pertigaan Tempatan Lengkap (CLTP) adalah salah satu pemerihal berasaskan LBP yang penting. Walau bagaimanapun, CLTP menderita dari dua batasan utama: pemilihan nilai ambang berasaskan secara manual dan keamatan yang tinggi yang memberi kesan negatif kepada prestasi deskriptor dan membawa kepada pengiraan yang tinggi. Kajian ini bertujuan untuk meningkatkan ketepatan klasifikasi CLTP dan mengatasi had komputasi dengan mencadangkan pemerihal baru yang diilhamkan oleh CLTP. Oleh itu, penyelidikan ini memperkenalkan dua sumbangan: Yang pertama adalah pemerihal baru yang dicadangkan yang menggabungkan transformasi wavelet diskrit yang berlebihan (RDWT) dengan CLTP asal, iaitu, wavelet menyelesaikan pola ternary tempatan (WCLTP). Mengeluarkan CLTP dalam bentuk jelmaan gelombang kecil dapat meningkatkan ketepatan pengelasan disebabkan oleh sifat peralihan tak varian dalam RDWT. Pertamanya, imej diuraikan kepada empat sub-kumpulan (LL, LH, HL dan HH) dengan menggunakan RDWT. Kemudian, CLTP dikeluarkan berdasarkan kepada koefisien gelombang kecil LL. Sumbangan kedua pula ialah pengurangan daya kedimensian WCLTP dengan mengurangkan saiz dan mencadangkan pemerihal tekstur baru, iaitu Corak Pertigaan Tempatan Lengkap Gelombang Kecil Berdasarkan Fitur (Feat-WCLTP). Pemerihal cadangan ini dapat meningkatkan prestasi CLTP dan mengurangkan kedimensian tinggi. Oleh itu, Feat-WCLTP merupakan gabungan antara bahagian isyarat, fitur dan pusat. Prestasi kaedah WCLTP dan Feat-WCLTP yang dicadangkan telah dinilai menggunakan empat set data tekstur (Outex, CURet, UIUC dan Kylberg) dan dua set data perubatan (2D HeLa dan Breast Cancer) dan kemudian dibandingkan dengan beberapa varian LBP yang terkenal. WCLTP berjaya mengatasi pemerihal lain dan mencapai ketepatan pengelasan tertinggi dalam semua eksperimen. Keputusan kaedah cadangan ini bagi set data tekstur ialah 99.35% dalam OuTex, 96.57% dalam CURet, 94.80% dalam UIUC dan 99.88% dalam Kylberg. Manakala, keputusan WCLTP dalam set data perubatan ialah 84.19% dalam 2D HeLa and 92.14% dalam set data Breast Cancer. Feat-WCLTP pula bukan sahaja dapat mengatasi masalah kedimensian, malah meningkatkan daya ketepatan pengelasan. Keputusan Feat-WCLTP dalam set data tekstur ialah 99.66% dalam OuTex, 96.89% dalam CURet, 95.23% dalam UIUC dan 99.92% dalam Kylberg. Manakala, keputusannya dalam set data perubatan ialah 84.42% dalam set data 2D HeLa dataset and 89.12% dalam set data Breast Cancer. Di samping itu, kaedah cadangan Feat-WCLTP dapat mengurangkan saiz fitur bagi corak tekstur (1,8) daripada 400 bin kepada 160 bin dalam WCLTP. Kedua-dua kaedah WCLTP dan Feat-WCLTP mempunyai daya ketepatan dan kedimensian yang lebih baik berbanding kaedah CLTP asal.

ABSTRACT

Nowadays, texture image descriptors are used in many important real-life applications. The use of texture analysis in texture and medical image classification has attracted considerable attention. Local Binary Patterns (LBP) is one of the simplest yet effective texture descriptors. But it has some limitations that may affect its accuracy. Hence, different variants of LBP were proposed to overcome LBP's drawbacks and enhance its classification accuracy. Completed local ternary pattern (CLTP) is one of the significant LBP variants. However, CLTP suffers from two main limitations: the selection of the threshold value is manually based and the high dimensionality which is negatively affected the descriptor performance and leads to high computations. This research aims to improve the classification accuracy of CLTP and overcome the computational limitation by proposing new descriptors inspired by CLTP. Therefore, this research introduces two contributions: The first one is a proposed new descriptor that integrates redundant discrete wavelet transform (RDWT) with the original CLTP, namely, wavelet completed local ternary pattern (WCLTP). Extracting CLTP in wavelet transform will help increase the classification accuracy due to the shift invariant property of RDWT. Firstly, the image is decomposed into four sub-bands (LL, LH, HL, HH) by using RDWT. Then, CLTP is extracted based on the LL wavelet coefficients. The latter one is the reduction in the dimensionality of WCLTP by reducing its size and a proposed new texture descriptor, namely, feature-based wavelet completed local ternary pattern (Feat-WCLTP). The proposed Feat-WCLTP can enhance CLTP's performance and reduce high dimensionality. The mean and variance of the values of the selected texture pattern are used instead of the normal magnitude texture descriptor of CLTP. The performance of the proposed WCLTP and Feat-WCLTP was evaluated using four textures (i.e. OuTex, CURET, UIUC and Kylberg) and two medical (i.e. 2D HeLa and Breast Cancer) datasets then compared with several well-known LBP variants. The proposed WCLTP outperformed the previous descriptors and achieved the highest classification accuracy in all experiments. The results for the texture dataset are 99.35% in OuTex, 96.57% in CURET, 94.80% in UIUC and 99.88% in the Kylberg dataset. The results for the medical dataset are 84.19% in the 2D HeLa dataset and 92.14% in the Breast Cancer dataset. The proposed Feat-WCLTP not only overcomes the dimensionality problem but also considerably improves the classification accuracy. The results for Feat-WCLTP for texture dataset are 99.66% in OuTex, 96.89% in CURET, 95.23% in UIUC and 99.92% in the Kylberg dataset. The results for the medical dataset are 84.42% in the 2D HeLa dataset and 89.12% in the Breast Cancer dataset. Moreover, the proposed Feat-WCLTP reduces the size of the feature vector for texture pattern (1,8) to 160 bins instead of 400 bins in WCLTP. The proposed WCLTP and Feat-WCLTP have better classification accuracy and dimensionality than the original CLTP.

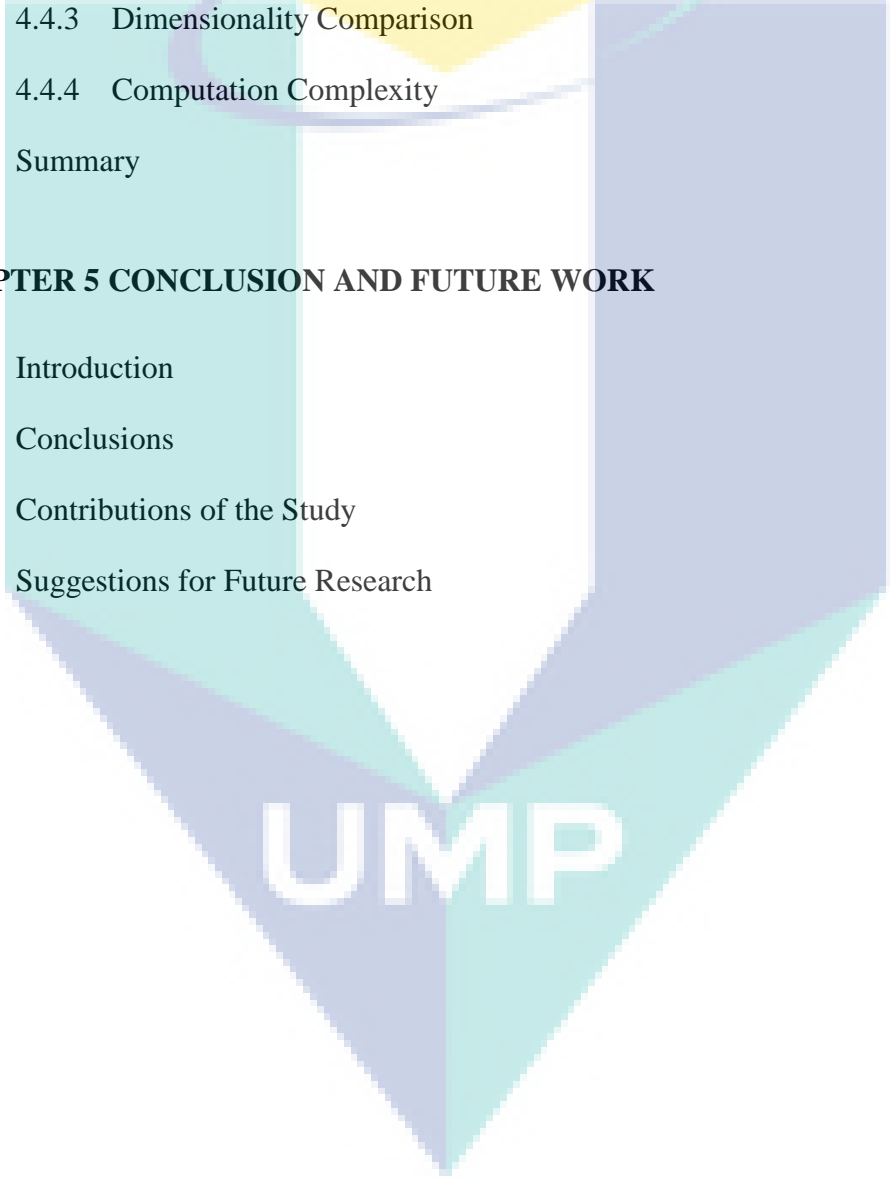
TABLE OF CONTENT

DECLARATION	
TITLE PAGE	
ACKNOWLEDGEMENTS	ii
ABSTRAK	iii
ABSTRACT	iv
TABLE OF CONTENT	v
LIST OF TABLES	ix
LIST OF FIGURES	x
LIST OF SYMBOLS	xii
LIST OF ABBREVIATIONS	xiii
CHAPTER 1 INTRODUCTION	1
1.1 Background	1
1.2 Motivation	2
1.3 Problem Statement	3
1.4 Research Objectives	3
1.5 Research Scope	4
1.6 Thesis Organisation	4
CHAPTER 2 LITERATURE REVIEW	6
2.1 Introduction	6
2.2 Texture Analysis	6
2.2.1 Texture Classification	7

2.2.2	Texture Segmentation	7
2.2.3	Texture Synthesis	7
2.2.4	Texture Compression	7
2.2.5	Shape from Texture	8
2.3	Texture Classification	8
2.3.1	Pre-processing	8
2.3.2	Feature Extraction	9
2.3.3	Feature Selection	9
2.3.4	Classification	10
2.4	Textural Feature Extraction	11
2.4.1	Structural Methods	12
2.4.2	Model-based Methods	12
2.4.3	Transform-based methods	13
2.4.4	Statistical-based Methods	13
2.5	Texture Descriptor	14
2.5.1	Local Binary Pattern	14
2.5.2	Local Ternary Pattern	17
2.5.3	Completed Local Binary Pattern	18
2.5.4	Completed Local Binary Count	20
2.5.5	Robust Local Binary Pattern	21
2.5.6	Noise Resistant Local Binary Pattern	22
2.5.7	Binary Rotation Invariant and Noise Tolerant	23
2.5.8	Completed Local Ternary Pattern	24
2.5.9	Dominant Rotated Local Binary Patterns	26
2.5.10	Feature-based Local Binary Pattern	27
2.6	Wavelet Transform (WT)	29

2.6.1	Continuous wavelet transforms (CWT)	30
2.6.2	Discrete Wavelet Transform	30
2.6.3	Redundant discrete wavelet transforms	31
2.7	Datasets	33
2.7.1	Texture Datasets	34
2.7.2	Medical Datasets	37
2.8	Summary	38
CHAPTER 3 METHODOLOGY		39
3.1	Introduction	39
3.2	Methodology of the Proposed Descriptors	39
3.3	General proposed model	40
3.3.1	Wavelet Completed Local Ternary Pattern	42
3.3.2	Feature-based WCLTP	46
3.3.3	Summary	51
CHAPTER 4 RESULTS AND DISCUSSION		53
4.1	Introduction	53
4.2	Experimental setup	53
4.2.1	Datasets	54
4.2.2	Confusion Matrix	54
4.2.3	Cross-Validation	55
4.2.4	Classifier	55
4.2.5	Dissimilarity measurement	56
4.3	Performance Evaluation for the Proposed WCLTP	56
4.3.1	Robustness of WCLTP Against Noise	56

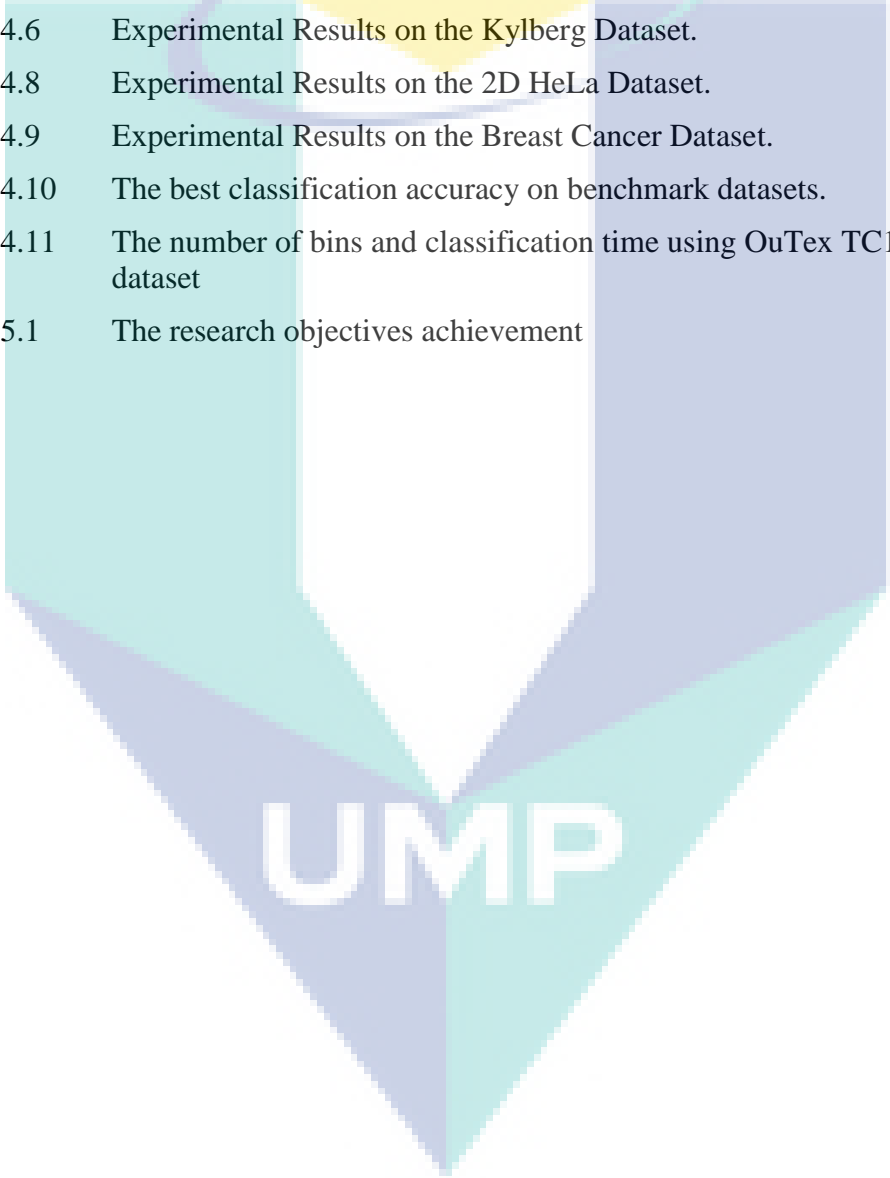
4.3.2	Experimental Results of WCLTP for Texture Image Classification.	59
4.3.3	Experimental Results of WCLTP for Medical Datasets.	64
4.4	Performance Evaluation for the Proposed Feat-WCLTP	67
4.4.1	Experimental Results of Feat-WCLTP Using Texture Dataset.	67
4.4.2	Experimental Results of Feat-WCLTP Using Medical Dataset.	75
4.4.3	Dimensionality Comparison	77
4.4.4	Computation Complexity	79
4.5	Summary	83
CHAPTER 5 CONCLUSION AND FUTURE WORK		84
5.1	Introduction	84
5.2	Conclusions	84
5.3	Contributions of the Study	86
5.4	Suggestions for Future Research	86



UMP

LIST OF TABLES

Table 2.1	The well-known LBP variants texture descriptors.	29
Table 4.1	The benchmark datasets used in the experiments	54
Table 4.2	Confusion Matrix	54
Table 4.3	Classification rates (%) on the OuTex dataset	59
Table 4.4	Classification rates (%) on the CURET dataset	61
Table 4.5	Experimental Results on the UIUC Dataset	62
Table 4.6	Experimental Results on the Kylberg Dataset.	64
Table 4.8	Experimental Results on the 2D HeLa Dataset.	65
Table 4.9	Experimental Results on the Breast Cancer Dataset.	66
Table 4.10	The best classification accuracy on benchmark datasets.	82
Table 4.11	The number of bins and classification time using OuTex TC10 dataset	82
Table 5.1	The research objectives achievement	85



UMP

LIST OF FIGURES

Figure 2.1	Framework of texture classification	8
Figure 2.2	Example of a simple SVM model	10
Figure 2.3	Example of KNN classification process.	11
Figure 2.4	Textural feature extraction methods	12
Figure 2.5	LBP operator	14
Figure 2.6	Examples of different patterns	15
Figure 2.7	Example of the LBP operator's noise sensitivity	16
Figure 2.8	Example of classifying falsely problem.	16
Figure 2.9	LTP operator	18
Figure 2.10	(a) a 3×3 pattern. (b) CLBP_S. (c) magnitude component. (d) CLBP_M.	19
Figure 2.11	The framework of CLBP	20
Figure 2.12	LBC operator	21
Figure 2.13	The RLBP	22
Figure 2.14	The uncertain code "11 \times 100 \times 0" is encoding and resulting in three NRLBP codes comparing with LBP and LTP in (a), (b),(c), and (d). (e) shows that no uniform code can be formed.	23
Figure 2.15	The overall framework of BRINT descriptor	24
Figure 2.16	The CLTP sign and magnitude operators.	26
Figure 2.17	The overall calculation process of FbLBP	28
Figure 2.18	RDWT and DWT with (512 x 512) image size (a) single-level Haar RDWT with size 512x512 for each sub-band (b) single-level Haar DWT with size (256 x 256) for each sub-band.	32
Figure 2.19	RDWT analysis and synthesis filter banks	33
Figure 2.20	Some images from CuReT dataset	34
Figure 2.21	Some images from OuTeX dataset.	35
Figure 2.22	some sample images in UIUC database	36
Figure 2.23	Some images from Kylberg dataset	36
Figure 2.24	Images from 2D Hela dataset	37
Figure 2.25	Image from BR Database	38
Figure 3.1	Illustration of the methodology	40
Figure 3.2	General Framework for the proposed work	41
Figure 3.3	Flowchart of WCLTP extraction process	43
Figure 3.4	Example of WCLTP sign extraction process	44
Figure 3.5	Example of WCLTP magnitude extraction process	45

Figure 3.6	Feat-WCLTP extraction process.	47
Figure 3.7	Example of the calculation process for magnitude component for Feat-WCLTP	50
Figure 4.1	Examples of the images with the noise.	57
Figure 4.2	Classification rates on the noisy CURET dataset with different SNR values for pattern size (R=1, P=8)	57
Figure 4.3	Classification rates on the noisy CURET dataset with different SNR values for pattern size (R=2, P=16).	58
Figure 4.4	classification accuracy of noisy CURET dataset when (R=3, P=24)	58
Figure 4.5	Performance comparison of proposed Feat-WCLTP with CLTP using CURET dataset under different pattern size (a) (R=1,P=8). (b) (R=2,P=16). (c) (R=3,P=24).	68
Figure 4.6	Performance comparison of proposed descriptors with CLTP using OuTex dataset.(a) OuTex TC12(h). (b) OuTex TC12(t) (c) OuTex TC10	70
Figure 4.7	Performance comparison of proposed descriptors with CLTP using UIUC dataset. (a) with pattern size (R=1,P=8). (b) with pattern size (R=2,P=16). (c) with pattern size (R=3, P=24).	72
Figure 4.8	Performance comparison of proposed descriptors with CLTP using Kylberg dataset. (a) with pattern size (R=1,P=8). (b) with pattern size (R=2,P=16). (c) with pattern size (R=3, P=24).	74
Figure 4.9	Performance comparison of proposed descriptors and CLTP using 2D HeLa dataset.	76
Figure 4.10	Performance comparison of proposed descriptors with CLTP using Breast Cancer dataset.	77
Figure 4.11	Dimensionality comparison of proposed descriptors with CLTP using P=8 and R= 1,2,3 and 4.	78
Figure 4.12	Dimensionality comparison of proposed descriptors with CLTP using P=16,24 and R= 1,2,3 and 4	78
Figure 4.13	Classification time comparison of proposed descriptors and CLTP using OuTex dataset with different radius (i.e. R=1,2,3,4) (a) using P =8 (b) using P=24	80
Figure 4.14	Classification time comparison of proposed descriptors using 2D HeLa dataset with different radius (i.e. R=1,2,3,4) (a) using P =8 (b) using P=24.	81

LIST OF SYMBOLS

R	The radius of symmetric neighbourhood circle
p	The number of neighbourhood pixels
i_c	The grey value of the centre pixel
i_p	The grey value neighbour pixel
U	Uniformity
u2	Uniform patterns
riu2	Rotation invariant uniform pattern
t	Threshold value
s_p	Sign component
m_p	Magnitude component
c_l	The average grey level of the whole image
μ_m	Mean of the magnitude vector
σ_m^2	Variance of the magnitude vector
t_μ	Local threshold value for mean
t_σ	Local threshold value for variance
t_c	Local threshold value for centre
Ψ	Mother wavelet function
*	Convolution operator
↓	Downsampling operator
c_j	Output coefficients of highpass filter
d_j	Output coefficients of lowpass filter
N	Number of training images
χ^2	Distance between two histograms
H	Histogram

UMP

LIST OF ABBREVIATIONS

ANN	Artificial Neural Network techniques
AR	Autoregression
BRINT	Binary Rotation Invariant and Noise Tolerant
CLBC	Completed Local Binary Count
CNN	Convolutional Neural Network
CLBP	Completed Local Binary Pattern
CLTP	Completed Local Ternary Pattern
CuReT	Columbia-Utrecht Reflectance and Texture Database
CWT	Continuous Wavelet Transforms
WT	Wavelet Transform
DRLBP	Dominant Rotated Local Binary Patterns
DWT	Discrete Wavelet Transform
FbLBP	Feature-based Local binary pattern
Feat-WCLTP	Feature-based Completed Local Ternary Pattern
GLCM	Gray Level Co-occurrence Matrix
HH	High-High
HL	High-Low
K-NN	K-Nearest Neighbor
LBC	Local Binary Count
LBP	Local Binary Patterns
LH	Low-High
LL	Low-Low
LTP	Local Ternary Pattern
MRF	Markov Random Field
MLP	Multi-Layer Perceptron
NRLBP	Noise Resistant Local Binary Pattern
PET	Positron Emission Tomography
RDWT	Redundant Discrete Wavelet Transform
RBF	Radial Basis Function
RGB	Red, Green and Blue
RLBP	Robust Local Binary Pattern

CHAPTER 1

INTRODUCTION

1.1 Background

Nowadays, computer vision technologies have been developed along with the growth in the manufacturing of advanced image capture devices. This development has enabled images to be captured efficiently at a high resolution, thereby reinforcing the active role of images in most real-life fields (i.e. medical, military, educational, satellite and entertainment) (Aziz et al. 2017). Consequently, the image processing field has experienced many relevant issues, such as the image classification problem.

The image classification problem refers to the task of categorising and classifying images into known classes based on their content features. A successful classification requires the extraction of the best features that can represent the image effectively. An image has many significant features, such as texture, edge, shape, spatial relationship and colour (Liu et al., 2017). Texture features are considered one of the most essential characteristics that can describe an image. No specific definition for texture has been given. However, texture can be defined as a set of features (i.e. uniformity, roughness, intensity and density) (Davies 2018). The significance of texture property has inspired researchers to make great progress in developing efficient texture classification descriptors.

Texture classification is increasingly recognised as a serious issue in the texture analysis field. In general, texture classification aims to design an algorithm that can address a sample image to a reference image in a pre-defined image database based on image texture property (Davarzani et al. 2015). Accordingly, numerous feature extraction algorithms have been proposed over the past decades. The common purpose of all

descriptors is how to extract distinctive texture features that enable them to perform well in real-life applications.

Texture classification plays a key role in a wide variety of real-life applications, such as medical image analysis (Depeursinge et al. 2014; Li et al. 2017; Liu et al. 2018), remote sensing (Anwer et al. 2018), the manufacturing industry (Ruiz et al. 2018; Tang et al. 2015), face recognition (Nanni et al. 2017) and object tracking (Zoidi et al. 2014).

Medical image analysis is a wide area where texture classification algorithms are used extensively in many medical imaging tasks, such as disease diagnosis and surgical planning. The evolution in the medical domain leads to the use of sophisticated medical equipment that helps in making a correct medical diagnosis, such as magnetic resonance imaging, electron microscopy, computed tomography and ultrasound devices. These equipment and methods are considered basic sources of medical images. However, given the abundant details and sensitivity of images obtained through these methods, manual screening is difficult and insufficient. Researchers have found that texture presents reliable and effective features that could enhance the accuracy and the time consumed in examining these images (Tech & Somwanshi 2017).

1.2 Motivation

Texture analysis has played a significant role in various fields. The human eye can extract a number of obvious texture features from an image. However, it cannot notice fine details that play a significant role in understanding the image contents. Such inadequacy leads to incorrect image representation. Therefore, developing a robust texture classification descriptor will overcome human mistakes as well as save time and cost. Recently, considerable attention has been paid to the use of texture analysis in the medical image field because of many reasons. Firstly, medical images may contain several and complex textures that cause the human visual system to struggle in discriminating textural information, thereby possibly leading to diagnosis errors, which are not tolerated due to the sensitivity of medical images (Depeursinge et al. 2017). Secondly, experts sometimes need to understand the progress of specific diseases, thereby requiring the analysis of a large number of images over a long period of time, which entails great effort and time. Automating this process will help reduce time consumption and improve the functionality of the diagnosis of diseases (Weese & Lorenz 2016).

Accordingly, developing a reliable and robust texture classification descriptor that works effectively on texture and medical images is an urgent need.

1.3 Problem Statement

An effective texture classification descriptor is the Local Binary Pattern (LBP), which was proposed over two decades ago (Ojala et al., 1996). LBP gained popularity due to its superior advantages (i.e. simplicity, flexibility and high distinguishing ability), which make LBP a preferred choice for many applications. However, it suffers from obvious limitations such as noise sensitivity, rotation, illumination variations and limited discriminative capability (Liu et al. 2014). Therefore, many descriptors based on LBP have been proposed to overcome its limitations, enhance its performance accuracy and preserve its advantages. Examples of these descriptors are Completed Local Binary Pattern (CLBP) (Guo et al. 2010), Local Ternary Pattern (LTP) (Tan & Triggs 2010) and Completed Local Binary Count (CLBC) (Zhao et al. 2012). Although these LBP variants improved the performance of the original LBP descriptor to some extent, they inherited some of LBP's limitations, such as noise sensitivity.

The Completed Local Ternary Pattern (CLTP) (Rassem et al., 2017) is one of the descriptors that eliminate noise sensitivity. CLTP achieved impressive classification accuracy rates in different image classification systems. However, CLTP suffers from some limitations, such as high dimensionality, where the size of CLTP is double that of CLBP, thereby increasing the computation time and needing a large memory space. Moreover, it may affect classification accuracy. In addition, the threshold value in CLTP is selected manually. Overcoming the high dimensionality of the CLTP texture descriptor will help improve its recognition and classification performance. The possibility of wrong matching and classification is higher with the high-dimensional descriptor in the classification stage using some classifiers, thereby reducing the descriptor's performance. Therefore, proposing a new descriptor that is robust to noise, illumination invariances and rotation invariances and has a low dimension is a challenge that must be overcome.

1.4 Research Objectives

On the basis of the aforementioned problems in the Section 1.3, this study seeks to implement an accurate texture and medical image classification system using texture features. The objectives of this research are as follows:

1. To improve the classification accuracy of CLTP.
2. To propose a new feature-based texture descriptor by overcoming the computational limitation of the wavelet CLTP.
3. To evaluate the performance of the proposed texture descriptors for medical and texture image classification tasks.

1.5 Research Scope

This research focuses on the feature extraction task and investigates improvements of the CLTP descriptor. It will improve the classification performance of CLTP in two ways: by enhancing the classification accuracy of CLTP and introducing a new wavelet CLTP (WCLTP) texture descriptor and by reducing the high dimensionality and introducing the feature-based WCLTP (Feat-WCLTP) texture descriptor. Four standard textures (i.e. OuTex, CURET, UIUC and Kylberg) and two medical (i.e. 2D HeLa and Breast Cancer) datasets were used to evaluate the performance of both WCLTP and Feat-WCLTP. In addition to estimate the validity of the results, a confusion matrix was used to calculate the classification accuracy.

1.6 Thesis Organisation

This thesis is organised as follows:

Chapter One presents a general overview of the texture analysis issue, especially the texture classification problem. The research motivations, problems, objectives and scope are identified.

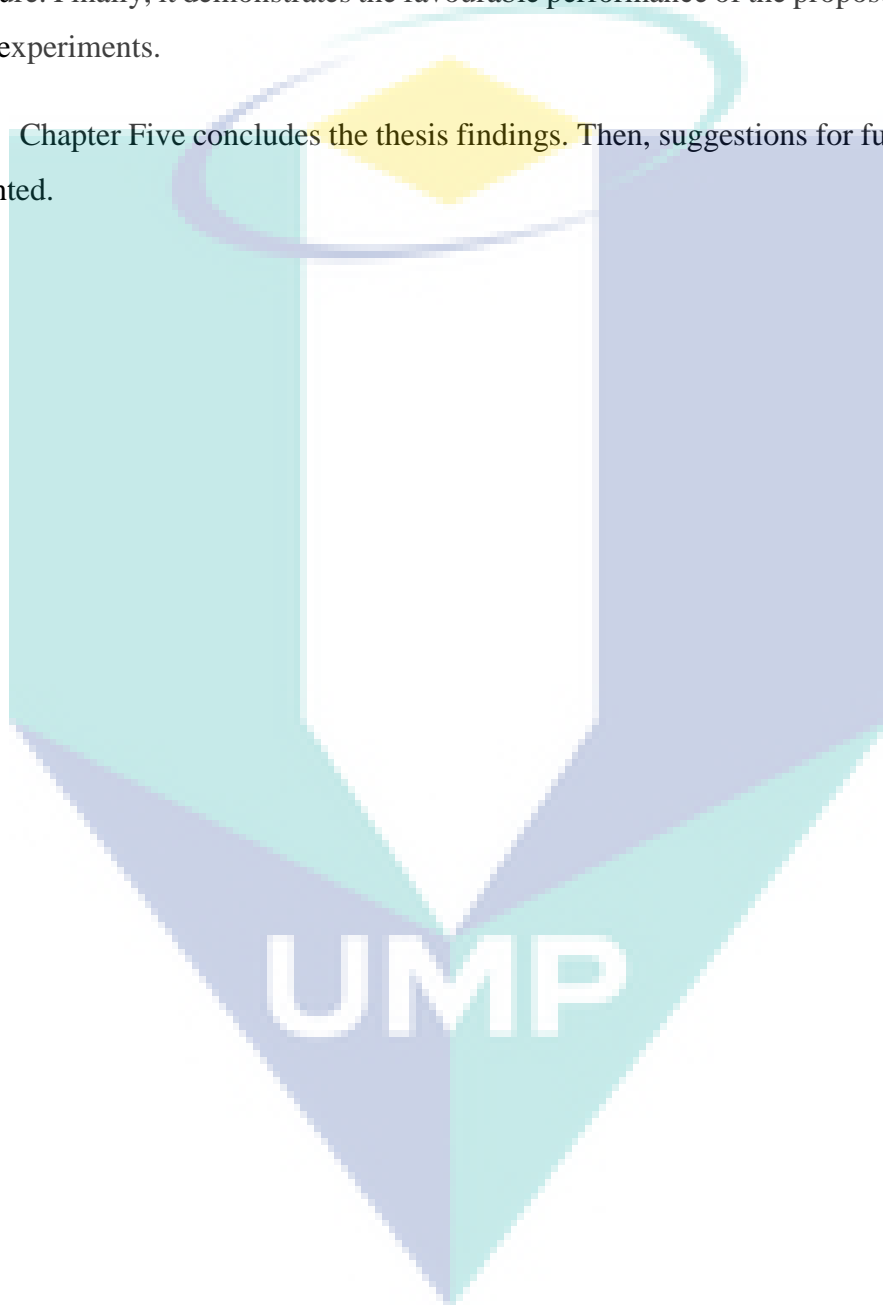
Chapter Two presents a general review of texture analysis, reviews of the LBP descriptor and some of its significant variants. It illustrates and explains the mathematical presentation for each method in the literature, as well as highlights the main advantages and limitations of each method. Finally, this chapter presents information about the benchmark datasets.

Chapter Three presents the methodology of the research. Then, it introduces the general proposed work, which consists of two proposed descriptors (WCLTP and Feat-

WCLTP) to address the research objectives. Also, this chapter investigates and discusses the proposed descriptors in detail and highlights their advantages.

Chapter Four presents the experimental results for the evaluation of the proposed descriptors. Moreover, it compares the evaluation results with those of the methods in the literature. Finally, it demonstrates the favourable performance of the proposed descriptors in all experiments.

Chapter Five concludes the thesis findings. Then, suggestions for future work are presented.



CHAPTER 2

LITERATURE REVIEW

2.1 Introduction

This chapter presents a literature review of texture analysis and its general research domains, highlighting the texture classification process and its general framework. In addition to providing a brief review of the main feature extraction methods, this chapter investigates the LBP descriptor and some of its variants and briefly introduces wavelet transform. Then, some benchmark databases are explored. Finally, the chapter summarises the review.

2.2 Texture Analysis

A digital image in computer vision applications can be described by a set of features, such as colour, shape, edge and texture. The texture is considered the most important and fundamental feature in image analysis. However, no official definition of this term has been given yet. Texture may provide good information about the physical properties of an image, such as roughness or smoothness. It can also be used to differentiate one object from another. As a result, texture analysis has been a universal research area in image processing and is applied in a variety of important computer vision applications (Liu et al., 2017). Texture analysis includes five general research domains: texture classification, texture segmentation, texture synthesis, texture compression and shape from texture.

2.2.1 Texture Classification

Texture classification aims to design an algorithm for classifying different unknown images into several groups based on a given set of training images. It has been used in many areas of application, such as medical image analysis (Tang et al. 2017), content-based image retrieval (Singh et al. 2018), object recognition (Pham et al. 2018), and remote sensing (Anwer et al. 2018).

2.2.2 Texture Segmentation

The goal of segmentation is to divide an image into individual homogeneous regions of similar texture. Therefore, additional analysis is conducted in these regions. The segmentation can be categorised into two types: supervised and unsupervised. The supervised scheme needs prior information or training samples that consist of textures from the classes presented in the image. In the unsupervised scheme, training samples do not need to be trained, and the pixels are grouped together based on their similarity. Many applications of texture segmentation exist, such as medical image analysis (Smistad et al. 2015) and document processing (Eskenazi et al. 2017).

2.2.3 Texture Synthesis

The goal of synthesis is to produce an output image from a particular input. Both images must be similar, but matching is not necessary. Texture synthesis is applied to many applications. For example, it can be used to synthesise high-resolution images in low-resolution images while retaining the image details (Yoo et al. 2016). It has been also used for image reconstruction, where a destroyed textured section of an image is replaced by a similar texture region (Colombo et al. 2011).

2.2.4 Texture Compression

The goal of texture compression is to minimise the amount of data required to store a textured image (Amin et al. 2018). The difference between texture compression and the normal image compression is that the first one is designed to utilise the statistical textured images by retaining all important high-frequency signals and simultaneously blocking artefacts. Compression is mainly used when storing or transmitting large amounts of data and multimedia such as digital encyclopaedias, videos and games (Jha et al. 2017).

2.2.5 Shape from Texture

This process mainly aims to reconstruct the 3D shape of a textured object from its image. This process requires some measurement of the image structure in addition to some information about surface texture to obtain a three-dimensional shape (Colombo et al. 2011).

2.3 Texture Classification

Texture classification is one of the most important and popular research topics in texture analysis and has recently become an active research field because it has been widely applied in many different important applications. Generally, texture classification aims to design an algorithm that can address a sample image to defined class where training examples have been given based on the image texture property (Suresha & Naik 2017). A general structure for texture classification includes four main processes which are: Pre-processing, feature extraction, feature selection and classification, as shown in Figure 2.1.

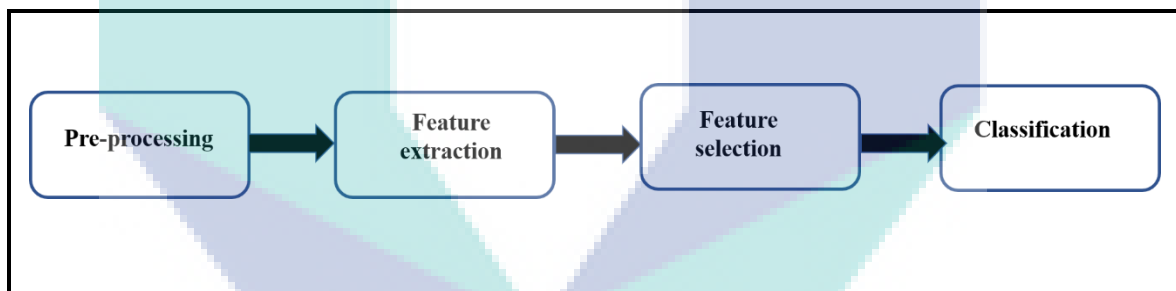


Figure 2.1 Framework of texture classification

2.3.1 Pre-processing

Pre-processing is a set of operations applied to the input image to prepare it for the next stage. This process aims to remove the variation from the input image without affecting the essential information in the image (Joshi & Karule 2018). Many examples of various sources during the image acquisition are given, such as the image device manufacturer, difference in sizes of the field of view, variations in illumination, image blurring and exposure duration. Preprocessing aims to remove these sources as much as possible. This process is performed by using a set of operations such as binarization,

scaling the image and removing the covered area, noise removal and illumination correction (Joshi & Karule 2018).

2.3.2 Feature Extraction

Image features are a distinctive characteristic of an image that helps in distinguishing between the categories of the images. Image features have two main types, namely, global and local features. The global features describe the image as a whole set and can represent an entire image with a single vector. Examples of global features are shape matrices and histogram-oriented gradients (HOG) (Lisin et al. 2005). Local features describe image patches, such as lines, spots and edges. Local features can be computed at multiple points in the image; thus, they are considered robust in representing an image. The texture features are a set of mathematical parameters that are calculated from the pixel's distribution in an image. Therefore, they are considered the best property that can describe an image properly. The main purpose of feature extraction is to extract the useful information that is required to describe a texture from the input image. The researchers agreed that feature extraction is the most significant step in the texture classification process (Liu et al. 2019). A successful classification result depends mainly on the efficiency of the feature extraction method (Bala & Scholar 2017). Many texture feature extraction descriptors have been proposed and tested since 1960. Given that this research focuses on texture descriptors, this matter will be further explained in detail in Section 2.4.

2.3.3 Feature Selection

Feature selection involves choosing a subset of relevant and useful discriminative features from whole extracted features according to certain criteria. In the feature extraction process, the number of extracted features may be large and some of the features may not be helpful. Thus, removing irrelevant and redundant features will reduce the dimensionality of data, decrease the mathematical computation and increase the classification accuracy, thereby improving the performance of the classification model (Jović et al. 2015). Feature selection is an optional step, and many classification systems were proposed without it.

2.3.4 Classification

The last step is classification, where the extracted features are used to distinguish between different textural classes where each image is sorted to one of the pre-defined texture classes. Many classification algorithms are used to classify textural images. Examples of the most common classifiers are support vector machines (SVMs) (Ashour et al. 2016), and the K-nearest neighbour (KNN) classifiers (Polat & Kayaalp 2019), convolutional neural network (CNN) (Han et al. 2017) and artificial neural network (ANN) (Deepa & Devi 2011). In the following subsection, K-NN and SVM are explained given that they are used mostly with texture descriptors.

2.3.4.1 Support Vector Machines (SVM)

The SVM is one of the popular classifiers that used in image classification in recent years. It is first proposed by (Vapnik & Kotz 1982). The SVM aims to build a model that able to classify two separable classes of data, using a decision surface. In SVM the examples are represented as points in space and it divided by a gap as wide as possible, the data points which are nearest to the gap are called support vectors. The decision surface is computed by determining the maximum gap between the two supporting vectors. Figure 2.2 shows a simple SVM model.

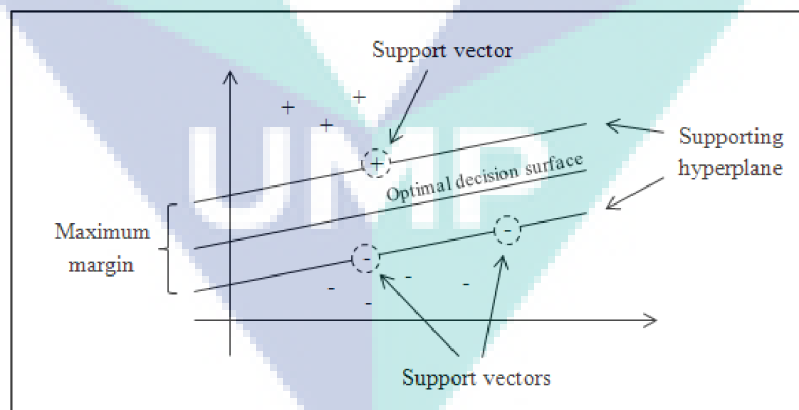


Figure 2.2 Example of a simple SVM model

Source: Hamel (2011)

The SVM classifier is working directly on the given input data space and is a good choice for a dataset with a large number of features (Yadav et al. 2017).

2.3.4.2 K-Nearest Neighbour (KNN)

The KNN algorithm is one of the simplest classification algorithms (Wan et al. 2012) and was first proposed by (Cover & Hart 1967). KNN depends on feature similarity. In this algorithm, a positive integer K is set. With each new sample, it specifies how many nearest neighbours are present near the test example. Then, the object is classified by a majority vote of its neighbours and is assigned to the class that is most common among its K -nearest neighbours. Figure 2.2 illustrates the process of the KNN algorithm.

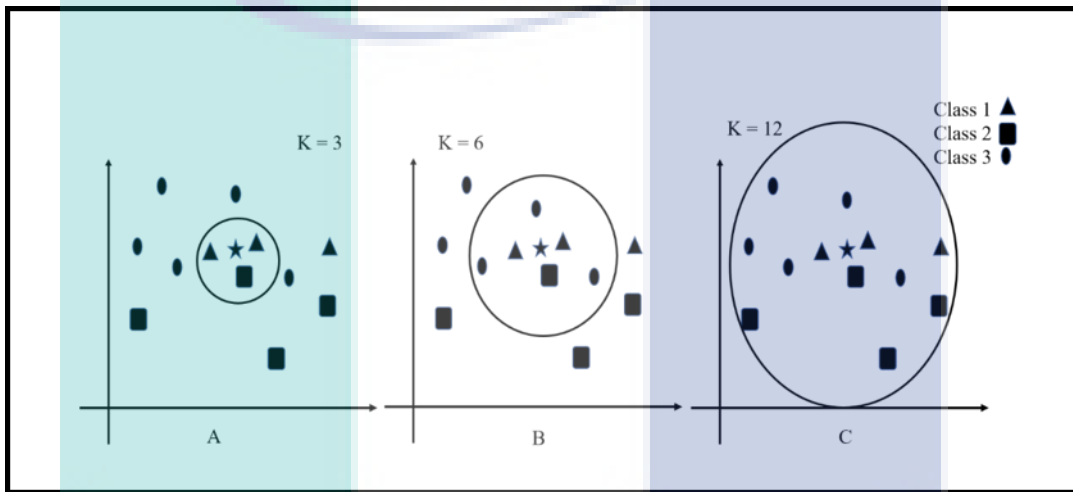


Figure 2.3 Example of KNN classification process.

To determine the class of the star, the star can be circle, square or triangle, and nothing else. The ‘ K ’ in the KNN algorithm is the nearest neighbours to take a vote from. In (A) $K = 3$. Hence, a circle with a star as the centre is made; it should be big to enclose only three data points on the plane. The star in (A) is assigned to the first class because 2 triangles and only 1 square are present inside the inner circle. In (B), $K = 6$, it is assigned to class 3 (3 circles, 2 triangles, 1 square) inside the circle. In (c), $K = 12$, it is assigned to class 3 also (5 circles, 3 triangles, 4 square) inside the circle. The k -nn algorithm is a good choice for classification in case no prior knowledge exists about the distribution data, such as nonlinear data (Yu et al. 2016).

2.4 Textural Feature Extraction

Numerous feature extraction methods have been developed and introduced for efficient texture classification. The common main purpose of all texture descriptors is to extract distinctive texture features that are robust to image effects such as noise, rotation,

blurriness and illumination variations (Bala & Scholar 2017). The existing methods can be categorised into four main groups as shown in Figure 2.4.

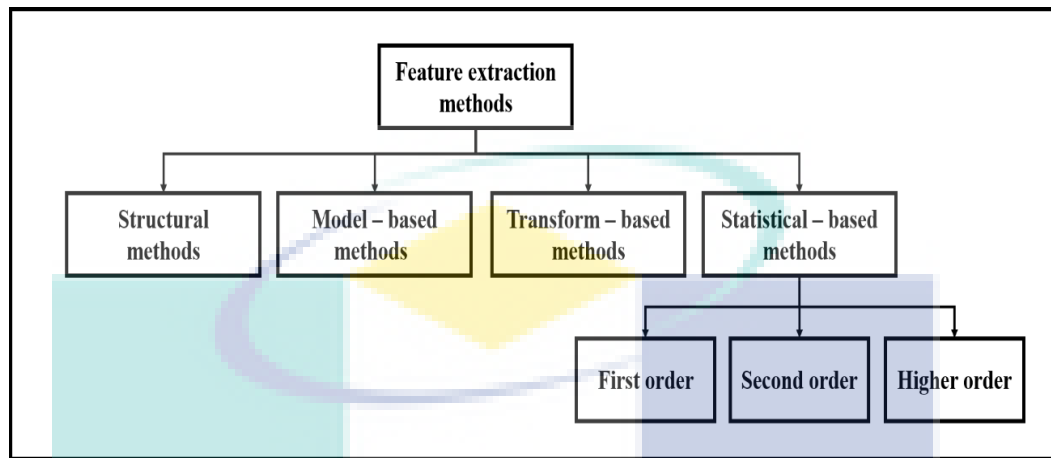


Figure 2.4 Textural feature extraction methods

2.4.1 Structural Methods

The algorithms in this approach consider that textures are formed of a set of elements called primitives or texel. These elements are arranged based on particular spatial rules, then the texel and their rules are used to describe textures and extract features. Many methods based on structural approach are applied to finding texels and extracting their features such as mathematical morphological operation (Velasco-Forero & Angulo 2013), fractal analysis (Xu et al. 2011) and the topographic map method (Jasiewicz & Stepinski 2013). However, this method is seldom used in texture classification because it is not adequate for analysing complex textures. It is suitable for textures with uniform patterns because the textures are well-defined, and it is not appropriate for micro textures' structures; it works well with large structures only (Cataldo & Ficarra 2017).

2.4.2 Model-based Methods

These methods suppose that textural images could be represented by some experimental models, and the parameters of the model are determined and used as the image features. Many popular models use this approach, such as Markov random field (Gu et al. 2017), Autoregression (Sahu et al. 2015), and fractals (Al-Kadi 2015).

The main trouble in the model-based methods is the process of choosing the proper model for a specific texture and mapping textures into the selected model effectively. Moreover, these models require many parameters, which may be difficult to determine especially if the neighbourhood size is not small. Therefore, the use of model-based methods in texture classification is still limited.

2.4.3 Transform-based methods

Transform-based methods are also known as filter-based methods because they are based on applying a filter to an image and converting it into a new domain, after which discriminative features are extracted. The fundamental step in this method is filtering. The filter is used to extract the relevant image features, then the filter response is performed by a local energy function to evaluate the energy in the filter output. The local energy function output is a series of images, which are considered the basis for classification. Many filters have been used in this approach, such as Fourier transform (Prakash & Chaudhury 2017), WT (Nayak et al. 2016) and Gabor transform (Jia et al. 2016). The main challenge is the selection of the filter, in addition to the large number of features produced by the filter, which results in computational complexity (Cataldo & Ficarra 2017).

2.4.4 Statistical-based Methods

These methods can be considered the most popular and effective methods for texture analysis. These methods use statistical measurements of different textural patterns based on spatial distribution of the grey value for the pixel to extract texture features. The statistical methods can be categorised into three different sets depending on its statistics order. The first set is the first-order statistical methods, which depend on the individual extraction features from every single pixel and ignoring the relationships between image pixels. Thus, they are not discriminative enough to be applied in classifying complex textures. The second set is the second-order statistical methods, which obtain properties from two or more-pixel values that share relative locations to each other like the grey-level co-occurrence matrix. The third set is the higher-order statistical operators, which are mainly used to overcome the limitations of the aforementioned sets. In this case, the features are extracted based on the spatial relationships between micropatterns. A well-known example of higher-order statistical method is LBP (Ojala et al., 1996).

2.5 Texture Descriptor

A representation of texture is also known as texture features. A texture descriptor is used to calculate the texture features numerically using one of the aforementioned methods. Selecting an appropriate texture descriptor is not easy, because no single descriptor is suitable for all applications. In the following, different texture descriptors will be discussed.

2.5.1 Local Binary Pattern

LBP is a simple yet powerful greyscale invariant texture descriptor proposed by Ojala two decades ago (Ojala et al., 1996). LBP has made a great contribution to the texture analysis field. It has been applied in a wide variety of application and has achieved good performance in medical image analysis (Nanni et al. 2010), texture classification (Davarzani et al. 2015) and face recognition (Taouche et al. 2014). LBP was initially defined within the concept of 8 grey pixels with a centre pixel. The LBP encoding process is illustrated in Figure 2.5, where the grey-level difference between the centre pixel and its neighbourhood pixel is calculated. The neighbourhood pixel is set to 1 if the difference is positive or 0 if it is negative; then, these values are used to obtain a binary code, which is generated later to represent a histogram that describes the image texture and the centre pixel value.

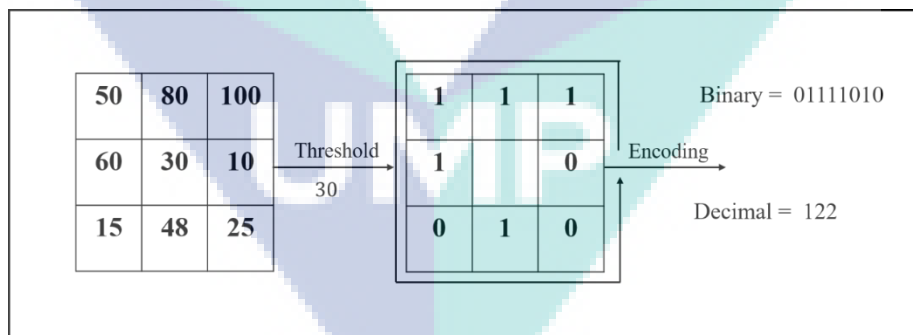


Figure 2.5 LBP operator

In 2002, authors developed the idea of LBP to use neighbourhoods with different sizes by using a symmetric circle neighbourhood defined by R and P , where R denotes the radius of the circle while P denotes the number of neighbourhood pixels (Ojala et al. 2002). The mathematical equation of LBP is shown below.

$$\text{LBP}_{P,R} = \sum_{p=0}^{P-1} 2^p s(i_p - i_c) , s(x) = \begin{cases} 1, & x \geq 0 \\ 0, & x < 0 \end{cases} \quad 2.1$$

where i_c and i_p denote the grey values of the centre pixel and the neighbour pixel, respectively. The neighbours' pixels that do not locate strictly in the centre of pixels are estimated by interpolation (Chowriappa et al. 2013). Figure 2.5 shows examples of three different texture patterns with different values of R and P .

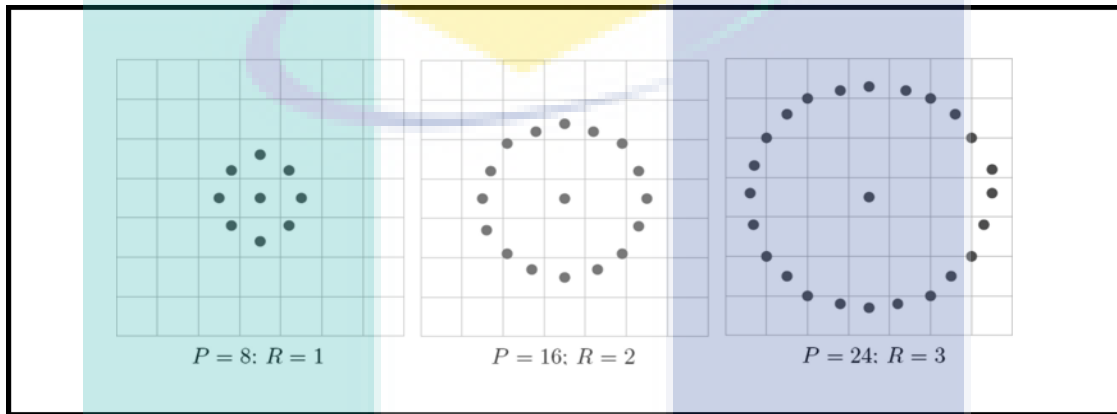


Figure 2.6 Examples of different patterns

Source : Chowriappa et al. (2013)

Together with this generalisation, the authors presented ‘uniform patterns’ of LBP (Ojala et al. 2002). LBP is called uniform if its uniformity measure is equal to at most 2. Uniformity (U) is the number of bitwise transitions from 0 to 1 or 1 to 0 when the bit pattern is considered circular. For example, patterns 11111111, 10001111 and 01010011 have 0, 2 and 6 transitions, respectively. The first two patterns are uniform because the uniformity measure is 2 or less, and the third pattern is non-uniform because it consists of more than two transitions. In the uniform-pattern LBP, each pattern is assigned a separate label, and all non-uniform patterns are assigned under a single label. This makes the uniform pattern LBP, $\text{LBP}_{P,R}^{u2}$ histogram size smaller compared with the original LBP, the superscript u2 stands for “uniform pattern”. With uniform patterns, for P neighbours, $P*(P-1) + 3$ different uniform patterns will be present as opposed to 2^P patterns in the original LBP. To achieve rotation invariance, a local rotation invariant pattern is presented as

$$LBP_{P,R}^{riu2} = \begin{cases} \sum_{p=0}^{P-1} 2^p s(i_p - i_c) & \text{if } U(LBP_{P,R}) \leq 2 \\ p + 1 & \text{otherwise} \end{cases}$$

Where i_c , i_p , P and R are as described in Equation 2.1 and the superscript $riu2$ stands for “rotation invariant uniform pattern”

The mapping from $LBP_{P,R}$ to $LBP_{P,R}^{riu2}$ (Ojala et al. 2002) can be implemented using a lookup table with a $P+2$ output values. Perhaps the most serious disadvantages of this method are its high sensitivity to noise and sometimes the different patterns of LBP possibly could be classified into the same class (Guo et al. 2012). Examples of these two weaknesses are shown in Figures 2.7 and 2.8.

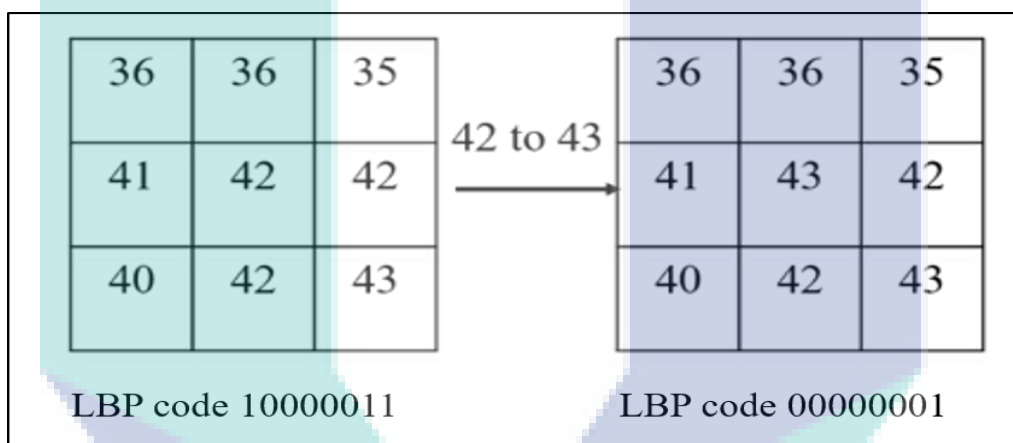


Figure 2.7 Example of the LBP operator's noise sensitivity

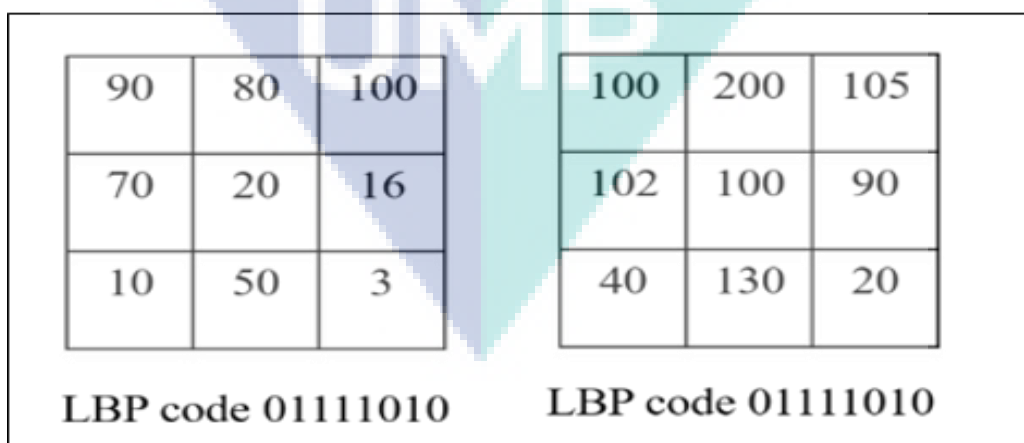


Figure 2.8 Example of classifying falsely problem.

As Figure 2.7 shows, a slight change in the centre grey pixel value from 42 to 43 due to noise may change the whole LBP binary code. In this example, this slight change from 42 to 43 changes the LBP code. Figure 2.8 shows that the LBP binary code for two different patterns is the same, thereby possibly leading to false classification of both patterns under the same class.

LBP has gained high popularity due to its simplicity, flexibility and high distinguishing power, thereby making LBP a foundation for new research directions (Pietikäinen & Zhao 2015). Thus, many different variants of LBP have been proposed to improve its discriminative power for texture classification and overcome its limitations. In the following, some well-known LBP variants will be explained.

2.5.2 Local Ternary Pattern

In 2010, Tan and Triggs modified the general LBP descriptor to overcome noise sensitivity by using a threshold value (t) and encoded the neighbour pixel values into 3-value instead of 2-valued codes (Tan & Triggs 2010). This new descriptor is called LTP, which is mathematically defined as follows:

$$LTP_{P,R} = \sum_{p=0}^{P-1} 2^p s(i_p - i_c), s(x) = \begin{cases} 1, & t \geq 0 \\ 0, & -t < x < t \\ -1, & x < -t \end{cases} \quad 2.3$$

where i_c , i_p , R and P are defined previously in Equation (2.1), and t indicates the threshold value.

The extraction of LTP can be shown in Figure 2.9 where the threshold value is set to 5; thus, the interval tolerance becomes [26, 36]. The values belong to the interval encoded to 0, and the values above 36 are encoded to 1. The values below 26 are encoded to -1.

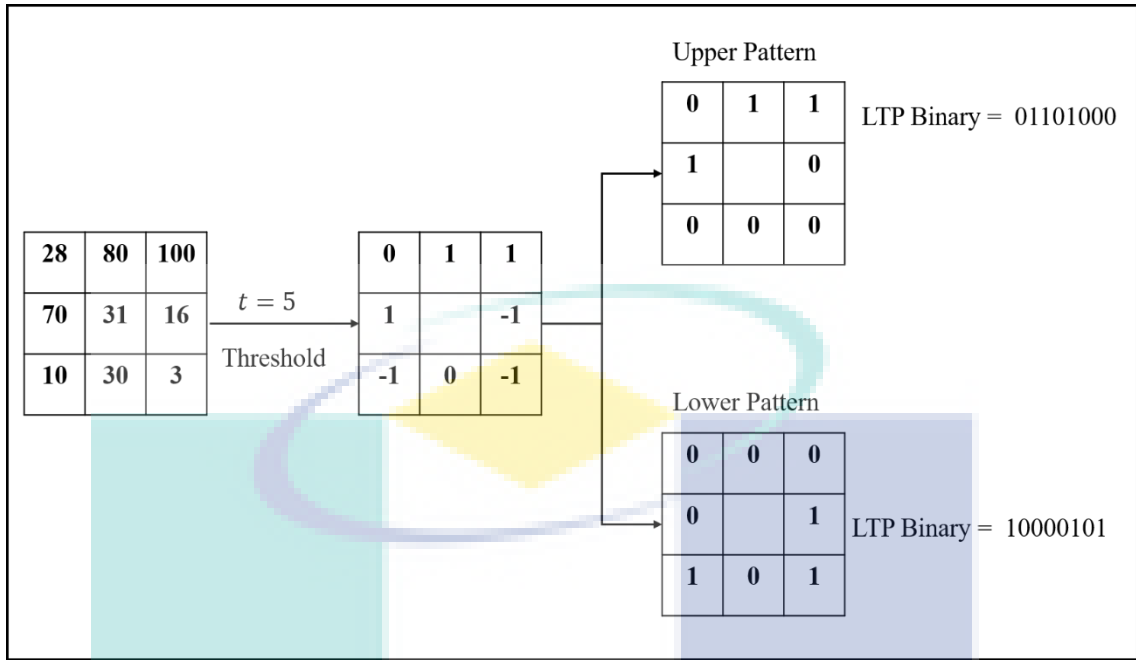


Figure 2.9 LTP operator

Tan and Triggs used LTP for face image classification. Since then, LTP has been used in many other fields. Although LTP reduces noise sensitivity, it is no longer strictly invariant to greyscale changes and still inherited the second weakness of LBP which is classifying some different LBP patterns into the same class (Ren et al. 2013).

2.5.3 Completed Local Binary Pattern

CLBP was introduced by Guo et al (Guo et al., 2010) as a new descriptor for texture classification to improve rotation invariant texture classification results. The authors adopted a broader perspective for feature extraction more than LBP by including the information from the magnitude vectors and the centre pixels. The information was used to construct three operators, namely, CLBP_S, CLBP_M and CLBP_C. In CLBP, the local difference is disassembled into two complementary components: the sign component s_p and magnitude component m_p . The sign component is used to build (CLBP_S) operator, which is equivalent to the conventional LBP. The magnitude component is used to construct the (CLBP_M) operator that measures the local variance of the magnitude. CLBP_S and CLBP_M can be expressed as in Equation (2.4) and Equation (2.5), respectively.

$$CLBP_{S_{p,R}} = \sum_{p=0}^{P-1} 2^p s(i_p - i_c), s(p) = \begin{cases} 1, & i_p \geq i_c \\ 0, & i_p < i_c \end{cases} \quad 2.4$$

$$\text{CLBP_M}_{P,R} = \sum_{p=0}^{P-1} 2^{pt} t(m_p, c), \quad t(m_p, c) = \begin{cases} 1, & |i_p - i_c| \geq c \\ 0, & |i_p - i_c| < c \end{cases} \quad 2.5$$

where i_c , i_p , R and P are defined previously in Equation (2.1), m_p is the magnitude component and c denotes the mean value of m_p . Figure 2.10 shows a clarification example for calculating the sign and magnitude of CLBP operators.

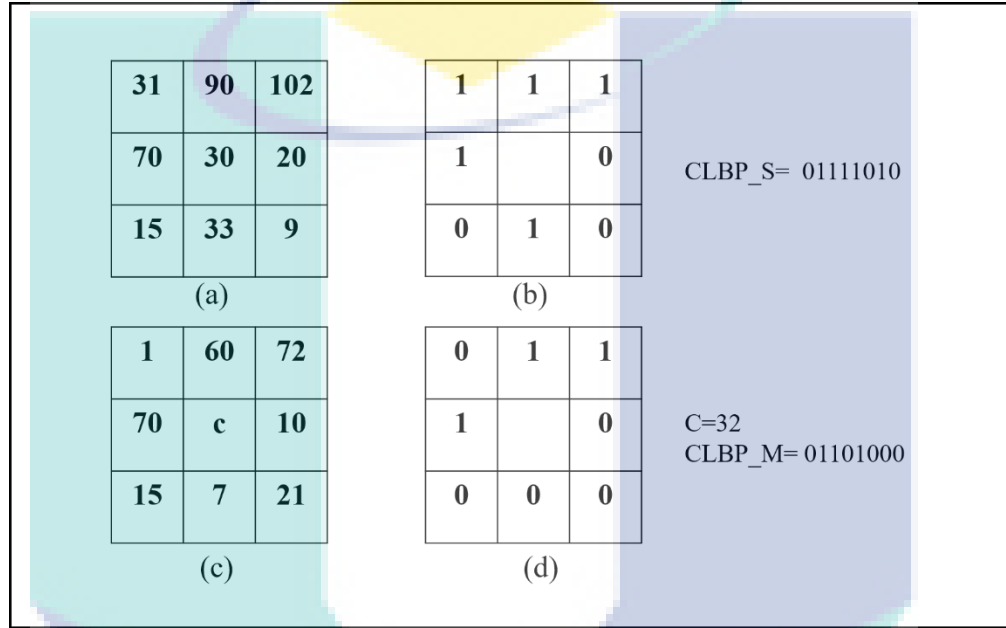


Figure 2.10 (a) a 3×3 pattern. (b) CLBP_S. (c) magnitude component. (d) CLBP_M.

The CLBP_C operator is constructed by thresholding the centre pixel of the 3×3 neighbourhood pattern at the average greyscale value of the whole image. It is mathematically expressed as in Equation (2.6).

$$\text{CLBP_C}_{P,R} = t(i_c, c_I) \quad 2.6$$

where i_c denotes the grey value of the centre pixel of the pattern, and c_I denotes the average grey level of the entire image. The three operators could be combined into joint or hybrid distributions. At first, the CLBP_S and CLBP_M could be combined in two ways: concatenation or jointly. In concatenation, the histograms of the CLBP_S and CLBP_M codes are calculated separately and then concatenated together, thereby constructing the CLBP_S_M. In the joint approach, a joint 2D histogram of the CLBP_S and CLBP_M codes is calculated to construct the CLBP_S/M. The three operators CLBP_S, CLBP_M and CLBP_C could also be combined in two ways: jointly or hybrid.

In the joint method, a 3D joint histogram is built, which is represented as CLBP_S/M/C. In the hybrid approach, a 2D joint histogram CLBP_S/C or CLBP_M/C is built firstly, and then the histogram is converted to a 1D histogram, which is then concatenated with CLBP_M or CLBP_S to generate a joint histogram, denoted by CLBP_M_S/C or CLBP_S_M/C (Guo et al. 2010).

The CLBP considerably improves texture classification. However, the CLBP suffers from some problems, such as noise sensitivity; similar sizes of the dimensionality of the CLBP_M and the CLBP_S, which means that the size of the histogram grows sharply; and the need to exploit the complementary between the sign component and the magnitude component (Sree 2015). Figure 2.11 demonstrates the general framework of the CLBP generation process.

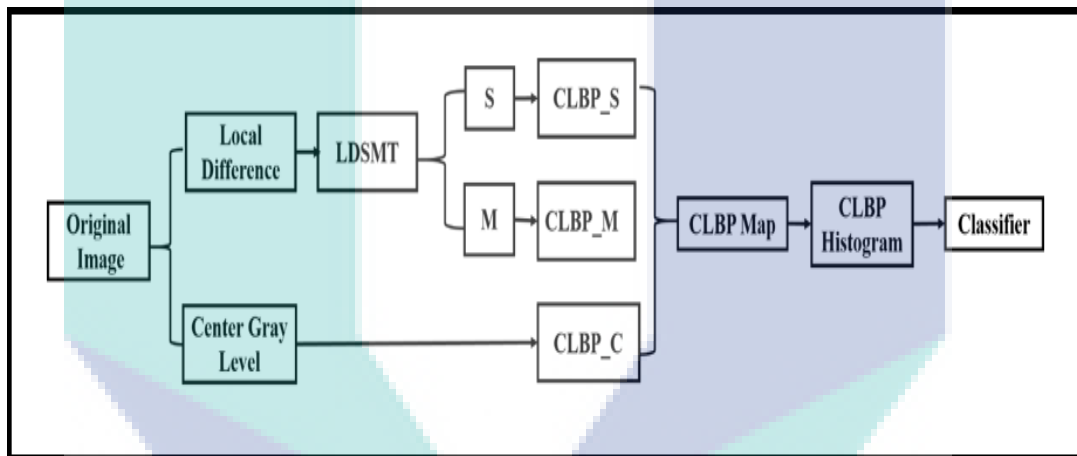


Figure 2.11 The framework of CLBP

Source: Guo et al. (2010)

2.5.4 Completed Local Binary Count

In 2012, a new texture descriptor called Local Binary Count (LBC) was proposed by (Zhao et al. 2012) for texture classification. Unlike LBP and its variants, the concept of LBC depends on computing the number of values of 1s that resulted from the thresholding step without the encoding step. An example of this operator is shown in Figure 2.12.

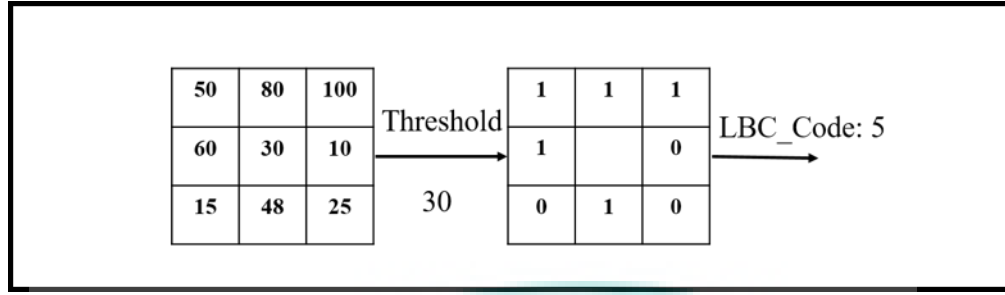


Figure 2.12 LBC operator

Mathematically, the following equation describes the LBC operator.

$$LBC_{P,R} = \sum_{p=0}^{P-1} s(i_p - i_c), s(x) = \begin{cases} 1, & x \geq 0 \\ 0, & x < 0 \end{cases} \quad 2.7$$

where i_c , i_p , R and P are defined in Equation 2.1. Similar to CLBP, the LBC was extended to completed LBC (CLBC), where the three operators CLBC_S, CLBC_M and CLBC_C are combined in joint or hybrid distributions. The CLBC_S is equal to the original LBC described above in Equation 2.7. The magnitude and centre operators can be described mathematically as follows:

$$CLBC_{M,P,R} = \sum_{p=0}^{P-1} t(m_p, c), t(m_p, c) = \begin{cases} 1, & |i_p - i_c| \geq c, \\ 0, & |i_p - i_c| < c, \end{cases} \quad 2.8$$

$$CLBC_{C,P,R} = t(i_c, c_1) \quad 2.9$$

where i_c , i_p , R , P , c , m_p and c_1 are defined in Equations (2.1), (2.5) and (2.6). The CLBC can achieve similar accurate classification rates as the CLBP. However, it reduces the computational complexity for the training and classification process and suffers from the same limitations of LBP (Nair & Jacob 2017).

2.5.5 Robust Local Binary Pattern

RLBP was proposed in 2013 by (Chen et al. 2013) to overcome the noise sensitivity problem in LBP. The concept of RLBP is finding the possible bit in LBP that was changed by the noise and then amending the changed bit of the LBP pattern. RLBP is used only in case of $P = 8$ and $R = 1$, in where the set of any neighbouring three-bit substring is $Y = \{y_1 = (000), y_2 = (001), y_3 = (010), y_4 = (011), y_5 = (100), y_6 = (101), y_7 = (110), y_8 = (111)\}$. The cases of y_3 and y_6 are assumed to be noisy, so they changed

to a new sub-string $y'3 = (000)$ and $y'6 = (111)$. Figure 2.13 shows a clear example of the RLBP process.

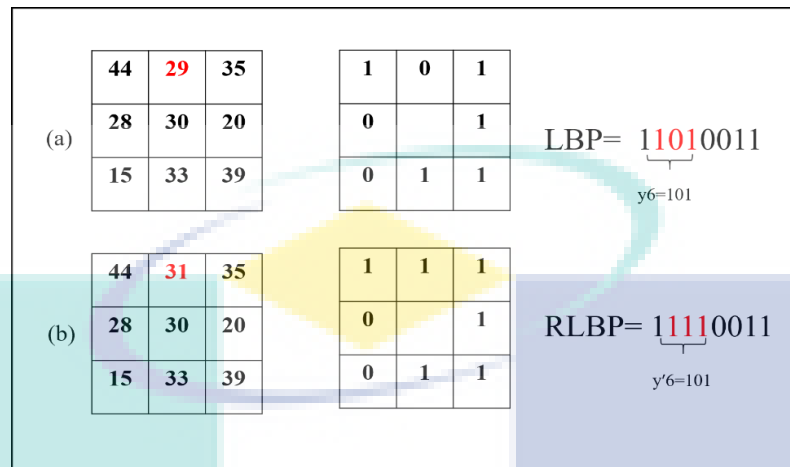


Figure 2.13 The RLBP

Figure 2.13 shows a pattern with an LBP binary code 11010011. The pixel with a value of 29 has a high possibility of being noisy because it results in a noisy substring 101 ($y6$). Thus, the RLBP changes the noisy substring 101 to the corresponding substring 111. The new code is 11110011, which denotes a local edge, which is a more meaningful pattern for texture representation. Thus, for each bin, the RLBP operator searches all its neighbouring three-bit substrings and maps its $y3$ or $y6$ to $y'3$ or $y'6$. Despite the simplicity of the idea, it works well. However, the main problem of this method is that the nonuniform patterns may be mapped to uniform ones and it is limited to one scale.

2.5.6 Noise Resistant Local Binary Pattern

NRLBP was mainly proposed to overcome the drawbacks of LTP and enhance its robustness to noise sensitivity (Ren et al. 2013). The connotation of NRLBP is based on the generation of different LBP patterns at the one-pixel place. The small pixel difference is most susceptible to noise. Thus, the NRLBP encodes the small pixel difference as the undetermined bit before determining its value depending on the other different bits of the LBP code. In the end, all the uncertain bit values are assigned to form all possible uniform LBP codes and change the noisy non-uniform patterns back to the uniform code. The main problems in NRLBP are its limited neighbourhood size because it needs a 3^P size table for P neighbouring pixels, and using a larger number of neighbouring pixels will be computationally expensive. Figure 2.14 shows an example of NRLBP calculation compared with LBP and LTP.

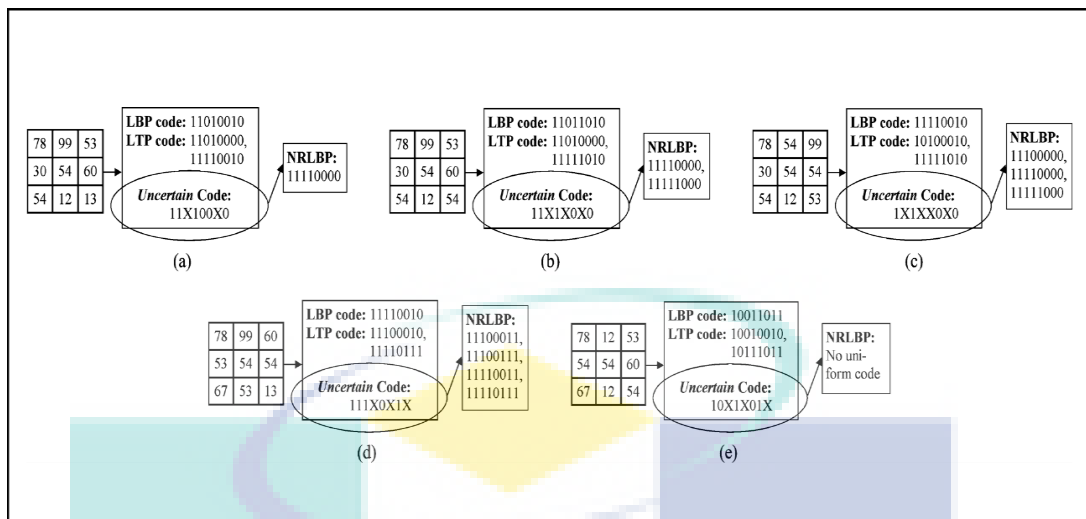


Figure 2.14 The uncertain code “11×100×0” is encoding and resulting in three NRLBP codes comparing with LBP and LTP in (a), (b),(c), and (d). (e) shows that no uniform code can be formed.

Source: Ren et al. (2013)

2.5.7 Binary Rotation Invariant and Noise Tolerant

Motivated by CLBP (Guo et al. 2010), a new feature extraction descriptor called Binary Rotation Invariant and Noise Tolerant (BRINT) descriptor was proposed (Liu et al. 2014). The BRINT combines three individual descriptors, namely, BRINT_S, BRINT_M and BRINT_C. Unlike the CLBP, which used only rotation invariant uniform patterns, BRINT considers all rotation invariant patterns. The BRINT can deal with a large number of different scales because the neighbour’s pixels are placed in a symmetric circle of radius R . Thus, adjusting the radius R creates operators for several spatial resolutions. The final representation histogram is a concatenation of binary histograms from multiple resolutions. Figure 2.15 illustrates the overall framework of the BRINT descriptor. BRINT has low dimensionality and noise robustness. However, the BRINT_M performs exactly the same as CLBP_M in extracting the magnitude information, which can be easily affected by rotation and illumination changes; thus, it still suffers the same limitations of CLBP_M.

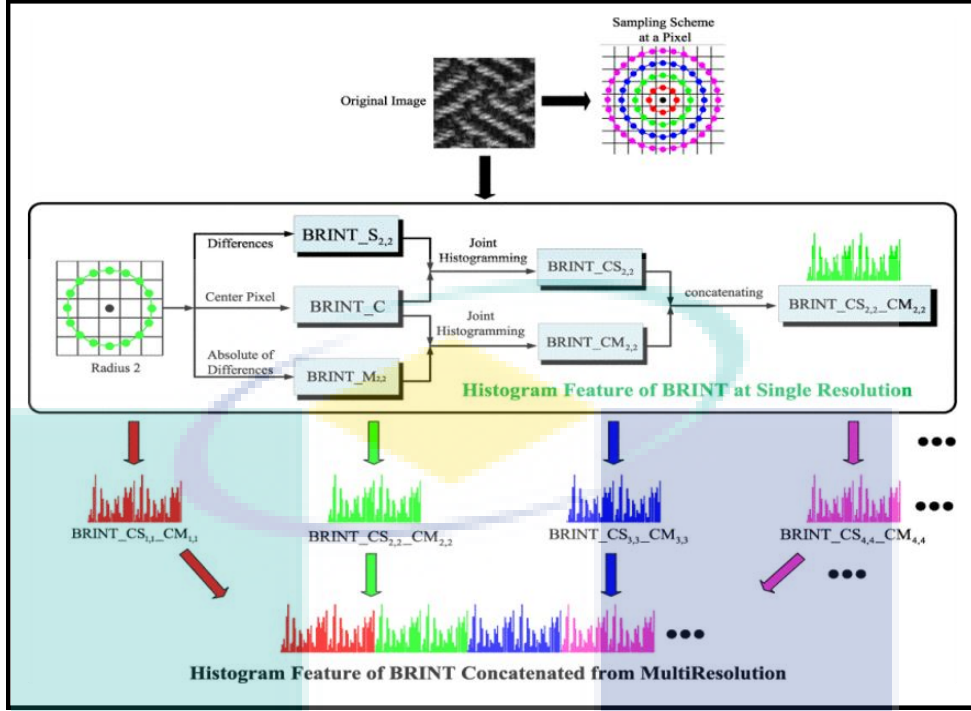


Figure 2.15 The overall framework of BRINT descriptor

Source: Liu et al. (2014)

2.5.8 Completed Local Ternary Pattern

Despite the significant accuracy in invariant rotation texture classification that has been achieved by CLBP, it also inherits the same challenges of LBP. (Rassem & Khoo 2014) proposed a more powerful texture operator called CLTP by combining CLBP and LTP. In CLTP, the local difference is decomposed into four complementary components; the first two are the upper and lower sign components, and the second two are the upper and lower magnitude components, which can be expressed as follows:

$$S_p^{\text{upper}} = S(i_p - (i_c + t)) \quad 2.10$$

$$S_p^{\text{lower}} = S(i_p - (i_c - t)) \quad 2.11$$

$$M_p^{\text{upper}} = |i_p - (i_c + t)| \quad 2.12$$

$$M_p^{\text{lower}} = |i_p - (i_c - t)| \quad 2.13$$

Then the sign components are used to build the $CLTP_{P,R}^{\text{upper}}$ and $CLTP_{P,R}^{\text{lower}}$ as follows:

$$CLTP_{S_{P,R}}^{\text{upper}} = \sum_{p=0}^{P-1} 2^{ps}(i_p - (i_c + t)), S_p^{\text{upper}} = \begin{cases} 1, & i_p \geq i_c + t, \\ 0, & \text{otherwise,} \end{cases} \quad 2.14$$

$$CLTP_{S_{P,R}}^{\text{lower}} = \sum_{p=0}^{P-1} 2^{ps}(i_p - (i_c - t)), S_p^{\text{lower}} = \begin{cases} 1, & i_p < i_c - t, \\ 0, & \text{otherwise,} \end{cases} \quad 2.15$$

where i_c , i_p , R and P are defined in Equation (2.1), and t is the threshold value, which is manually set to 5.

The two operators are then concatenated to form $CLTP_{S_{P,R}}$ as follows:

$$CLTP_{S_{P,R}} = [CLTP_{S_{P,R}}^{\text{upper}} \quad CLTP_{S_{P,R}}^{\text{lower}}] \quad 2.16$$

With the use of m_p^{upper} and m_p^{lower} , the $CLTP_{M_{P,R}}$ is built m_p^{lower} as follows

$$CLTP_{M_{P,R}}^{\text{upper}} = \sum_{p=0}^{P-1} 2^{pt}(m_p^{\text{upper}}, c), t(m_p^{\text{upper}}, c) \quad 2.17$$

$$= \begin{cases} 1, & |i_p - (i_c + t)| \geq c, \\ 0, & |i_p - (i_c + t)| < c, \end{cases}$$

$$CLTP_{M_{P,R}}^{\text{lower}} = \sum_{p=0}^{P-1} 2^{pt}(m_p^{\text{lower}}, c), t(m_p^{\text{lower}}, c) \quad 2.18$$

$$= \begin{cases} 1, & |i_p - (i_c - t)| \geq c, \\ 0, & |i_p - (i_c - t)| < c, \end{cases}$$

where i_c , i_p , R and P are defined previously in Equation (2.1), and c is the mean value of the magnitude component.

$$CLTP_{M_{P,R}} = [CLTP_{M_{P,R}}^{\text{upper}} \quad CLTP_{M_{P,R}}^{\text{lower}}] \quad 2.19$$

Figure 2.16 shows a clear example for calculating the sign and magnitude in CLTP operator where the local difference is computed twice based on the upper and lower value of the centre pixel. The sign is computed directly using the new value of the centre pixel after using the threshold, while the magnitude is computed based on the upper and lower magnitudes calculated according to c .

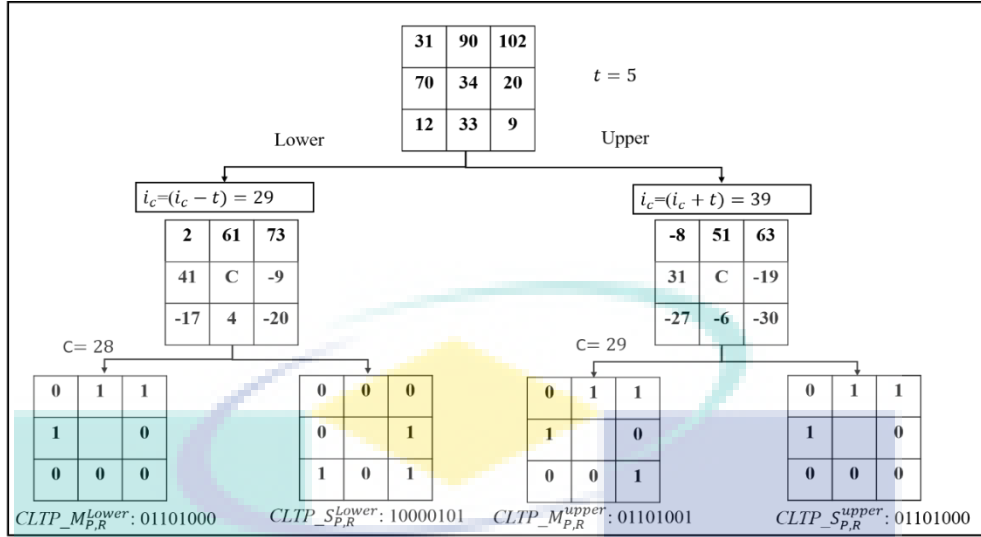


Figure 2.16 The CLTP sign and magnitude operators.

Similar to the above process, $CLTP_{P,R}^{upper}$ and $CLTP_{P,R}^{lower}$ can be mathematically expressed as follows:

$$CLTP_{C_{P,R}}^{upper} = t(i_c^{upper}, C_I) \quad 2.20$$

$$CLTP_{C_{P,R}}^{lower} = t(i_c^{lower}, C_I) \quad 2.21$$

where $i_c^{upper} = i_c + t$, $i_c^{lower} = i_c - t$ and C_I is the average pixel intensities of the whole image. The final CLTP operator is built the same as the CLBP operator by combining the three CLTP operators into joint or hybrid distributions to build the final histogram, which is double the size of the CLBP histogram. This feature may be considered a weak point of this operator.

2.5.9 Dominant Rotated Local Binary Patterns

In 2016, Mehta and Egiazarian challenged the rotation invariance problem, which is one of the most significant limitations in LBP, by proposing the dominant rotated LBP (DRLBP) descriptor (Mehta & Egiazarian 2016). DRLBP achieved rotation invariance by using a reference direction that was selected by the authors as the dominant direction as a reference direction based on experiments. The dominant direction is computed locally from the neighbourhood as the index of the neighbouring pixel, which has the maximum difference from the centre pixel as in Equation (2.22)

$$D = \arg \max |i_p - i_c| \quad 2.22$$

DRLBP captures structural information by using both sign and magnitude components. Similar to conventional LBP, DRLBP obtains a binary code that represents the neighbourhood by calculating the local differences between a centre pixel and its neighbours. Mathematically, the DRLBP descriptor is defined as Equation (2.23)

$$\text{DRLBP}_{P,R} = \sum_{p=0}^{P-1} S(i_p - i_c) \times 2^{\text{mod}(p-P,D)}, \quad 2.23$$

$$S(i_p - i_c) = \begin{cases} 1, & \text{if } i_p \geq i_c \\ 0, & \text{if } i_p < i_c \end{cases}$$

where i_c , i_p , R and P are defined by Equation (2.1), mod denotes the modulus operator and the weight depending on D , and D is the dominant direction. The DRLBP is invariant to both rotation and illumination variations and has a high discriminative power. However, it is sensitive to noise, and the calculating process of dominant orientation requires more computation.

2.5.10 Feature-based Local Binary Pattern

Recently, Pan et al. (2017), influenced by CLBP, proposed a new algorithm called feature-based LBP (FbLBP) to enhance LBP and overcome the limitations of its variants (Pan et al., 2017). The technique of constructing the final histogram of FbLBP is similar to that used by the CLBP where three binary codes are generated from three complementary parts, namely, the sign, feature and the centre pixel components. The sign operator (FbLBP_S) is qualified for conventional LBP, whilst the feature part (FbLBP_F) includes two features, namely, the mean and the variance. The mean and variance are encoded into binary format by using an adaptive local threshold proposed by the authors. They divided the image into $n \times n$ non-overlapping sub-images, then the adaptive threshold is determined for each sub-image. Thus, the FbLBP_F is defined as in Equation (2.24) and Equation (2.25).

$$\text{FbLBP_F}\mu(i_c) = S(\mu_m - t\mu) \quad 2.24$$

$$\text{FbLBP_F}\sigma(i_c) = S(\sigma_m^2 - t\sigma) \quad 2.25$$

where (μ_m) and (σ_m^2) are the mean and variance of the magnitude vector m_p , and the local threshold t_μ and t_σ are the average values of (μ_m) and (σ_m^2) in the sub-image. In a similar way, the centre pixel component is encoded to binary. as in Equation (2.26). Figure 2.17 summarises the overall calculation process of the FbLBP.

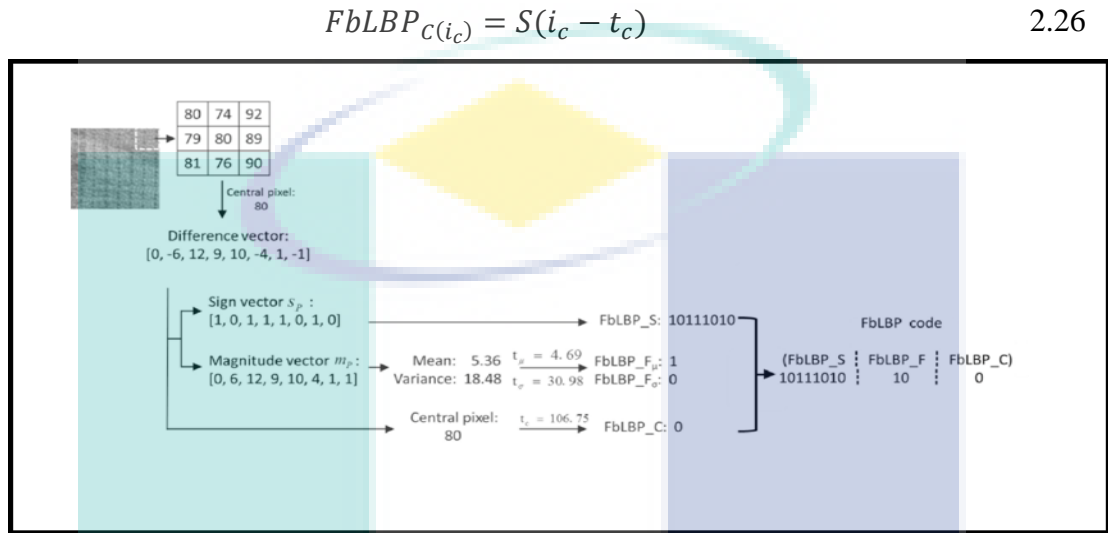


Figure 2.17 The overall calculation process of FbLBP

Source: Pan et al. (2017)

The FbLBP achieves good discrimination accuracy and solves the dimensionality problem, as indicated by the reduced dimensionality of the final histogram compared with that of the CLBP operator. However, the first problem, which is noise sensitivity, still appears in FbLBP as in CLBP and CLBC.

Table 2.1 compares all the previous descriptors in terms of noise sensitivity, illumination sensitivity, rotation sensitivity, the use of tuning parameters, computational complexity, high dimensionality and the histogram size. The table shows the limitations of the original LBP and some of its variants. All LBP variants aimed to increase the classification accuracy of LBP and handle its limitations. However, most of LBP variants still inherited at least one of LBP's limitations, (i.e. noise sensitivity, rotation sensitivity and illumination sensitivity). CLTP is one of the LBP-based descriptors that eliminate noise sensitivity problem and achieved impressive classification accuracy rates in different image classification tasks. However, CLTP suffers from the high dimensionality issue, where the size of CLTP is double that of CLBP. Moreover, the threshold value in CLTP is selected manually. Thus, this work aims to enhance the classification accuracy of CLTP and addressing the high dimensionality problem. Overcoming the high

dimensionality will reduce the computational time. To achieve these objectives this research will introduce two texture descriptors: the WCLTP descriptor, which mainly aims to enhance the classification accuracy, and Feat-WCLTP, which is mainly aims to overcome the high dimensionality and reduces the computational time.

Table 2.1 The well-known LBP variants texture descriptors.

Descriptor	Limitations						
	Noise Sensitivity	Illumination sensitivity	Rotation sensitivity	Using tuning parameter	Computational complexity	High dimensionality	Histogram size (for single-scale R)
LBP	Yes	Yes	Yes	No	No	Yes	2^P
$LBP_{P,R}^{ri}$	Yes	Yes	No	No	No	Yes	2^P
$LBP_{P,R}^{u2}$	Yes	Yes	No	No	No	Yes	$P*(P-1) + 3$
$LBP_{P,R}^{riu2}$	Yes	Yes	No	No	No	No	$P+2$
LTP	Yes	Yes	No	Yes	No	No	$(P+2)*2$
CLBP	Yes	Yes	No	No	Yes	Yes	$(P+2)*(P+2)*2$
CLBC	Yes	Yes	No	No	Yes	Yes	$(P+1)*(P+1)*2$
NRLBP	No	Yes	Yes	Yes	No	Yes	3^P
RLBP	Yes	No	No	No	No	Yes	$P*(P-1) + 3$
CLTP	No	No	No	Yes	Yes	Yes	$((P+2)*(P+2)*2)2$
BRINT	No	Yes	No	No	No	No	144
DRLBP	Yes	No	No	Yes	Yes	No	Not constant
FbLBP	Yes	Yes	No	No	No	No	$(P+2)*(2+2)*2$

Yes, indicates the limitation still exists
No indicates the limitation has been overcome.

2.6 Wavelet Transform (WT)

WT considers a unified framework for image multiresolution decomposition. It allows the examination of the texture under several resolutions while preserving spatial resolution (Sree 2015). The main concept of the WT is analysing the signal as a superposition of wavelets across multiple scales. It was developed to overcome the problems of Fourier transform related to frequency and time resolution properties (Cataldo & Ficarra 2017). For example, some important features in the image are

localised in the spatial domain. Fourier transform failed to represent these features in their transform coefficients. To solve such a problem, WT is used. WT extracts features from the input image by decomposing the original image into a series of sub-band images. Several WT types can be found in the literature, such as continuous WTs (CWT) (Rahimi & Moghaddam 2015), discrete WT (DWT) (Kovac et al. 2018) and redundant WT (RDWT) (Subhedar & Mankar 2016).

2.6.1 Continuous wavelet transforms (CWT)

CWT divides a continuous time function into wavelets (Rioul & Vetterli 1991). CWT has the ability to structure a time-frequency representation of an image with a good time and frequency localisation. CWTs $f(x)$ is presented as in Equation (2.26)

$$W(a, b) = \frac{1}{\sqrt{a}} \int x(t) \Psi * \left(\frac{t - b}{a} \right) dt. \quad a > 0, b \in \mathfrak{R} \quad 2.26$$

where Ψ represents the mother wavelet function, a and b denote the scale parameters and $*$ represents the convolution operator. The main problem in CWT is that it generates a large amount of unnecessary information because it calculates wavelet coefficients at every possible scale and position, thereby leading to high cost.

2.6.2 Discrete Wavelet Transform

DWT was proposed to overcome the drawbacks of CWT and makes WT more efficient in real-life applications (Mallat 1989). DWT selects only a subset of scales and positions during the analysis process. It represents the image in the time domain by employing a digital filter. DWT analyses an image by passing it over filters with several cut-off frequencies at different scales. This process includes three main steps: transforming the image into the frequency domain before multiplying it with the frequency filter function and then re-transforming the result into the spatial domain. Figure 2.18 illustrates an example of DWT.

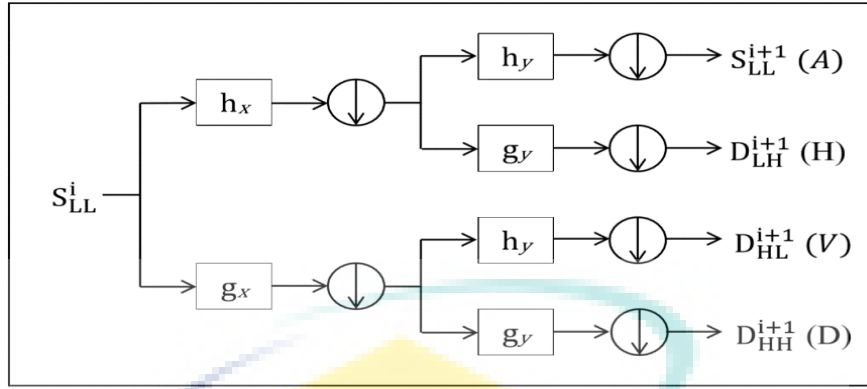


Figure 2.18 Example of DWT

Source: Li et al., (2003)

In the figure, the image S is decomposed into four sub-bands. The sub-band with low frequency represents an approximation of the image S , and the other three sub-bands with high-frequency represent detail images in different orientations, i.e. vertical, horizontal and diagonal.

The sub-band images can be computed by using the following equations:

$$A = [h_x * (h_y * S)_{\downarrow 2,1}]_{\downarrow 1,2} \quad 2.27$$

$$H = [h_x * (g_y * S)_{\downarrow 2,1}]_{\downarrow 1,2} \quad 2.28$$

$$V = [g_x * (h_y * S)_{\downarrow 2,1}]_{\downarrow 1,2} \quad 2.29$$

$$D = [g_x * (g_y * S)_{\downarrow 2,1}]_{\downarrow 1,2} \quad 2.30$$

where h , g and S , represent the high-pass filter, the low-pass filter and the input image, respectively. \downarrow represents the downsampling operator. For further decompositions, the approximation image LL is used to achieve higher levels of decomposition. This operation is continued until the final scale is reached. Despite the widespread use of DWT in the image classification field, it suffers from the main drawback, which is translation variance. Moreover, the DWT sub-bands are half the size of the original image, thereby leading to the loss of much spatial information during this type of decomposition.

2.6.3 Redundant discrete wavelet transforms

RDWT was proposed to overcome the limitations of the DWT (Fowler 2005). One major drawback of DWT is the shift variance problem, which is a result of

downsampling operation. The downsampling process removes useless samples from sub-band images, thereby helping reduce the redundant samples in the decomposition process. However, this approach leads to translation variance of the decomposition results. For example, a slight shift in the input image leads to a large amendment in wavelet coefficients, thereby causing incorrect feature extraction. RDWT overcomes this problem by eliminating the downsampling operation and producing an overcomplete representation (Irani Mehr et al. 2013). RDWT decomposes an image into four sub-bands that each have the same size as the input image: LL, HL, LH and HH. In DWT, the sub-band size is decreased by half the input image size in each decomposition level. Thereby, in RDWT, the texture features in each sub-band and input image will be identical in spatial location, thereby efficiently acquiring the local texture (Subhedar & Mankar 2016). Figure 2.19 shows the size of each band for DWT and RDWT.

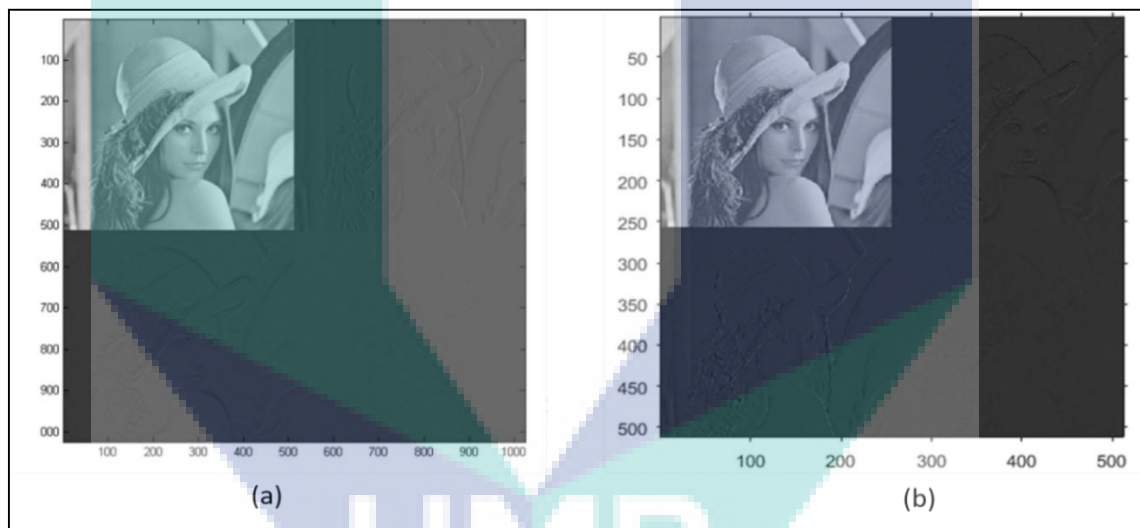


Figure 2.18 RDWT and DWT with (512 x 512) image size (a) single-level Haar RDWT with size 512x512 for each sub-band (b) single-level Haar DWT with size (256 x 256) for each sub-band.

RDWT has one more distinctive feature, which is the introduction of over-complete frame expansion, thereby making it more robust to noise than DWT (Jarholiya 2016). Figure 2.20 shows the RDWT analysis and synthesis filter bank, where $f(n)$ denotes the input image and $f'(n)$ denotes the retrieved image. $h[-k]$ and $g[-k]$ are low-pass and high-pass filters for analysis, respectively. $h[k]$ and $g[k]$ are corresponding synthesis filters. The output coefficients are symbolised by c_j and d_j at level j .

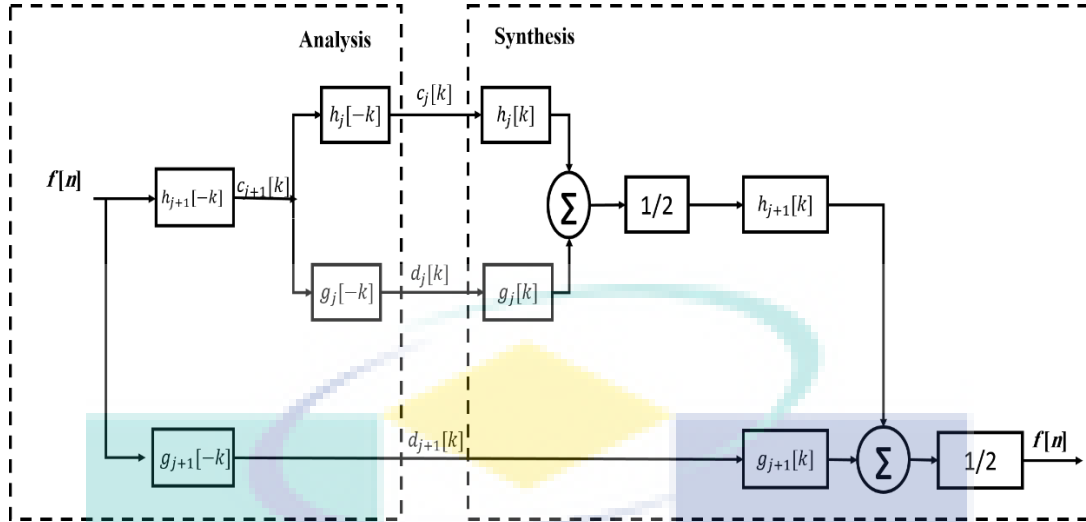


Figure 2.19 RDWT analysis and synthesis filter banks

Source : Hien et al. (2006)

Mathematically, RDWT analysis can be expressed as:

$$c_j [k] = (c_{j+1} [k] * h_j [-k]) \quad 2.31$$

$$d_j [k] = (d_{j+1} [k] * g_j [-k]) \quad 2.32$$

RDWT synthesis can be expressed a

$$c_{j+1} [k] = \frac{1}{2} (c_j [k] * h_j [k] + d_j [k] * g_j [k]) \quad 2.33$$

The redundancy of RDWT consumes more memory space. However, this increases the number of extracted features from the image.

The previous literature suggests that all LBP variants have inherited at least one or more of the limitations set out in Table 2.1. Therefore, this thesis will address the computational limitation and enhance the classification accuracy of the CLTP descriptor. These objectives will be achieved by introducing two descriptors: the WCLTP descriptor, which mainly aims to enhance the classification accuracy, and Feat-WCLTP, which is mainly proposed to overcome the computational limitation.

2.7 Datasets

To evaluate the effectiveness of the proposed work, two types of dataset were used, namely, texture dataset and medical dataset. These datasets are described in detail in section 2.7.1 and 2.7.2, respectively.

2.7.1 Texture Datasets

Four representative texture datasets were used, namely, CuReT(Dana et al. 1999), OuTeX (Ojala et al. 2002), UIUC (Lazebnik et al. 2005), and Kylberg (Kylberg 2011). These datasets are mostly used in recent research for assessment purposes. Using these datasets will help to compare the proposed descriptors with others to achieve a fair evaluation.

2.7.1.1 CuReT Dataset

The CuReT dataset contains 61 texture classes, and every class has 205 images obtained from several viewpoints and lighting directions (Dana et al. 1999). A total of 118 images are shot from a viewing angle of less than 60° . Of these 118 images, 92 images were selected, from which a sufficiently large region could be cropped ($200 * 200$) across all texture classes (Guo et al. 2010). A different number of images N ($N = 6, 12, 23, 46$) are selected randomly as training data from every class. Some images from the CuReT dataset are shown in Figure 2.21.

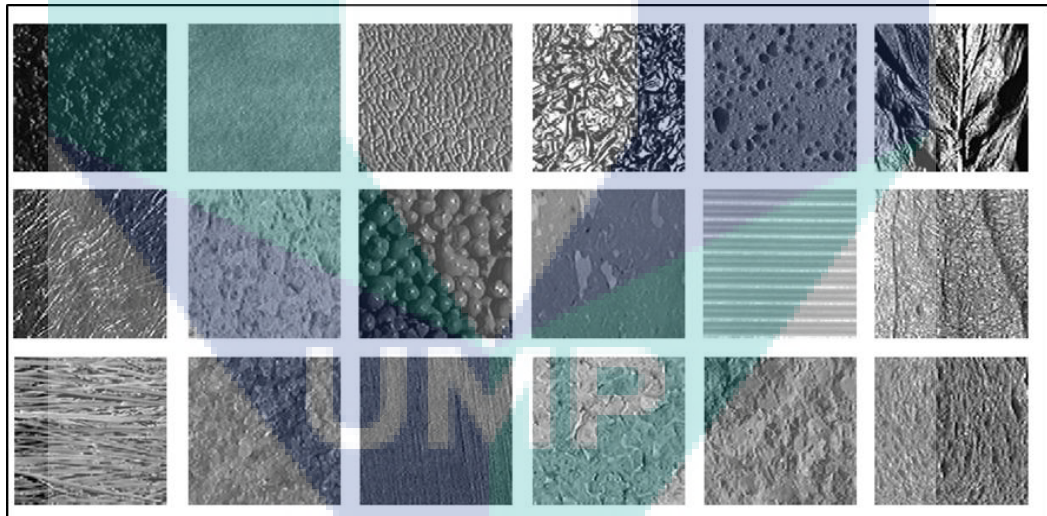


Figure 2.20 Some images from CuReT dataset

2.7.1.2 OuTeX Dataset

The OuTeX dataset family has 16 different suits. In these experiments, OuTeX-TC-0010 and OuTeX-TC-0012 were selected. Each of them has 24 classes of texture images taken under 3 illuminations ('inca') for TC-0010 and ('t184' and 'horizon') for TC-0012, and 9 rotation angles ($0^\circ, 5^\circ, 10^\circ, 15^\circ, 30^\circ, 45^\circ, 60^\circ, 75^\circ$ and 90°) (Ojala et al. 2002). Twenty 128×128 images are available for each rotation angle under a given

illumination condition. The 24×20 images of TC-0010 and rotation 0° were used for the training sample; the rest of the images at different rotations were adopted as the testing sample. The whole sample in TC-0012 taken under lighting ‘t184’ and ‘horizon’ was adopted as the testing sample. Some images from the OuTeX dataset are shown in Figure 2.22.

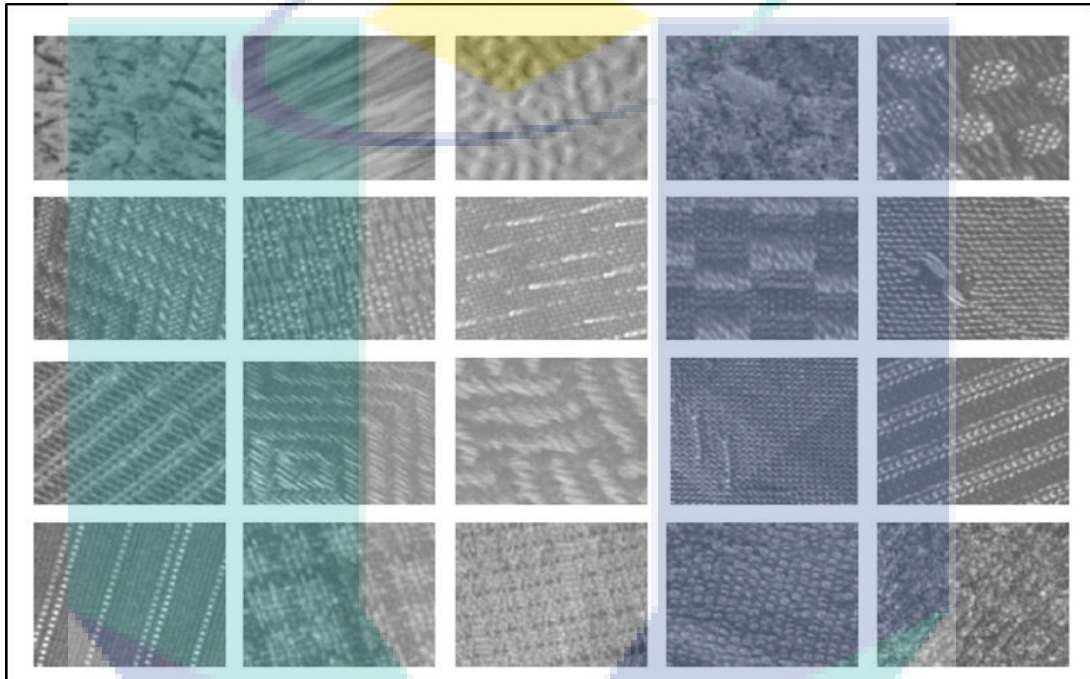


Figure 2.21 Some images from OuTeX dataset.

2.7.1.3 UIUC Dataset

The UIUC database includes 25 texture classes with 40 texture images in each class. The images were collected under different illuminations and viewpoint angles (Lazebnik et al. 2005). From each class, N number of images were selected randomly for training, while the remaining $40-N$ images were used for testing. The final classification accuracy is the average percentage of over 100 random splits. Figure 2.23 shows some sample images in the UIUC dataset.

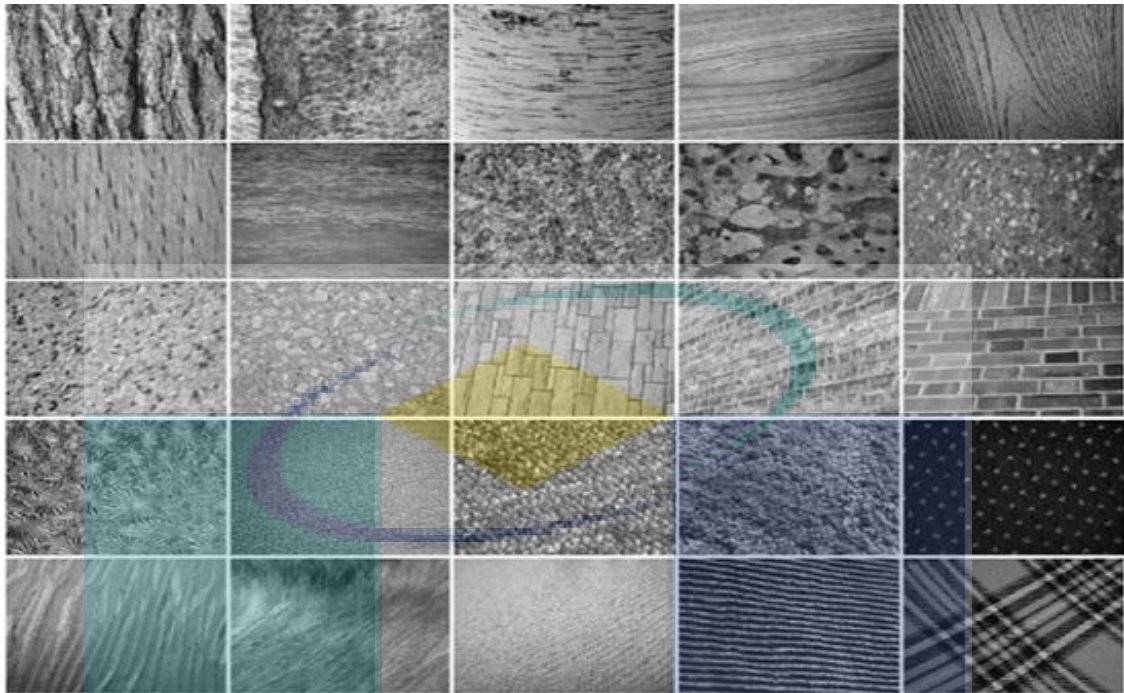


Figure 2.22 some sample images in UIUC database

2.7.1.4 Kylberg Dataset

Kylberg is a texture dataset that contains 28 texture classes of different natural and man-made surfaces, with each class consisting of 160 images (Kylberg 2011). The image size is 576×576 pixels and stored as greyscale 8-bit PNG images, as shown in Figure 2.24.

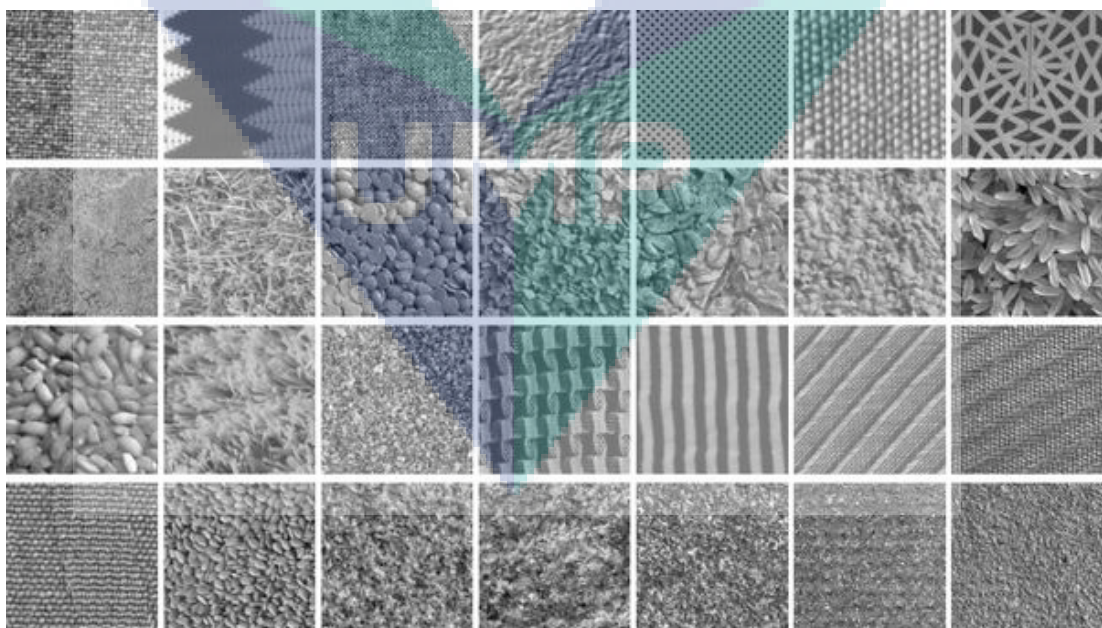


Figure 2.23 Some images from Kylberg dataset

2.7.2 Medical Datasets

To evaluate the performance of the proposed work, two medical datasets were used: 2D-HeLa database (Boland & Murphy 2001) and Breast Cancer dataset (Junior et al. 2009).

2.7.2.1 2D HeLa Dataset

The 2D-HeLa database contains 10 classes, namely, DNA, Actin, Endosomes, ER, Golgi GPP130, Golgia, Lysosomes, Microtubules, Nucleolus and Mitochondria (Boland & Murphy 2001). Each class has a different number of images; the highest number of images is 87. Four-fifths of images from every class were randomly chosen as training data, and the remaining 1/5 of images were adopted as testing data, similar to (Rassem et al. 2015). The final classification accuracy is the average percentage over 10 random splits. Figure 2.25 shows an example of a 2D HeLa image dataset.

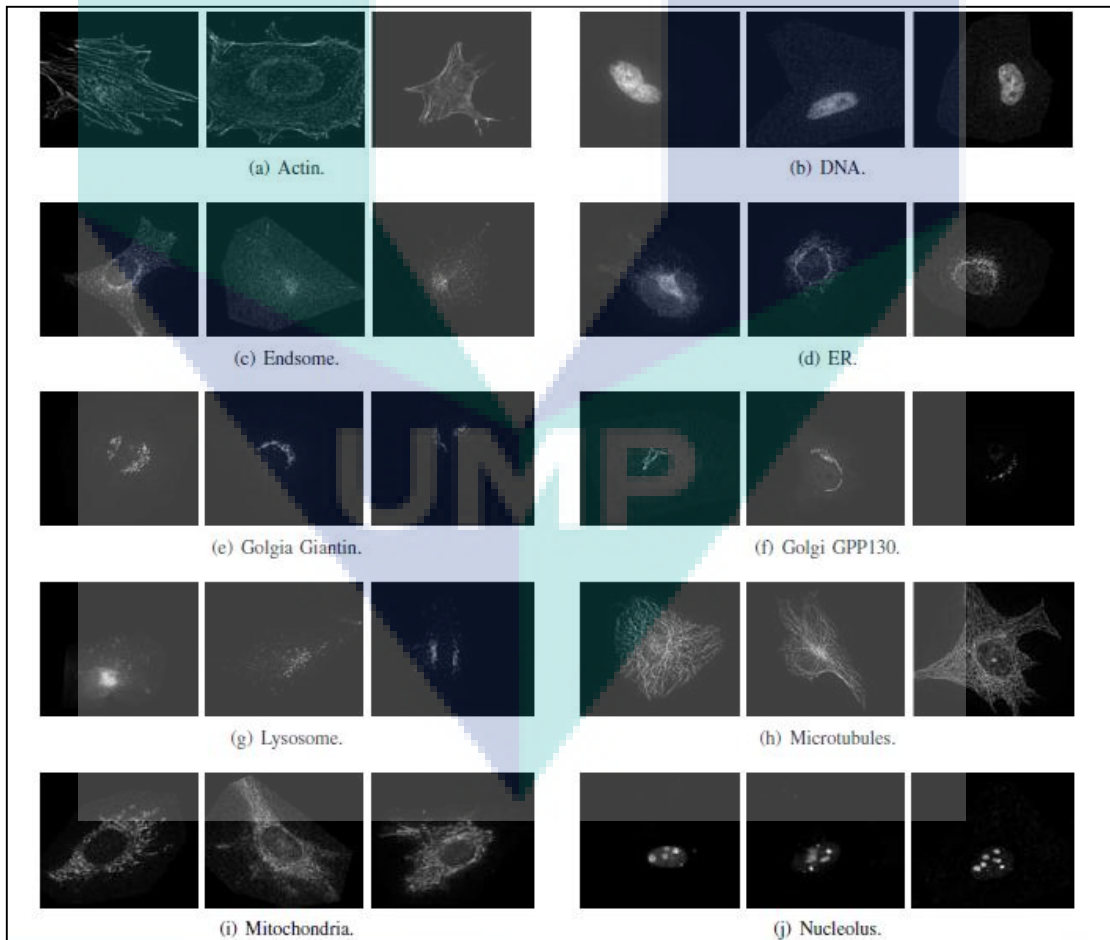


Figure 2.24 Images from 2D Hela dataset

2.7.2.2 Breast Cancer Dataset

The Breast Cancer dataset has three classes, namely, benign, control and malignant, and has a total of 1394 images (Junior et al. 2009). The setup of this dataset is the same as that of 2D-Hela where 4/5 of the images from every class were randomly chosen as training data, and the remaining 1/5 of images was adopted as testing data. The final classification accuracy is the average percentage over 10 random splits. Some examples of the Breast Cancer dataset images are shown in Figure 2.26.

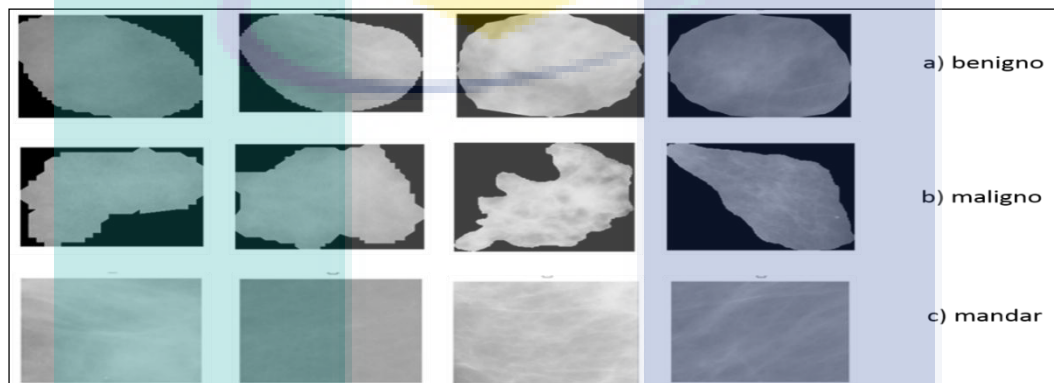


Figure 2.25 Image from BR Database

2.8 Summary

This chapter presented a review of texture analysis methods. Texture analysis consists of five general domains: classification, segmentation, synthesis, compression and the shape from texture. The general structure for texture classification is produced and the main steps for the classification process are discussed. Texture feature extraction is presented as it is an important step in texture classification. Texture feature extraction methods are classified into four groups: statistical, structural, model-based and signal processing-based. Furthermore, LBP was presented as one of the simplest and popular texture descriptors. Other well-known and popular texture descriptors (i.e. LBP, LTP, CLBP, CLBC, CLTP, NRLBP, RLBP, BRINT, DRLBP and FbLBP) were introduced. The main advantages and limitations of each descriptor were highlighted. CLTP is one of the most important LBP variants that was proposed to overcome the drawbacks of LBP. However, despite the impressive performance of CLTP, it suffers from some limitations, such as high dimensionality and the problem of selecting the threshold value. At the end, a brief introduction about WT was included. In addition, some information about benchmark datasets that used was presented.

CHAPTER 3

METHODOLOGY

3.1 Introduction

This chapter presents the research methodology used in this research. The following section illustrates the overall research methodology. The next section introduces the proposed descriptors, which include two main stages: Wavelet Completed Local Ternary Pattern (WCLTP) and Feature-based WCLTP (Feat-WCLTP). A summary is given in the last section.

3.2 Methodology of the Proposed Descriptors

The overall research methodology of this research is divided into three main stages: literature review, design and implementation, and the evaluation stage, which are summarised as follows:

The literature review phase involves identifying the texture descriptors applied to different real-world problems, i.e. medical, face and fingerprint. This phase shows that many texture descriptors were proposed in previous years, each one having different strengths and weaknesses. CLTP is one of these descriptors and was proposed in 2014 (Rassem & Khoo 2014). Although CLTP showed good performance, it still suffers from some limitations, which are summarised in Table 2.1.

The design and implementation stage involve overcoming the limitations of CLTP by proposing new texture descriptors inspired by CLTP for the image classification task. Firstly, a new descriptor called WCLTP is proposed by extracting CLTP after converting an image to transform domain. This conversion is performed because of the properties of the WT compared with the spatial domain. The original descriptor suffers from the high dimensionality problem; therefore, the WCLTP suffers from the same problem. To overcome this problem, further enhancement is proposed, which involves reducing the extracted features and combining the extracted features in a single vector, as will be explained in the coming sections.

Finally, the evaluation phase is performed, which consists of two main steps: assessing the new descriptor using different benchmark datasets, such as medical image and texture image databases, and discussing the final outcome. The performance of the new descriptors is compared with that of other descriptors especially CLBP, CLBC and the original CLTP. These stages are illustrated in Figure 3.1.

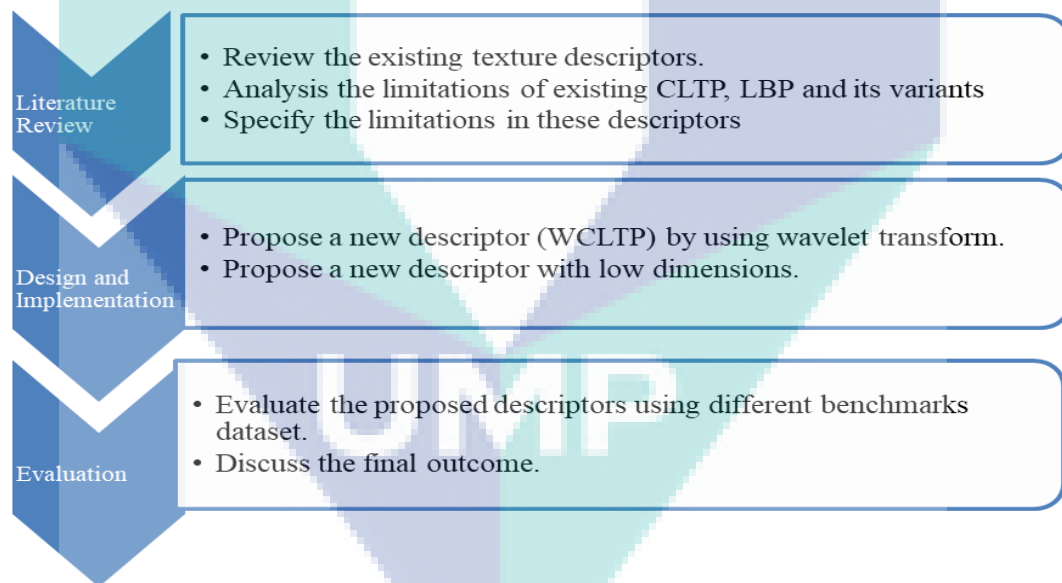


Figure 3.1 Illustration of the methodology

3.3 General proposed model

Generally, the texture classification aims to design an algorithm that can address a sample image to one of a set of known classes whose training examples have been provided. As mentioned in the literature, this process requires a set of steps:

preprocessing, feature extraction, feature selection and classification. Many researchers agree that the feature extraction step is the most important step (Liu et al. 2019) because the powerful extracted features play a crucial role in the final classification results. However, if the best classifier is fed by weak features, then it will fail to achieve good results (Liu et al. 2019). Therefore, given this work's focus on the feature extraction task, CLTP is selected as its backbone model. Accordingly, the performance of CLTP is improved in two ways: by introducing the WCLTP descriptor, which mainly aims to enhance the classification accuracy rate of CLTP, and by introducing the Feat-WCLTP descriptor to reduce the high dimensionality problem that was inherited from the original CLTP descriptor and causes high memory consumption. Figure 3.2 shows the general framework of the proposed method.

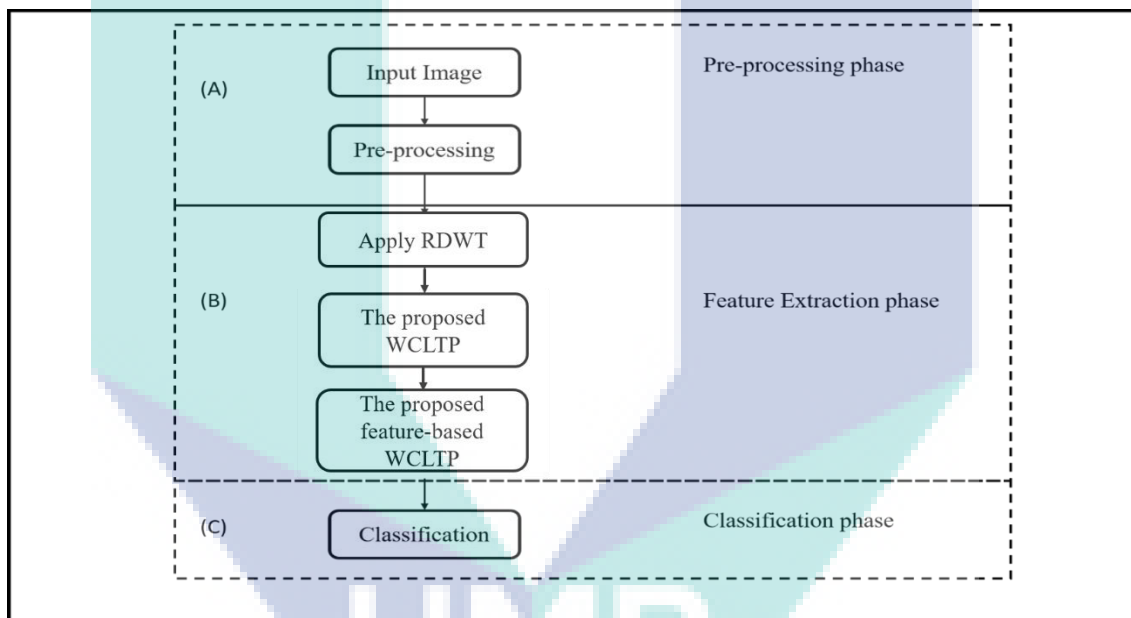


Figure 3.2 General Framework for the proposed work

As shown in Figure 3.2, the proposed work generally consists of three main phases, namely, (A) preprocessing, (B) feature extraction and (C) classification. The aim of preprocessing is to enhance the input image and present it in a way that can be measured consistently for strong classification. In this work, the preprocessing process is shortened by normalising the image, converting images to greyscale and resizing them. In phase (B), the feature extraction process is implemented to extract useful information from the preprocessed image. Thus, this phase will be implemented in two stages: Firstly, the WCLTP descriptor is proposed by integrating RDWT with CLTP to extract more useful features and improve the accuracy rate. Secondly, a feature-based descriptor is

proposed to reduce the size of the extracted features. In the classification phase, the extracted features are fed to a classifier to assign the image to one of the pre-defined classes. Different kinds of classifiers were introduced in the past. In this research, KNN is used because of its good performance with different texture descriptors and for a fair comparison with other descriptors. The following sections will introduce each proposed model in detail.

3.3.1 Wavelet Completed Local Ternary Pattern

The proposed WCLTP mainly aims to enhance the performance of CLTP and improve its classification accuracy. In image processing, the method of transforming the images from the spatial forms (pixel values) to the wavelet form has been used to enhance many applications due to the properties of WTs, such as the ability to analyse data at different scales and the low computational complexity (Irani Mehr et al. 2013).

RDWT transform is considered one of the robust WTs. It was proposed to overcome the limitations of DWT (Fowler 2005). The downsampling in DWT gains shift variance even for a slight shift in the input image, thereby leading to incorrect feature extraction. RDWT addresses the shift variance problem of DWT. It decomposes an image into four sub-bands, where the size of each sub-band equals the size of the original image unlike DWT where the sub-band size is only the half size of the original image. As a result, the important textures in the image will be at the same spatial location in each sub-band, thereby ensuring an accurate capture of the local texture and its exact measure.

The implementation steps of the proposed WCLTP are described as follows: Firstly, RDWT is applied to the preprocessed input image and decomposes the image into four sub-bands: LL, HL, LH and HH. LH, HL and HH represent the horizontal, vertical and diagonal detail, respectively. LL is approximate for the input image; thus, the power is more compact in the LL sub-band.

Therefore, the LL sub-band is selected. Then, CLTP_S, CLTP_M and CLTP_C are extracted from the LL sub-band. WCLTP_S, WCLTP_M and WCLTP_C are combined in different ways to evaluate the effectiveness of the WT. Figure 3.3 shows the WCLTP extraction process.

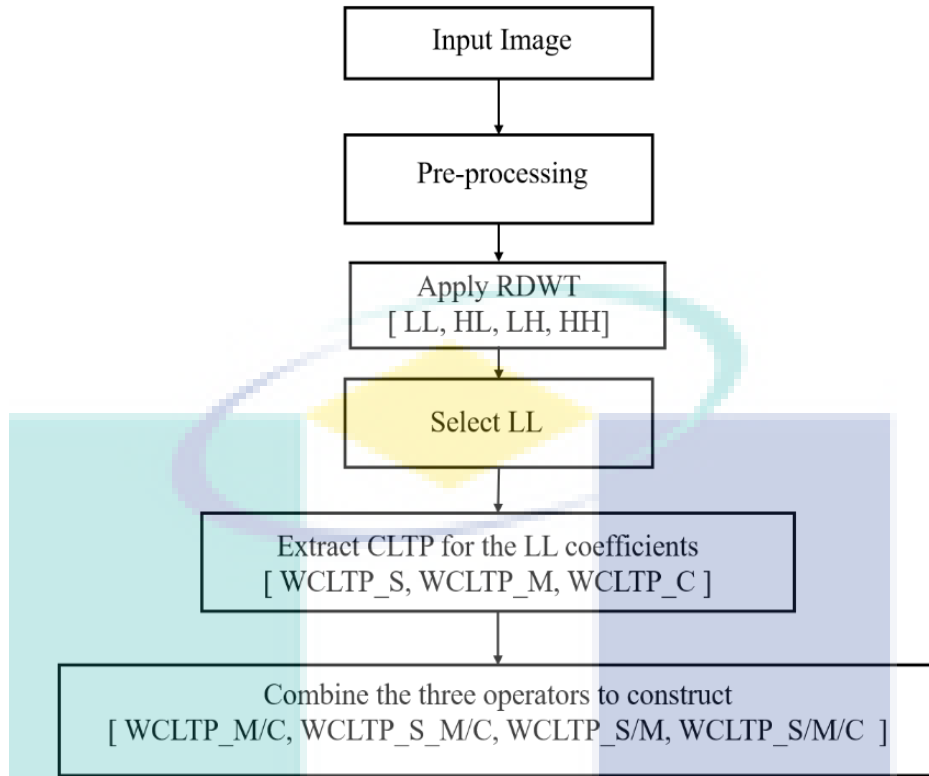


Figure 3.3 Flowchart of WCLTP extraction process

The WCLTP can be expressed mathematically as follows: Firstly, the upper and lower sign and magnitude components can be expressed as follows:

$$S_p^{\text{upper}} = s(i_p - (i_c + t)) \quad 3.1$$

$$S_p^{\text{lower}} = s(i_p - (i_c - t)) \quad 3.2$$

$$M_p^{\text{upper}} = |i_p - (i_c + t)| \quad 3.3$$

$$M_p^{\text{lower}} = |i_p - (i_c - t)| \quad 3.4$$

Then the sign components are used to build the $WCLTP_{P,R}^{\text{upper}}$ and $WCLTP_{P,R}^{\text{lower}}$, as follows:

$$\begin{aligned}
 WCLTP_{P,R}^{\text{upper}} &= \sum_{p=0}^{P-1} 2^p s(i_p - (i_c + t)), S_p^{\text{upper}} \\
 &= \begin{cases} 1, & i_p \geq i_c + t, \\ 0, & \text{otherwise,} \end{cases}
 \end{aligned} \quad 3.5$$

$$WCLTP_{P,R}^{lower} = \sum_{p=0}^{P-1} 2^{ps}(i_p - (i_c - t)), S_p^{lower} = \begin{cases} 1, & i_p < i_c - t, \\ 0, & \text{otherwise,} \end{cases} \quad 3.6$$

where i_c , i_p , R and P are as described previously in Equation (2.1), while t is the threshold value. The two operators are then concatenated to form $WCLTP_{S_{P,R}}$ as in Equation (3.7). Figure 3.4 illustrates an example of the $WCLTP_{S_{P,R}}$ calculation process.

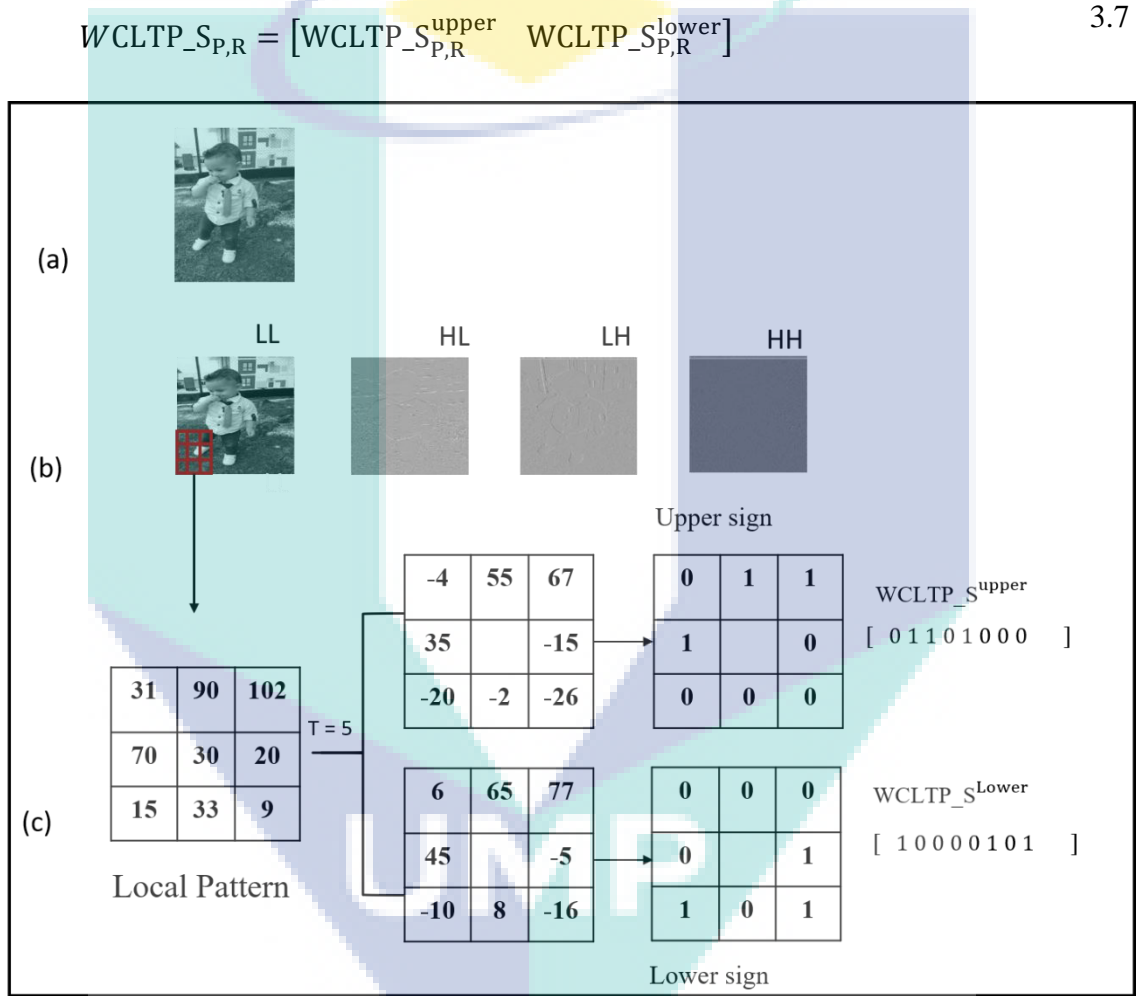


Figure 3.4 Example of WCLTP sign extraction process

As shown in Figure 3.4 (a) is the input grey-level image. In (b), RDWT is applied to the input image and decomposes the image into four sub-bands, where the LL sub-band is selected. (c) shows how the sign is calculated, where the local difference vector is firstly calculated according to Equations (3.1) and (3.2). Equations (3.5) and (3.6) are utilised to

calculate the upper and lower WCLTP_S, respectively. The histogram size for the WCLTP_S is $(P+2) * 2$ bins.

Similar to WCLTP_S_{P,R}, the WCLTP_M_{P,R} is built using the two magnitude complementary components m_p^{upper} and m_p^{lower} as follows:

$$WCLTP_M_{P,R}^{upper} = \sum_{p=0}^{P-1} 2^p t(m_p^{upper}, c), t(m_p^{upper}, c) \quad 3.8$$

$$= \begin{cases} 1, & |i_p - (i_c + t)| \geq c, \\ 0, & |i_p - (i_c + t)| < c, \end{cases} \quad 3.9$$

$$WCLTP_M_{P,R}^{lower} = \sum_{p=0}^{P-1} 2^p t(m_p^{lower}, c), t(m_p^{lower}, c)$$

$$= \begin{cases} 1, & |i_p - (i_c - t)| \geq c, \\ 0, & |i_p - (i_c - t)| < c, \end{cases}$$

$$WCLTP_M_{P,R} = [WCLTP_M_{P,R}^{upper} \quad WCLTP_M_{P,R}^{lower}] \quad 3.10$$

where i_c, i_p, P, R and c are defined in Equations (2.1) and (2.5). Figure 3.5 shows an example of the calculation process to construct the WCLTP_M_{P,R}

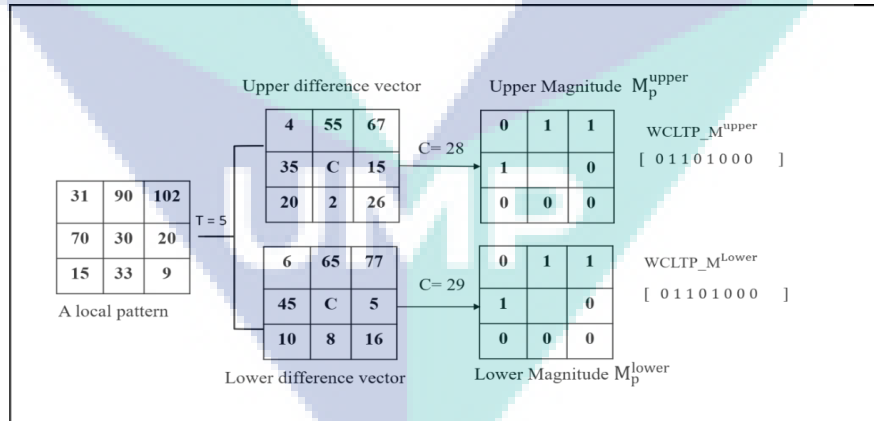


Figure 3.5 Example of WCLTP magnitude extraction process

As seen in Figure 3.5, the local difference is calculated while ignoring the sign by using Equations (3.3) and (3.4). Then, the neighbouring pixels are thresholded according to the C value, where C can be defined as the mean value of all m_p in the whole image. Equations (3.8) and (3.9) are used to build the upper- and lower-magnitude operators for the proposed WCLTP. The histogram size for the WCLTP_M is $(P+2) * 2$ bins.

Similar to the above process, $WCLTP_{C_{P,R}}^{upper}$ and $WCLTP_{C_{P,R}}^{lower}$ can be mathematically expressed as follows:

$$WCLTP_{C_{P,R}}^{upper} = t(i_c^{upper}, C_I) \quad 3.11$$

$$WCLTP_{C_{P,R}}^{lower} = t(i_c^{lower}, C_I) \quad 3.12$$

$$WCLTP_{C_{P,R}} = [WCLTP_{C_{P,R}}^{upper} \quad WCLTP_{C_{P,R}}^{lower}] \quad 3.13$$

where $i_c^{upper} = i_c + t$, $i_c^{lower} = i_c - t$ and C_I is the average grey level of the whole image. The histogram size for the $WCLTP_C$ is $2*2$ bins.

The proposed $WCLTP_S$, $WCLTP_M$ and $WCLTP_C$ operators are combined into joint or hybrid distributions to build the final operator histogram similar to CLTP. The operators of the same type of pattern, i.e. the upper and the lower pattern, are combined firstly into joint or hybrid distributions. Then their results are concatenated to build the final operator histogram that has a size of $((P+2)*(P+2)*2)/2$, which is considered relatively high dimensionality.

3.3.2 Feature-based WCLTP

The proposed WCLTP was evaluated in this work through a set of experiments that will be discussed in detail in the next chapter. The results show the effectiveness of the enhanced model in improving the performance of CLTP. However, the size of the resultant histogram is too large. This problem is inherited from the original CLTP. The high dimensionality negatively affected the performance of the descriptor and increased the running time. Moreover, high dimensionality needs large storage space. In addition, the classification process will be slow. In this section, the objective is to overcome the high dimensionality problem and maintain the improved performance.

In their major study, (Guo et al. 2010) confirmed by analysis that the sign vector of local difference possesses more information than the magnitude vector. This situation explains why texture classification using the sign operator achieves much higher accuracy than that achieved by the magnitude operator. On the basis of this finding, a new descriptor is proposed to overcome the high dimensionality problem by modifying the structure of the magnitude operator and reducing the number of extracted features.

Similar to the first model structure, the proposed Feat-WCLTP is constructed using three operators: sign, magnitude and centre operators. The Feat-WCLTP_S is equal to WCLTP_S and calculated using the same Equations (3.5), (3.6) and (3.7) to retain the powerful features of the sign component. Figure 3.6 illustrates the Feat-WCLTP extraction process.

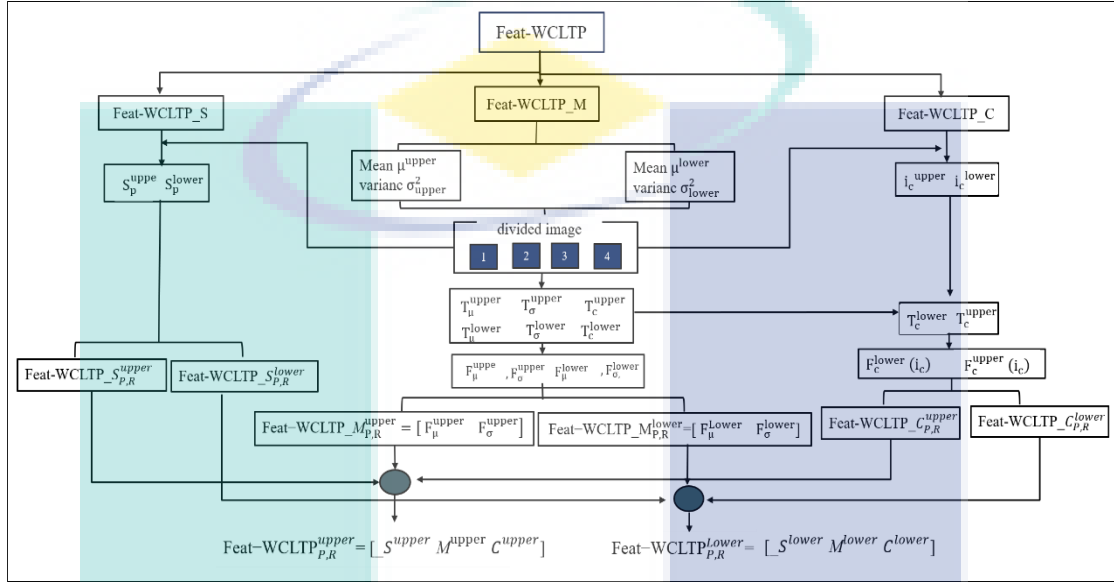


Figure 3.6 Feat-WCLTP extraction process.

As mentioned above, the proposed descriptor aims to solve the dimensionality problem without affecting the classification accuracy. Thus, the focus is to reduce the dimensionality of the magnitude vector. Accordingly, the feature-based is used to reduce the number of features generated from the magnitude from P -dimensional features to only two-dimensional features, which are the mean and variance of the magnitude vector. The mean feature μ indicates the average difference between the centre pixel and its neighbours, while the variance σ^2 indicates the total changes in the magnitude vector m_p . Mathematically, the Feat-WCLTP_M is computed by calculating the mean and the variance of the magnitude vector m_p by using the following equations:

$$\mu^{\text{upper}} = \frac{1}{P} \sum_{p=0}^{P-1} m_p^{\text{upper}} \quad 3.14$$

$$\mu^{\text{lower}} = \frac{1}{P} \sum_{p=0}^{P-1} m_p^{\text{lower}} \quad 3.15$$

$$\sigma_{\text{upper}}^2 = \frac{1}{P} \sum_{p=0}^{P-1} (m_p^{\text{upper}} - \mu^{\text{upper}})^2 \quad 3.16$$

$$\sigma_{\text{lower}}^2 = \frac{1}{P} \sum_{p=0}^{P-1} (m_p^{\text{lower}} - \mu^{\text{lower}})^2 \quad 3.17$$

where P is the number of neighbouring pixels. The mean and variance are the average values of all P elements in the magnitude vector. Thus, using these features can diminish the impact of noise, rotation and illumination. Moreover, when using these two features, all non-uniform patterns do not need to be integrated into a single bin as in CLBP_M and CLTP_M, which means better complementary information will be provided to the sign component. This approach will positively reflect on the descriptor performance.

However, the mean and variance values are needed to encode because they are continuous values, which means they cannot be used directly in the classification process. Thus, to convert them to discrete values, an adaptive threshold method is used. In this method, the input image is divided into four equal non-overlapping sub-images. Then, a threshold value for each mean and variance in each sub-image is calculated as follows:

The threshold values for the mean are:

$$T_{\mu}^{\text{upper}} = \frac{1}{N} \sum_{n=1}^N \mu^{\text{upper}} \quad 3.18$$

$$T_{\mu}^{\text{lower}} = \frac{1}{N} \sum_{n=1}^N \mu^{\text{lower}} \quad 3.19$$

where N is the number of local patterns in each sub-image. The following equations are used to determine the threshold values for upper and lower variances.

$$T_{\sigma}^{\text{upper}} = \frac{1}{N} \sum_{n=1}^N \sigma_{\text{upper}}^2 \quad 3.20$$

$$T_{\sigma}^{\text{lower}} = \frac{1}{N} \sum_{n=1}^N \sigma_{\text{lower}}^2 \quad 3.21$$

Using this threshold method helps properly exploit the relationships between pixels.

The upper and lower mean and variance features are converted to binary format by using the following equations:

$$F_{\mu}^{\text{upper}}(i_c) = s(\mu^{\text{upper}} - T_{\mu}^{\text{upper}}) \quad 3.22$$

$$F_{\mu}^{\text{lower}}(i_c) = s(\mu^{\text{lower}} - T_{\mu}^{\text{lower}}) \quad 3.23$$

$$F_{\sigma}^{\text{upper}}(i_c) = s(\sigma_{\text{upper}}^2 - T_{\sigma}^{\text{upper}}) \quad 3.24$$

$$F_{\sigma}^{\text{lower}}(i_c) = s(\sigma_{\text{lower}}^2 - T_{\sigma}^{\text{lower}}) \quad 3.25$$

where i_c is the centre pixel. In Equations (3.22 to 3.25), $s(x)$ is the same as defined in Equation (2.1).

The upper and lower features used to build the final (Feat-WCLTP_M) as follows:

$$\text{Feat-WCLTP_M}_{P,R}^{\text{upper}} = [F_{\mu}^{\text{upper}} \quad F_{\sigma}^{\text{upper}}] \quad 3.26$$

$$\text{Feat-WCLTP_M}_{P,R}^{\text{lower}} = [F_{\mu}^{\text{lower}} \quad F_{\sigma}^{\text{lower}}] \quad 3.27$$

$$\begin{aligned} \text{Feat - WCLTP_M}_{P,R} \\ = [\text{Feat - WCLTP_M}_{P,R}^{\text{upper}} \quad \text{Feat - WCLTP_M}_{P,R}^{\text{lower}}] \end{aligned} \quad 3.28$$

This process can be explained using an example, as shown in Figure 3.7.

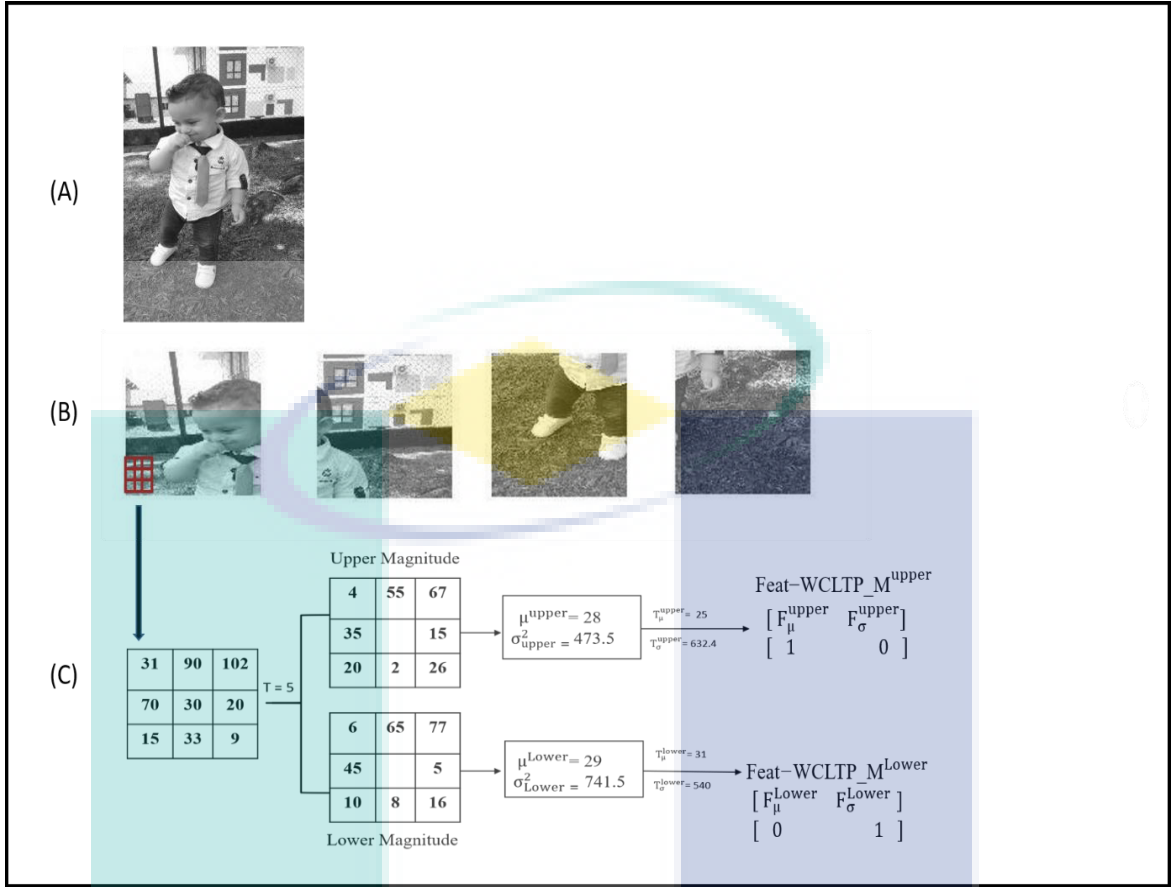


Figure 3.6 Example of the calculation process for magnitude component for Feat-WCLTP

Referring to Figure 3.7, A is the input image, which is the LL sub-band image that resulted from applying RDWT in the first model. B is the set of 2*2 sub-images. C is the calculation process where the local difference is computed according to Equations (3.3) and (3.4). Then, the mean and variance are calculated according to Equations (3.14) to (3.17). For each sub-image in B, the average of the means and variances is computed and used as a threshold value to encode the mean and variance features. Thus, the resultant Feat-WCLTP_M becomes a binary number with a histogram size of (2*2)*2 pins.

The next step is to compute the Feat-WCLTP_C. To extract more discriminative information from the centre pixel, it is encoded in the same way as the mean and variance. The threshold value for the centre pixel is the average grey values of the current sub-image they calculated as in Equation (3.29) and Equation (3.30).

$$T_c^{\text{upper}} = \frac{1}{N} \sum_{n=1}^N i_c^{\text{upper}} \quad 3.29$$

$$T_c^{\text{lower}} = \frac{1}{N} \sum_{n=1}^N i_c^{\text{lower}} \quad 3.30$$

where i_c^{upper} and i_c^{lower} are the centre pixels with adding and subtracting the threshold value, respectively. To construct the centre operator *Feat - WCLTP_C*, the following equations are used:

$$F_c^{\text{upper}}(i_c) = s(i_c^{\text{upper}} - T_c^{\text{upper}}) \quad 3.30$$

$$F_c^{\text{lower}}(i_c) = s(i_c^{\text{lower}} - T_c^{\text{lower}}) \quad 3.31$$

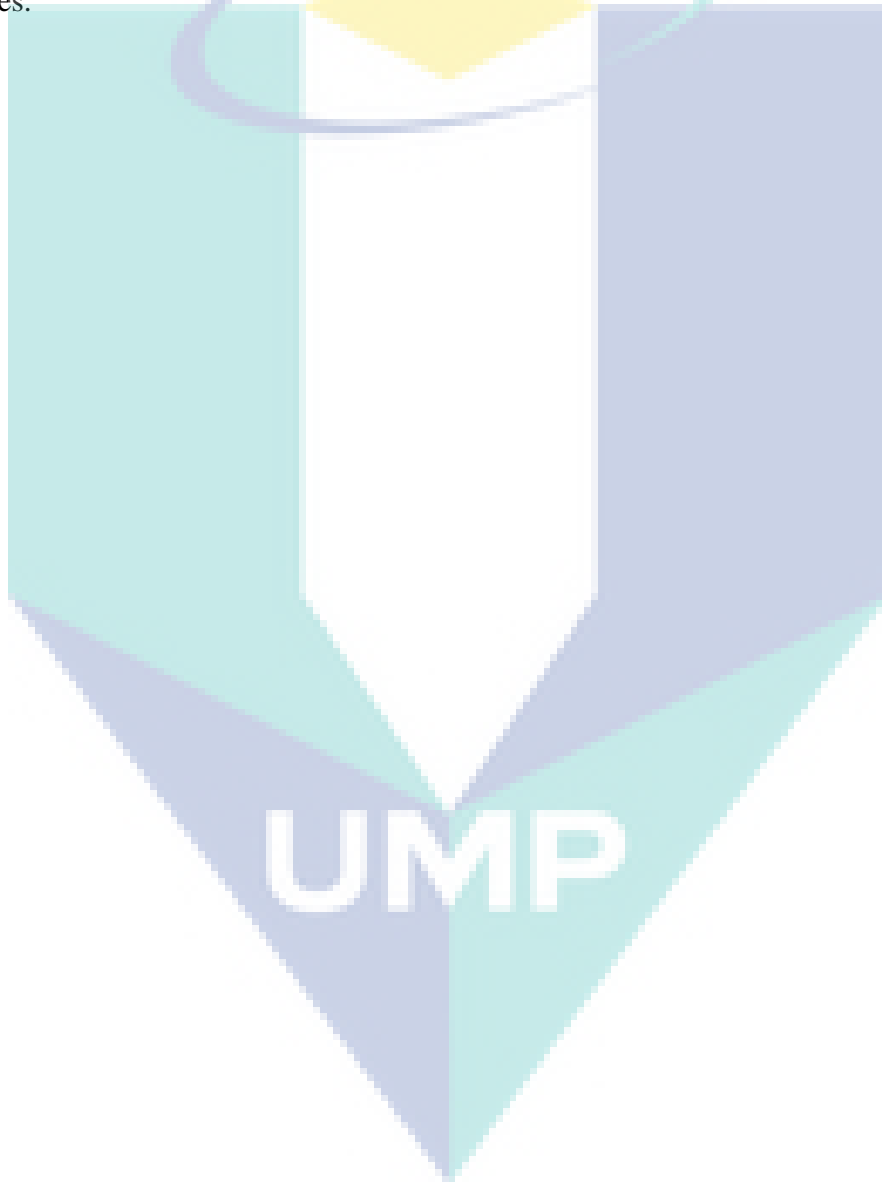
$$\text{Feat - WCLTP_C} = [F_c^{\text{upper}}(i_c) \quad F_c^{\text{lower}}(i_c)] \quad 3.32$$

where i_c is the centre pixel. After computing all features from *Feat-WCLTP_C*, *Feat-WCLTP_M* and *Feat-WCLTP_S*, the three operators are integrated into joint or hybrid distributions to build the final histogram as *WCLTP*. At first, the *Feat-WCLTP_S* and *Feat-WCLTP_M* could be combined in two ways: concatenation or jointly. In concatenation, the histograms of the *Feat-WCLTP_S* and *Feat-WCLTP_M* codes are calculated separately and then concatenated together, thereby constructing the *Feat-WCLTP_S_M*. In the joint approach, a joint 2D histogram of the *Feat-WCLTP_S* and *Feat-WCLTP_M* codes is calculated to construct the *Feat-WCLTP_S/M*. The three operators *Feat-WCLTP_S*, *Feat-WCLTP_M* and *Feat-WCLTP_C* could also be combined in two ways: jointly or hybrid. In the joint method, a 3D joint histogram is built, which is represented as *Feat-WCLTP_S/M/C*. In the hybrid approach, a 2D joint histogram *Feat-WCLTP_S/C* or *Feat-WCLTP_M/C* is built firstly, and then the histogram is converted to a 1D histogram, which is then concatenated with *Feat-WCLTP_M* or *Feat-WCLTP_S* to generate a joint histogram, denoted by *Feat-WCLTP_M_S/C* or *Feat-WCLTP_S_M/C*.

3.3.3 Summary

In this chapter, the general methodology for this research was presented. The methodology consists of three stages: literature review, design and implementation, and

evaluation. Two main contributions were introduced based on the problems in CLTP. The first one is the enhanced performance classification of CLTP through integration with RDWT and proposed WCLTP. The second is the solution to the high dimensionality problem by using feature-based technique and the proposed Feat-WCLTP. The proposed Feat-WCLTP can enhance CLTP's performance and reduce the high dimensionality. The magnitude operator in Feat-WCLTP is described using two features instead of the features of all neighbouring pixels. An adaptive threshold function is used to encode these features.



CHAPTER 4

RESULTS AND DISCUSSION

4.1 Introduction

This chapter presents a series of experiments that are performed to evaluate the effectiveness of the proposed work. The first section gives details about the experimental setup used in the evaluation process. Next, the efficacy of the proposed WCLTP descriptor is evaluated by conducting three sets of experiments: (i) evaluating its robustness against noise, (ii) evaluating the classification accuracy for texture image classification and (iii) evaluating the classification accuracy for medical image classification. The third section presents the experimental results of evaluating the proposed Feat-WCLTP where three sets of experiments are conducted: (i) evaluating the classification accuracy of Feat-WCLTP for texture image classification, (ii) evaluating the classification accuracy of Feat-WCLTP for medical image classification and (iii) evaluating the computation time of Feat-WCLTP. All results are compared with those of other well-known descriptors in the literature. Towards the end, a summary is included.

4.2 Experimental setup

In all experiments, the evaluation process depends on the classification accuracy measure because it is the most commonly used to evaluate the descriptor performance. This measurement can evaluate the overall efficiency of a descriptor. To estimate the validity of the results, a confusion matrix was used. In addition, four representative

texture datasets and two medical texture datasets were used in the experiments. The k-fold cross-validation method was used to estimate the generalisation error of the proposed models. The dataset is separated into two sets in which k-1 functions are for the training set and the Kth set is utilised for testing.

4.2.1 Datasets

All the experiments in this research were conducted using six publicly available benchmark datasets that were mostly used in recent research for assessment purposes. Thus, using these datasets helps compare the proposed descriptors with others for a fair evaluation. A detailed description of the datasets was provided in Section 2.8. Table 4.1 summarises the main characteristics of the datasets.

Table 4.1 The benchmark datasets used in the experiments

Data Type	Number	Dataset	Classes	Sample per class	Total
Texture datasets	1	OuTex TC-10	24	20	4320
	2	OuTex TC-12	24	20	8640
	3	CUReT	61	46	5612
	4	UIUC	25	40	1000
Medical datasets	1	Kylberg	28	160	4480
	2	2D HeLa	10	87	862
		Breast Cancer	3	Unfixed	1394

4.2.2 Confusion Matrix

As mentioned before, the evaluation process depends on the classification accuracy in all experiments. Thus, in this section, the confusion matrix was used to find the classification accuracy. In the confusion matrix, numbers of correctly and incorrectly classified cases exist for each class. Table 4.2 shows an example of the confusion matrix.

Table 4.2 Confusion Matrix

Predicted Class	Class	Actual Class	
		True	False
Class	True	True Positive (TP)	False Positive (FP)
	False	False Negative (FN)	True Negative (TN)

According to Table 4.2; True Positive (TP), False Positive (FP), True Negative (TN), False Negative (FN) are defined as follows:

True Positive (TP): the number of positive cases that were correctly identified.

False Positive (FP): the number of negative cases that were incorrectly classified as positive.

True Negative (TN): the number of negative cases that were classified correctly.

False Negative (FN): the number of positive cases that were incorrectly classified as negative.

Equation (4.1) and Equation (4.2) are used to calculate classification accuracy and classification error

$$\text{classification accuracy} = \frac{TP+TN}{TP+TN+FP+FN} \quad 4.1$$

$$\text{classification error} = \frac{FP+FN}{TP+TN+FP+FN} \quad 4.2$$

4.2.3 Cross-Validation

K-fold cross validation is used to evaluate classifier performance. In this method, the data is randomly divided into k mutually exclusive sets, where k = 3, k = 5 and k = 10 denote 3-fold, 5-fold and 10-fold cross-validation, respectively. In this process, the data are divided into two parts several times. Each time, one part is used as training data while the other part is used as testing. Then, the average error across all k trails is computed. In this research, a 100-round 5-fold cross validation is applied to compute the average results to ensure that each class properly appears in both training and testing sets.

4.2.4 Classifier

The final step in the classification process is feeding the extracted texture features to a classifier. The classifier will assign an unknown sample image to a known class. Numerous classifiers are used in texture classification. Selecting an appropriate classifier will have a good effect on classification results. In this study, the k-NN classifier is used

for classification because it reported a good classification result. In addition, it is widely used in most common descriptors, which helps in conducting a fair comparison.

4.2.5 Dissimilarity measurement

To measure the dissimilarity between two histograms, chi-square statistic is used, which is given as follows:

$$\text{Dissimilarity}_{x^2}(H, K) = \sum_{i=1}^B \frac{(h_i - k_i)^2}{h_i + k_i} \quad 4.3$$

where the x^2 is the distance between two histograms $H=h_i$ and $K= k_i$, where ($i=1,2,3,\dots,B$).

4.3 Performance Evaluation for the Proposed WCLTP

As being explained in Chapter 3, the WCLTP was proposed to enhance the classification accuracy of CLTP. Thus, to evaluate and examine the effectiveness of the WCLTP, three sets of experiments were conducted. The first set examined the robustness of WCLTP against noise by using a noisy dataset. The second set evaluated the performance of the proposed WCLTP for texture image classification. The third set evaluated the performance of the proposed WCLTP for medical image classification. Where possible, the results of all experiments were compared with those of other approaches in the literature.

4.3.1 Robustness of WCLTP Against Noise

The robustness of any texture descriptor toward a noisy image reflects the effectiveness of this descriptor and its ability to succeed in a real-life application. Thus, implementing any texture descriptor under idealised situations only is almost guaranteed to be ineffective in a real-world environment. Therefore, in this section, a challenging noisy dataset is utilised to evaluate the performance of WCLTP and compare it with that of some well-known descriptors. The CURET dataset is selected for this task because it has the largest number of classes among all selected datasets, thereby ensuring diverse image types. Figure 4.1 illustrates an example of noisy image.

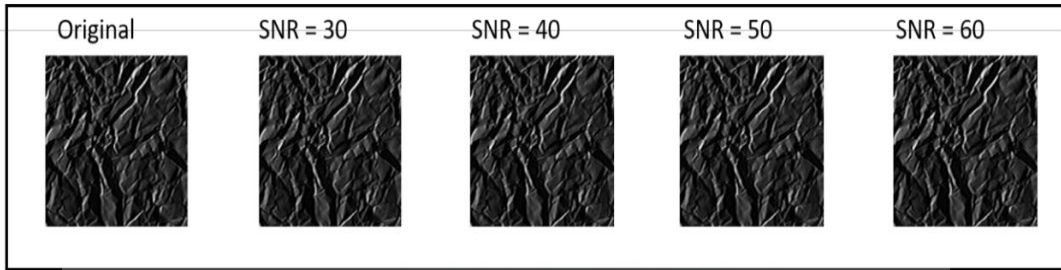


Figure 4.1 Examples of the images with the noise.

In these experiments, to follow the same experimental procedures as in (Sree & Rao 2017), all the CURET dataset images are corrupted by additive Gaussian noise with specific signal-to-noise ratio (SNR) values (SNR = 60, 50, 40 and 30). For each class, 46 images are randomly selected as training images. The range of variability and classification rate on average is noted by implementing the procedure 100 times for each SNR value. A varying value of radius ($R = 1, 2, 3$) and neighbouring pixels ($P = 8, 16, 24$) is used. The experimental results of a noisy CURET dataset for different pattern sizes are shown in Figures 4.2, 4.3 and 4.4.

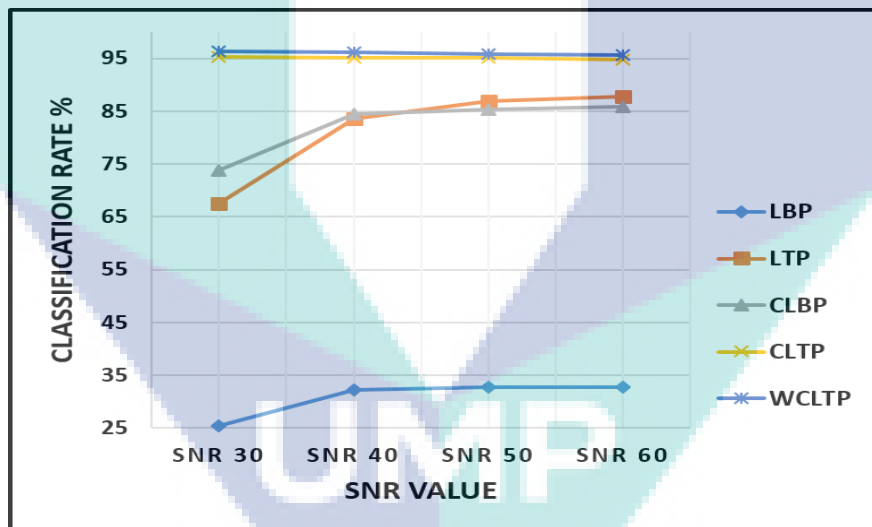


Figure 4.2 Classification rates on the noisy CURET dataset with different SNR values for pattern size ($R=1, P=8$)

From Figure 4.2, LBP is evidently the most sensitive to the noise descriptor, where its classification accuracy does not exceed 34% even with a high SNR value, while CLTP is more robust to noise and maintains its classification results around 95% at different SNR values. As can be observed, the proposed WCLTP obtained the best classification result and performed stably for noisy images of different SNR values.

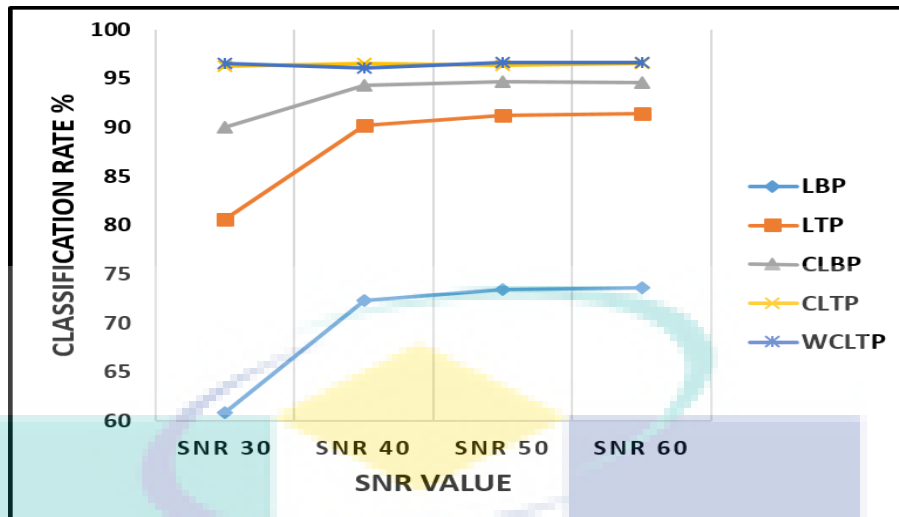


Figure 4.3 Classification rates on the noisy CURET dataset with different SNR values for pattern size (R=2, P=16).

In Figure 4.3, LBP with (R = 2, P = 16) shows more robustness to noise than LBP with (R = 1, P = 8). However, it still has the worst result among all the LBP variants. CLTP and WCLTP still performed well under different noise levels (above 95% accuracy). Even so, WCLTP is still the best.

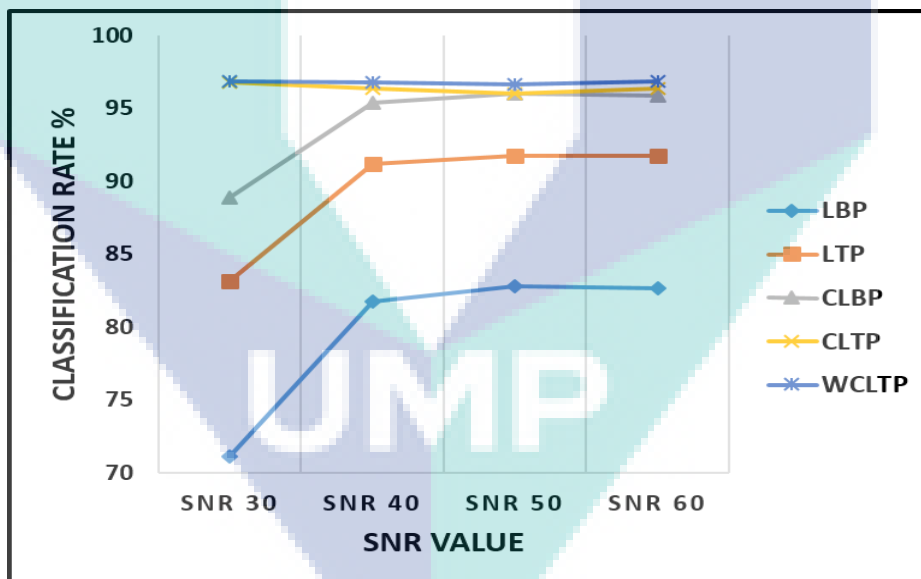


Figure 4.4 classification accuracy of noisy CURET dataset when (R=3, P=24)

Figure 4.4 shows that the proposed WCLTP is more robust to noise than LBP, LTP, CLBP and CLTP at different SNR values with texture pattern (R = 3 and P = 24). While LBP still had poor performance, WCLTP and CLTP maintained their performance at different SNR values. The performance of LBP, LTP and CLBP dropped suddenly when SNR decreased to 30. This drop ranges from about 10% for LBP and to less than

7% for CLBP. All the results confirmed that the proposed WCLTP is more robust to noise than other LBP variants, and its performance was not affected in all noise levels.

4.3.2 Experimental Results of WCLTP for Texture Image Classification.

In these experiments, four representative texture datasets were used. The proposed WCLTP and several texture descriptors, i.e. LBP, LTP, CLBP, CLBC, and CLTP, were compared in terms of accuracy.

4.3.2.1 Experimental Results on the OuTex Dataset

For experiments on the two suites (TC10) and (TC12), which are considered the two most well-known test suites in OuTex, were selected. Each of (TC10) and (TC12) has 24 texture classes captured under nine different rotation angles (0° , 5° , 10° , 15° , 30° , 45° , 60° , 75° and 90°) and three uneven type of illumination source ('horizon', 'inca' and 't184'). Twenty 128×128 non-overlapping images are available for each rotation angle under a given illumination condition. For TC10, 480 images with 'inca' illumination condition and 0° angle rotation were used as training set whereas the remaining 3840 images are used as testing set. For TC12 the training set is same to that of TC10 while 4320 images under 't184' or 'horizon' illumination conditions were used as testing set. The experimental results of OuTex dataset are presented in Table 4.3.

Table 4.3 Classification rates (%) on the OuTex dataset

Method	Parameters (R,P) . R =the radius of the circle, P =the number of											
	R =1, P = 8				R =2 , P = 16				R =3 , P = 24			
	TC10		TC12		TC10		TC12		TC12		TC10	
	t	h	Avg	t	h	Avg	t	h	Avg	t	h	Avg
LBP	84.81	65.46	63.68	71.32	89.40	82.27	75.21	82.29	95.08	85.05	80.79	86.97
LTP	94.14	75.88	73.96	81.33	96.95	90.16	86.94	91.35	98.2	93.59	89.42	93.74
CLBP_S	84.41	65.46	63.68	71.18	89.40	82.26	75.20	82.29	95.07	85.04	80.78	86.96
CLBC_S	82.94	65.02	63.17	70.38	88.67	82.57	77.41	82.88	91.35	83.82	82.75	85.97
CLTP_S	94.14	75.88	73.96	81.33	96.95	90.16	86.94	91.35	98.20	93.59	89.42	93.74
WCLTP_S	92.97	83.56	80.00	85.51	94.97	92.04	86.81	91.27	97.89	93.87	90.51	94.09
CLBP_M	81.74	59.30	62.77	67.94	93.67	73.79	72.40	79.95	95.52	81.18	78.65	85.12
CLBC_M	78.96	53.63	58.01	63.53	92.45	70.35	72.64	78.48	91.85	75.59	74.58	80.67
CLTP_M	94.04	75.86	74.05	81.32	97.32	83.40	84.40	88.37	98.00	85.39	84.65	89.35
WCLTP_M	94.51	77.36	77.71	83.19	97.11	82.71	86.53	88.78	97.89	83.54	84.42	88.62
CLBP_M/C	90.36	72.38	76.66	79.80	97.44	86.94	90.97	91.78	98.02	90.74	90.69	93.15

Table 4.3 Continued

Method	R =1, P = 8			R =2, P = 16			R =3, P = 24					
	TC10		TC12	TC10		TC12	TC10		TC12			
	t	h	Avg.	t	h	Avg.	t	h	Avg.			
CLTP_M/C	95.94	84.70	86.02	88.89	97.94	90.14	92.38	93.49	98.52	91.23	89.98	93.24
WCLTP_M/C	95.86	85.56	87.59	89.67	97.99	91.46	93.43	94.29	98.44	92.29	93.08	94.60
CLBP_S_M/C	94.53	81.88	82.52	86.31	98.02	90.99	91.08	93.36	98.33	94.05	92.40	94.93
CLTP_S_M/C	96.43	84.00	86.85	89.09	98.44	92.14	92.80	94.55	98.98	95.00	92.94	95.64
WCLTP_S_M/	97.27	88.98	89.26	91.84	97.94	93.63	92.94	94.84	98.78	95.56	94.40	96.24
CLBP_S/M	94.66	82.75	83.14	86.85	97.89	90.55	91.11	93.18	99.32	93.58	93.35	95.42
CLBC_S/M	95.23	82.13	83.59	86.98	98.10	89.95	90.42	92.82	98.70	91.41	90.25	93.45
CLTP_S/M	96.41	82.85	84.81	88.02	97.84	92.06	92.69	94.20	99.04	94.14	95.59	96.26
WCLTP_S/M	96.54	86.97	86.62	90.04	98.44	93.68	93.01	95.04	99.35	94.75	94.14	96.08
CLBP_S/M/C	96.56	90.30	92.29	93.05	98.72	93.54	93.91	95.39	98.93	95.32	94.53	96.26
CLBC_S/M/C	97.16	89.79	92.92	93.29	98.54	93.26	94.07	95.29	98.78	94.00	93.24	95.34
CLTP_S/M/C	96.88	90.25	92.92	93.35	98.83	93.59	94.26	95.56	99.17	95.67	94.28	96.37
WCLTP_S/M/	98.13	91.25	93.32	93.56	98.80	95.60	95.19	96.53	99.22	96.76	95.77	97.25

Bold values indicate the best result

* The results of LBP and LTP are from (Sree & Rao 2017)

As shown in Table 4.3, the classification accuracy for the individual operator that depends on sign difference calculation is mostly greater than the accuracy achieved by magnitude operators, thereby implying that the sign features are more discriminated than magnitude features. The proposed WCLTP apparently outperformed the other descriptors in most experiments using OuTex (TC10) and (TC12). In the TC10 dataset, the WCLTP achieved the highest accuracy rate of 99.35% with WCLTP_S/M_{24,3}, and the second rank for CLBP_S/M_{24,3} had a 99.32% accuracy rate, while the worst result was obtained by CLBP_M_{8,1} with an accuracy of 81.74%. In TC12, the WCLTP_S/M/C_{24,3} achieved the best accuracy rate of 96.76% and 95.77% with both TC12(t) and TC12(h), respectively. On average, the WCLTP_S/M/C_{24,3} achieved the highest accuracy for TC family, reaching 97.25%, compared with 96.37% achieved by CLTP_S/M/C_{24,3}, 96.26% achieved by CLBP_S/M/C_{24,3} and 95.34% achieved by CLBC_S/M/C_{24,3}. Given that the OuTex dataset is subjected to illumination changes, the improved results confirmed that the proposed WCLTP is more robust to illumination variations.

4.3.2.2 Experimental Results on the CURET Dataset

The CURET dataset has 61 texture classes. Each class includes 205 texture images which are subjected to different illumination and viewpoint conditions. 118 images out

of 250 images have viewing angles less than 60°. 92 images are selected after being converted to greyscale and cropped to 200 × 200 pixels. Out of 92 images N images are selected and used as training data, while the remaining (92-N) are used as testing data. The final classification accuracy is the average percentage over a hundred random splits. Table 4.4 shows the classification results for N = (6, 12, 23, 46) on CURET dataset.

Table 4.4 Classification rates (%) on the CURET dataset

Descriptor	Parameters (R,P) . R =the radius of the circle, P =the number of neighbourhood pixels											
	R=1, P=8				R=2, P=16				R=3, P=24			
	6	12	23	46	6	12	23	46	6	12	23	46
LBP ^{riu2}	60.36	69.05	74.64	81.32	63.38	72.70	79.28	84.53	67.86	75.51	81.65	86.35
LTP	65.17	74.61	80.85	87.74	68.72	80.18	86.17	91.16	72.76	82.42	87.19	91.52
CLBP_S	59.00	67.81	74.62	80.70	63.49	72.68	79.49	85.35	66.94	75.26	81.80	87.31
CLBC_S	56.88	66.21	72.89	78.82	60.42	68.95	74.42	79.78	60.82	70.57	74.21	80.14
CLTP_S	64.38	72.66	81.73	88.24	68.39	79.09	86.61	91.55	72.57	81.55	87.72	91.75
WCLTP_S	62.73	72.18	79.48	85.90	68.54	78.47	83.17	89.16	70.50	78.68	85.20	90.57
CLBP_M	51.77	60.33	67.73	75.16	58.557	68.28	76.11	83.03	62.57	71.93	79.89	68.49
CLBC_M	50.12	58.62	57.82	66.61	50.63	58.70	66.05	73.89	51.23	60.53	68.36	77.41
CLTP_M	61.37	71.17	80.53	86.67	63.33	74.47	82.14	88.83	67.14	76.93	85.16	90.52
WCLTP_M	58.22	67.94	76.14	83.74	64.49	72.82	82.19	88.00	64.89	74.86	82.89	89.11
CLBP_M/C	56.53	67.15	75.58	82.97	64.81	75.56	82.98	89.75	68.71	78.54	86.04	91.65
CLTP_M/C	62.07	72.94	82.26	88.98	66.77	77.12	85.51	91.67	70.10	80.12	89.02	93.58
WCLTP_M/C	61.83	73.01	81.68	88.96	66.61	77.96	86.43	92.52	71.55	80.99	88.20	93.60
CLBP_S_M/C	66.63	76.54	85.02	90.55	70.27	80.47	87.57	92.78	73.29	82.28	89.28	94.07
CLTP_S_M/C	67.54	78.89	85.46	91.27	71.55	82.16	87.82	94.04	74.36	85.14	91.03	94.69
WCLTP_S_M/C	67.70	77.89	86.81	92.63	70.12	83.44	88.94	94.06	74.55	83.37	90.34	94.87
CLBP_S/M	71.86	82.27	88.57	93.46	74.63	83.44	89.67	93.85	74.95	84.30	90.83	94.53
CLBC_S/M	69.89	79.88	86.62	93.10	72.16	81.71	89.60	93.78	70.52	81.57	89.12	93.60
CLTP_S/M	71.30	82.37	89.20	93.50	74.14	84.42	90.78	95.06	76.49	85.11	92.02	95.63
WCLTP_S/M	70.63	81.67	88.46	93.69	75.79	84.87	90.87	95.49	76.31	85.25	91.59	95.43
CLBP_S/M/C	74.35	85.06	91.52	95.07	76.07	85.73	92.15	95.67	76.80	86.54	92.00	95.72
CLBC_S/M/C	72.85	82.92	90.12	94.78	75.17	85.91	91.30	95.39	73.18	84.07	90.55	95.26
CLTP_S/M/C	75.18	84.06	90.45	94.78	77.72	85.54	92.44	95.95	77.97	87.50	92.72	96.11
WCLTP_S/M/C	72.81	83.96	91.10	95.86	77.85	86.68	92.53	96.27	78.30	87.27	93.28	96.57

Table 4.4 shows a similar conclusion to Table 4.3. The proposed WCLTP performs better than other descriptors in all cases on average. Its highest classification accuracy reaches 96.57% with WCLTP_S/M/C_{24,3}, while CLTP_S/M/C_{24,3} has an accuracy of 96.11%. Moreover, the CLBC obtained the worst results in all experiments. Although the WCLTP achieved the highest accuracy percentage, CLTP and CLBP showed better performance in some cases in this dataset. The performance varies based

on the texture pattern (i.e. $[R = 1, P = 8]$, $[R = 2, P = 16]$ and $[R = 3, P = 24]$) with a different number of training images. In general, the evaluation results confirmed that the WCLTP is more rotation invariant than other descriptors because of the RDWT's shift invariance.

4.3.2.3 Experimental Results on the UIUC Dataset.

The UIUC dataset includes 25 texture classes. Each class has 40 images captured in different illumination conditions and viewing points. Following the same procedure in (Rassem & Khoo, 2014), different training images (N) are randomly selected for each class where ($N = 5, 10, 15, 20$). The remaining $(40-N)$ images are used as the test set. Each random selection is repeated 100 times to obtain statistically valid experimental results. The experimental results of the UIUC dataset are shown in Table 4.5.

Table 4.5 Experimental Results on the UIUC Dataset

Method	Parameters (R,P) . R =the radius of the circle, P =the number of											
	R=1, P=8				R=2, P=16				R=3, P=24			
	5	10	15	20	5	10	15	20	5	10	15	20
LTP	50.0	58.2	64.6	67.8	61.2	71.3	74.4	78.2	60.9	74.5	78.7	83.4
CLBP_S	40.0	47.5	51.6	55.2	41.8	51.3	56.8	60.6	44.8	54.6	60.6	64.2
CLBC_S	39.8	46.6	51.1	55.6	43.3	53.0	59.1	62.3	47.1	57.4	63.4	66.9
CLTP_S	54.2	61.8	69.9	71.6	64.9	75.0	80.4	83.2	68.8	77.6	83.0	86.0
WCLTP_S	61.6	71.5	76.0	78.6	69.4	78.2	82.5	85.0	72.9	81.1	84.8	87.0
CLBP_M	42.3	49.9	54.4	57.5	56.0	65.6	69.5	72.0	56.1	65.9	71.0	74.3
CLBC_M	39.0	45.5	49.4	52.1	50.6	59.0	64.4	67.1	51.6	60.6	66.6	69.3
CLTP_M	57.4	64.6	69.6	73.6	70.2	79.3	83.3	85.4	69.9	79.3	82.5	85.2
WCLTP_M	66.1	74.0	77.9	80.2	70.2	77.9	81.8	83.4	69.4	76.8	80.4	82.8
CLBP_M/C	56.9	65.0	69.8	72.6	68.4	76.8	80.1	82.7	68.0	76.7	80.8	83.2
CLTP_M/C	70.0	76.9	80.4	81.8	77.3	83.6	87.0	89.4	76.8	83.4	87.2	88.6
WCLTP_M/C	69.8	77.3	81.5	83.7	75.4	82.7	86.0	87.7	76.1	83.2	86.5	88.4
CLBP_S_M/C	62.5	71.2	75.4	78.6	68.6	77.5	81.3	83.5	69.4	78.6	82.8	85.3
CLTP_S_M/C	68.8	77.3	80.4	83.6	77.3	84.2	87.8	89.8	77.2	84.6	88.4	90.6
WCLTP_S_M/	72.8	80.2	83.5	86.0	79.0	85.6	89.0	90.7	79.9	86.6	89.5	91.0
CLBP_S/M	64.7	74.6	79.5	82.5	71.8	80.8	85.3	87.6	72.0	82.6	86.8	89.5

Table 4.5 Continued

Method	Parameters (R,P) . R =the radius of the circle, P =the number of											
	R=1, P=8				R=2, P=16				R=3, P=24			
	5	10	15	20	5	10	15	20	5	10	15	20
CLBC_S/M	65.2	74.8	78.8	82.4	73.1	82.0	86.3	88.5	75.1	83.9	87.6	89.7
CLTP_S/M	65.0	74.4	79.6	83.0	77.1	85.6	89.4	91.8	79.3	87.7	90.5	93.2
WCLTP_S/M	74.9	82.3	86.1	88.0	82.5	89.1	91.5	92.8	83.8	89.9	92.2	93.8
CLBP_S/M/C	74.5	82.2	85.8	87.8	78.7	86.3	89.2	91.0	78.0	85.8	89.1	91.0
CLBC_S/M/C	74.5	82.3	85.6	87.8	79.4	86.6	89.6	91.0	79.7	86.4	90.1	91.3
CLTP_S/M/C	74.5	81.7	85.9	86.8	82.6	87.8	90.4	92.6	82.9	88.9	91.5	94.4
WCLTP_S/M/	77.5	84.7	87.6	89.2	84.2	90.1	92.2	93.4	84.6	90.2	92.7	94.8

* The results for CLBP, CLBC and CLTP are from (Rassem & Khoo, 2014)

A significant observation that can be drawn from Table 4.5 is that the UIUC dataset is difficult for most descriptors especially when using a single operator. Most variants such as LTP, CLBP and CLBC achieved classification accuracy less than 60% in single operator and even less than 50% in some cases because of the complex characteristics of the data, such as high resolution and nonrigid deformations. WCLTP shows on average the best performance compared with other methods in all cases. WCLTP achieved the highest accuracy rate of 94.80% when integrating the three operators together WCLTP_S/M/C_{2,3}. In some cases when (R = 2 and 3), CLTP_M and CLTP_M/C performed better than WCLTP_M and WCLTP_M/C, respectively.

4.3.2.4 Experimental Results on the Kylberg Dataset.

The Kylberg dataset consists of 28 classes, where each class contains 160 images. In this experiment, different training images (N = 16, 40, 64, 80) are randomly selected from each class, while the remaining (160-N) images in each class are used for testing. To obtain statistically valid experiment results, each random selection is executed 100 times and the average classification rate is used as the final experimental result. Table 4.6 shows the classification accuracy of WCLTP and other LBP variants using the Kylberg dataset.

Table 4.6 Experimental Results on the Kylberg Dataset.

Method	Parameters (R,P) . R =the radius of the circle, P =the number of neighbourhood pixels											
	R=1, P=8				R=2, P=16				R=3, P=24			
	16	40	64	80	16	40	64	80	16	40	64	80
CLBP_S	90.58	95.03	96.47	97.03	90.13	95.06	96.76	97.40	93.27	97.10	98.13	98.44
CLTP_S	90.63	94.97	96.36	96.84	95.73	98.35	99.01	99.20	96.86	99.18	99.52	99.60
WCLTP_S	93.11	96.64	97.61	98.01	95.56	98.53	99.14	99.31	95.78	98.71	99.33	99.47
CLBP_M	85.68	91.34	93.38	94.09	91.52	95.23	96.45	96.89	93.11	95.72	96.57	96.99
CLTP_M	93.01	96.82	97.86	98.23	96.00	98.28	98.87	99.08	97.19	98.99	99.35	99.47
WCLTP_M	94.44	97.04	97.97	98.32	96.49	98.30	98.87	98.99	96.98	98.76	99.20	99.36
CLBP_M/C	94.54	97.46	98.31	98.58	96.40	98.37	98.90	99.14	97.28	98.94	99.35	99.51
CLTP_M/c	95.92	98.03	98.72	98.87	97.58	98.88	99.28	99.40	98.21	99.36	99.62	99.66
WCLTP_M/C	96.19	98.28	98.96	99.22	97.48	99.03	99.49	99.62	98.46	99.41	99.68	99.73
CLBP_S_M/C	96.11	98.35	98.98	99.14	96.43	98.72	99.33	99.45	97.26	99.07	99.46	99.62
CLTP_S_M/C	95.94	98.02	98.62	98.82	97.46	98.98	99.37	99.51	97.92	99.41	99.67	99.75
WCLTP_S_M/C	96.20	98.21	98.87	99.14	97.36	99.12	99.53	99.66	98.05	99.36	99.69	99.70
CLBP_S/M	96.07	98.53	99.08	99.32	97.71	99.30	99.65	99.75	97.96	99.46	99.77	99.82
CLTP_S/M	95.21	97.85	98.60	98.80	97.58	99.31	99.65	99.75	98.11	99.54	99.78	99.80
WCLTP_S/M	96.56	98.65	99.21	99.37	97.88	99.42	99.67	99.76	98.17	99.58	99.72	99.81
CLBP_S/M/C	97.34	99.24	99.60	99.70	98.35	99.55	99.79	99.84	98.62	99.60	99.78	99.83
CLTP_S/M/C	96.61	98.39	98.92	99.11	98.36	99.49	99.71	99.78	98.67	99.65	99.82	99.87
WCLTP_S/M/C	97.42	98.97	99.74	99.84	98.46	99.63	99.79	99.86	98.79	99.68	99.84	99.88

Bold values indicate the best result

Table 4.6 clearly shows that almost all descriptors performed well on the Kylberg dataset. The proposed WCLTP achieved impressive results in most cases. The best classification result was obtained by WCLTP_S/M/C_{24,3} of 99.88%, with a slight difference of 0.01% for the CLTP_S/M/C_{24,3} result because of the simplicity of this dataset. The combination of the three operators in WCLTP (WCLTP S/M/C) performs much better than the CLBP S/M/C and CLTP S/M/C at every radius and training size. In general, the WCLTP outperforms other LBP variants in all texture dataset experiments.

4.3.3 Experimental Results of WCLTP for Medical Datasets.

In these experiments, the proposed WCLTP was evaluated using two medical datasets.

4.3.3.1 Experimental Results on the 2D HeLa Dataset.

The 2D HeLa dataset consists of 10 classes of Hela cells. Each class contains images ranging from 73 to 98. Table 4.7 shows the classification rates of the WCLTP and other LBP variants using this dataset. In this experiment, 5-fold cross-validation was used, where the images of each class were randomly split into five parts, with four parts for training and one part for testing. Different radius ($R = 1, 2, 3$) and pattern neighbours ($P = 8, 16, 24$) were utilised to show the effect of increasing the radius and neighbours on the classification rate.

Table 4.7 Experimental Results on the 2D HeLa Dataset.

Method	Parameters (R, P) . R =the radius of the circle, P =the number of neighborhoods pixels		
	R=1, P=8	R=2, P=16	R=3, P=24
CLBP_S	59.77	65.00	66.98
CLTP_S	70.35	73.14	77.21
WCLTP_S	73.72	77.44	79.42
CLBP_M	51.63	58.37	60.23
CLTP_M	63.02	66.98	68.26
WCLTP_M	67.67	70.93	71.16
CLBP_M/C	60.58	64.77	65.70
CLTP_M/C	70.93	72.33	73.14
WCLTP_M/C	76.16	77.33	79.30
CLBP_S_M/C	64.42	66.74	69.77
CLTP_S_M/C	71.98	75.58	75.70
WCLTP_S_M/C	77.56	82.21	81.05
CLBP_S/M	62.79	68.84	70.23
CLTP_S/M	78.02	79.77	78.60
WCLTP_S/M	78.49	81.40	81.74
CLBP_S/M/C	66.74	70.93	70.23
CLTP_S/M/C	78.84	79.88	80.81
WCLTP_S/M/C	81.40	83.73	84.19

Table 4.7 shows a significant variation in the results. CLTP and WCLTP achieved good performance at the expense of CLBP at every radius. The proposed WCLTP shows clear superiority in all experiments. In pattern ($R = 1, P = 8$), the classification accuracy of WCLTP_M/C and WCLTP_S_M/C has a significant 6% improvement compared with

the classification accuracy of CLTP_M/C and CLTP_S_M/C. With $R = 2,3$ and $P = 16,24$, WCLTP_S/M/C has on average a 6 to 7% higher classification accuracy than CLTP. The highest accuracy rate achieved by WCLTP_S/M/C_{24,3} is 84.19% with a considerable difference of more than 3% for the CLTP_S/M/C_{24,3} result. In general, the proposed WCLTP achieved satisfactory results.

4.3.3.2 Experimental Results on the Breast Cancer Dataset.

The Breast Cancer dataset has 3 classes with a total of 1394 images. In these experiments, the same setup of the 2D-HeLa dataset is used, where 4/5 of the images from every class are randomly chosen as training data and the remaining 1/5 is adopted as testing data. Table 4.8 shows the classification rate for different LBP variants using the Breast Cancer dataset.

Table 4.8 Experimental Results on the Breast Cancer Dataset.

Method	Parameters (R, P) . R =the radius of the circle, P =the number of neighborhoods pixels		
	R=1, P=8	R=2, P=16	R=3, P=24
CLBP_S	59.77	65.00	66.98
CLTP_S	70.35	73.14	77.21
WCLTP_S	73.72	77.44	79.42
CLBP_M	51.63	58.37	60.23
CLTP_M	63.02	66.98	68.26
WCLTP_M	67.67	70.93	71.16
CLBP_M/C	60.58	64.77	65.70
CLTP_M/C	70.93	72.33	73.14
WCLTP_M/C	76.16	77.33	79.30
CLBP_S_M/C	64.42	66.74	69.77
CLTP_S_M/C	71.98	75.58	75.70
WCLTP_S_M/C	77.56	82.21	81.05
CLBP_S/M	62.79	68.84	70.23
CLTP_S/M	78.02	79.77	78.60
WCLTP_S/M	78.49	81.40	81.74
CLBP_S/M/C	66.74	70.93	70.23
CLTP_S/M/C	78.84	79.88	80.81
WCLTP_S/M/C	81.40	83.73	84.19

Table 4.8 shows that WCLTP and CLTP outperform the CLBP descriptor in many cases. WCLTP achieved the highest classification accuracy of 92.14% when WCLTP_S_{16,2}, followed by CLTP_S_{8,1}, which reached 90.69%, and WCLTP_S_{24,3}, which reached 90.11%. In this dataset, the combination of the sign, magnitude and centre affects the accuracy because of the image formats used in the experiments. As shown in Figure 2.25, the segmented Breast Cancer images are used in these experiments. As a result of the segmentation, many of the pixels' values are 0s, thereby affecting the extracted texture features in particular with combinations of sign, magnitude and centre information.

4.4 Performance Evaluation for the Proposed Feat-WCLTP

The results obtained in the previous section show the effectiveness of the proposed WCLTP descriptor in improving CLTP's performance. However, the proposed WCLTP inherits the high dimensionality problem of the CLTP original descriptor. Thus, a second descriptor called Feat-WCLTP was proposed to overcome the high dimensionality problem and maintain the improved performance. To evaluate the performance of proposed Feat-WCLTP, three sets of experiments were conducted. In the first one, four texture benchmark datasets were used. In the second experiment, two medical benchmark datasets were utilised. In the third experiment, two medical and texture datasets were used to evaluate the computational time of Feat-WCLTP. In this section, the performance of the two proposed descriptors will be compared with that of CLTP. A dimensionality and time classification comparison is included. In these experiments, the evaluation results were obtained for the case where the three operators for each descriptor were combined (i.e. sign, magnitude and centre).

4.4.1 Experimental Results of Feat-WCLTP Using Texture Dataset.

In these experiments, the accuracy of the proposed Feat-WCLTP is evaluated and compared with that of CLTP. The dataset setup and evaluation metrics used to evaluate this descriptor are the same as those described in WCLTP experiments in Section 4.3.

4.4.1.1 Experimental Results on the CURET Dataset

Figure 4.5 illustrates the results of the proposed WCLTP, Feat-WCLTP and original CLTP over the CURET dataset under different texture patterns (i.e. [P = 8, R = 1],

[P = 16, R = 2] and [P = 24, R = 3]) using different numbers of training images N where (N = 6, 12, 23, 46).

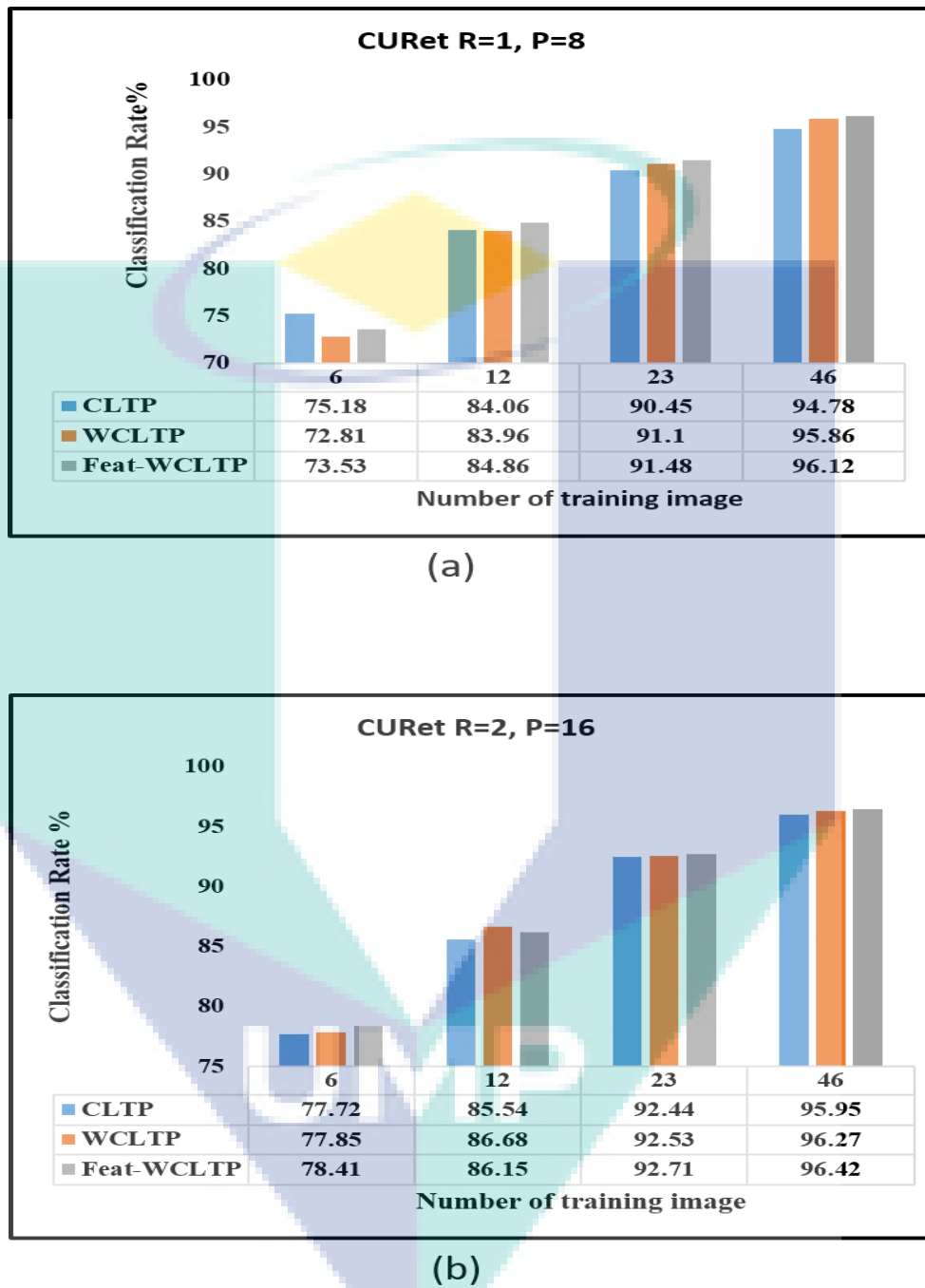


Figure 4.5 Performance comparison of proposed Feat-WCLTP with CLTP using CUREt dataset under different pattern size (a) (R=1,P=8). (b) (R=2,P=16). (c) (R=3,P=24).

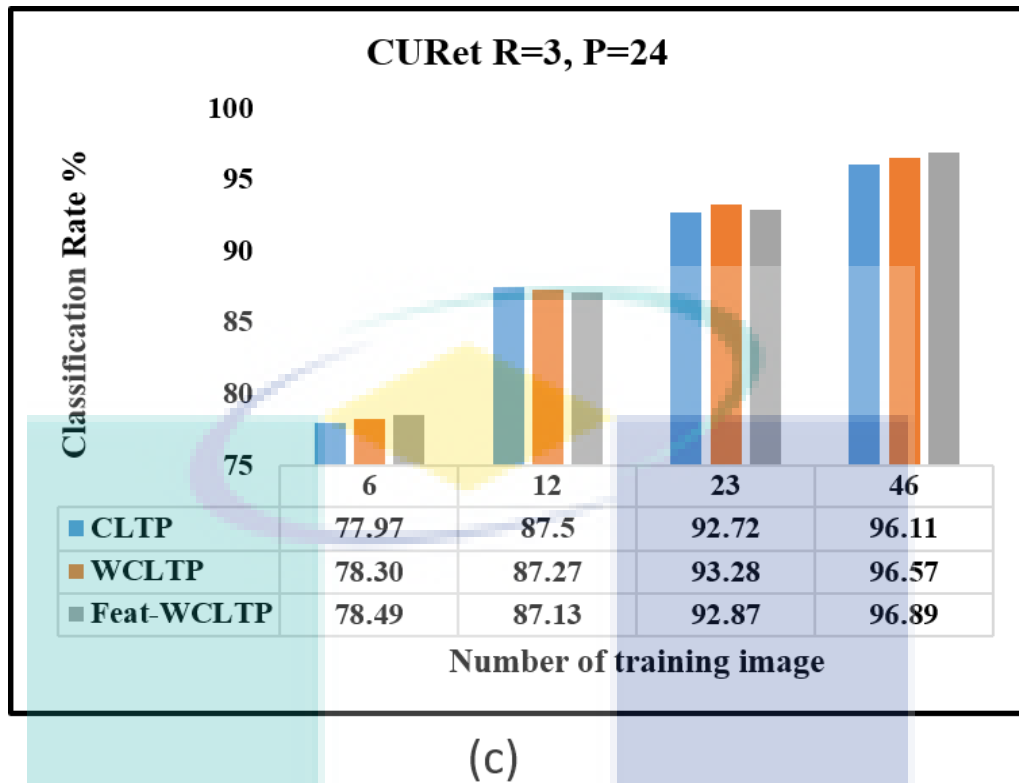
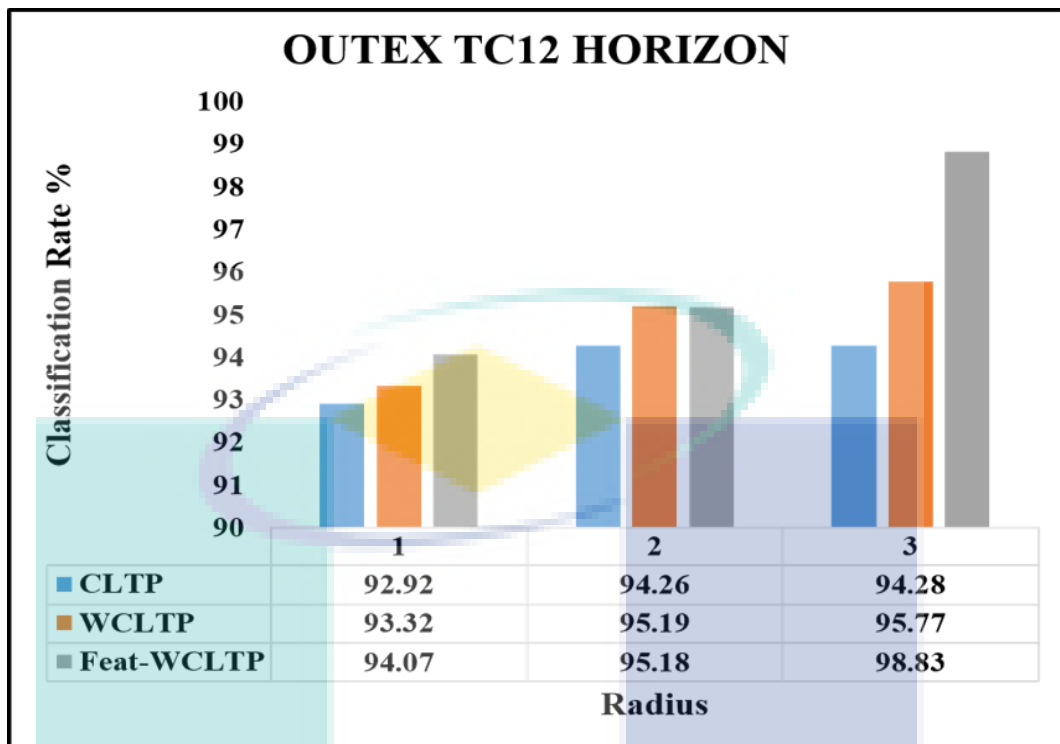


Figure 4.5 Continued

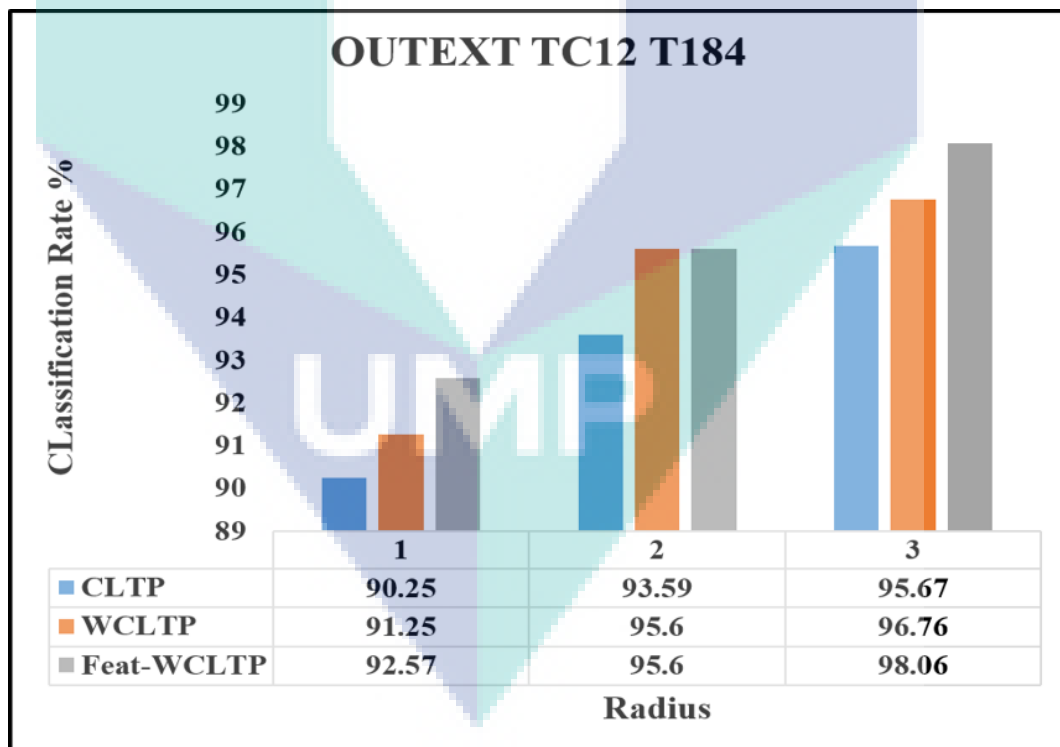
Figure 4.6 shows that the results for the three descriptors were competitive. The Feat-WCLTP achieved the highest classification accuracy rates of 96.12%, 96.42% and 96.89% at ($P = 8, R = 1$), ($P = 16, R = 2$) and ($P = 24, R = 3$) respectively. In general, the Feat-WCLTP performed better than WCLTP and CLTP using $P = 8, P = 1$ texture pattern with all N 's training images. With the bigger size of the texture patterns, the Feat-WCLTP performed better in most cases expect in three cases, as shown in Figure 4.6. In general, the proposed WCLTP and Feat-WCLTP performed better than the original CLTP.

4.4.1.2 Experimental Results on the OuTex Dataset

Figure 4.7 illustrates the accuracy results of the proposed WCLTP, Feat-WCLTP and original CLTP using the OuTex dataset under different texture pattern sizes (i.e. [$P = 8, R = 1$], [$P = 16, R = 2$] and [$P = 24, R = 3$]). In these experiments, three OuTex datasets were used, as shown in Figure 4.7.

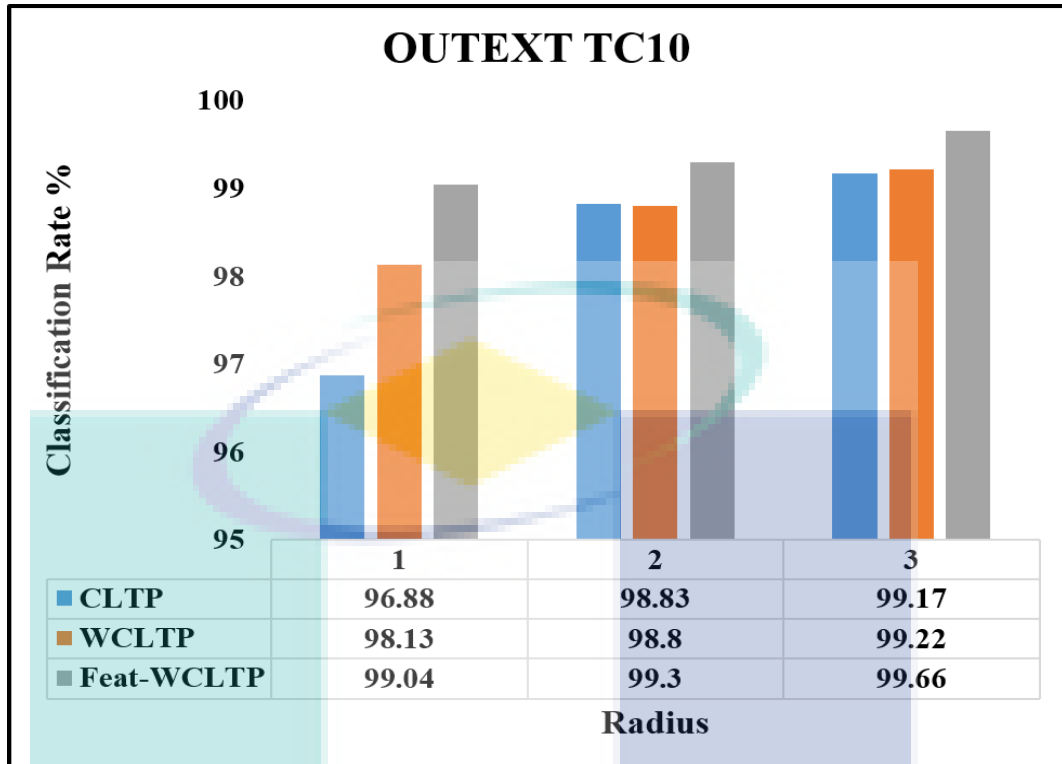


(a)



(b)

Figure 4.6 Performance comparison of proposed descriptors with CLTP using OuTex dataset.(a) OuTex TC12(h). (b) OuTex TC12(t) (c) OuTex TC10



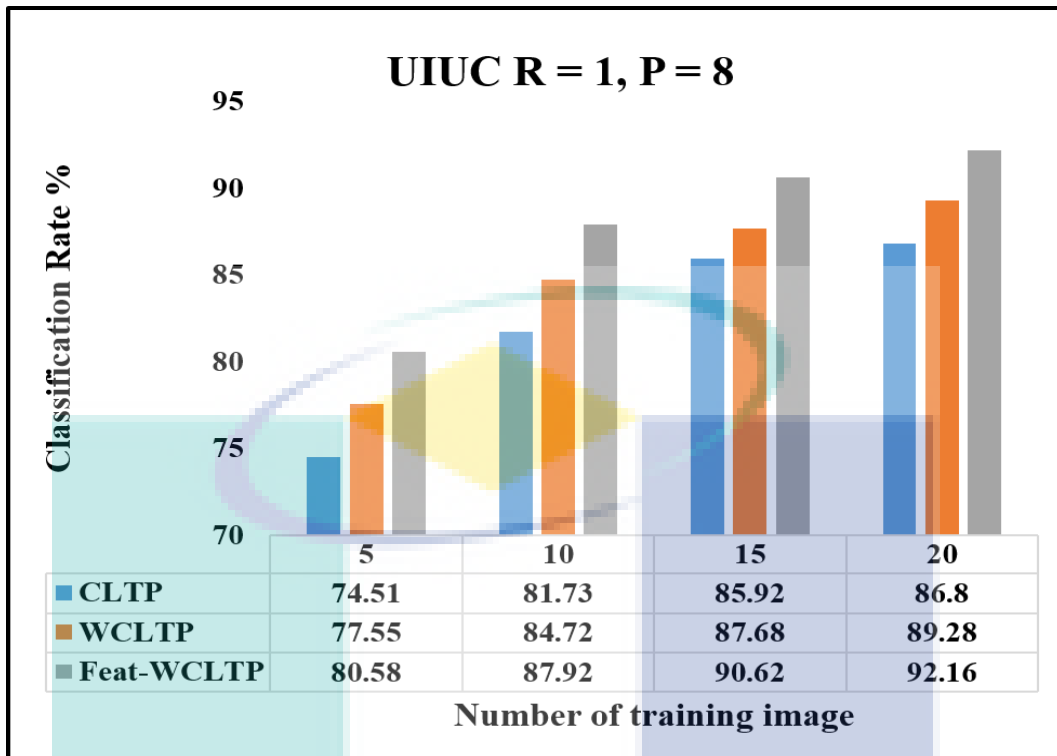
(c)

Figure 4.6 Continued

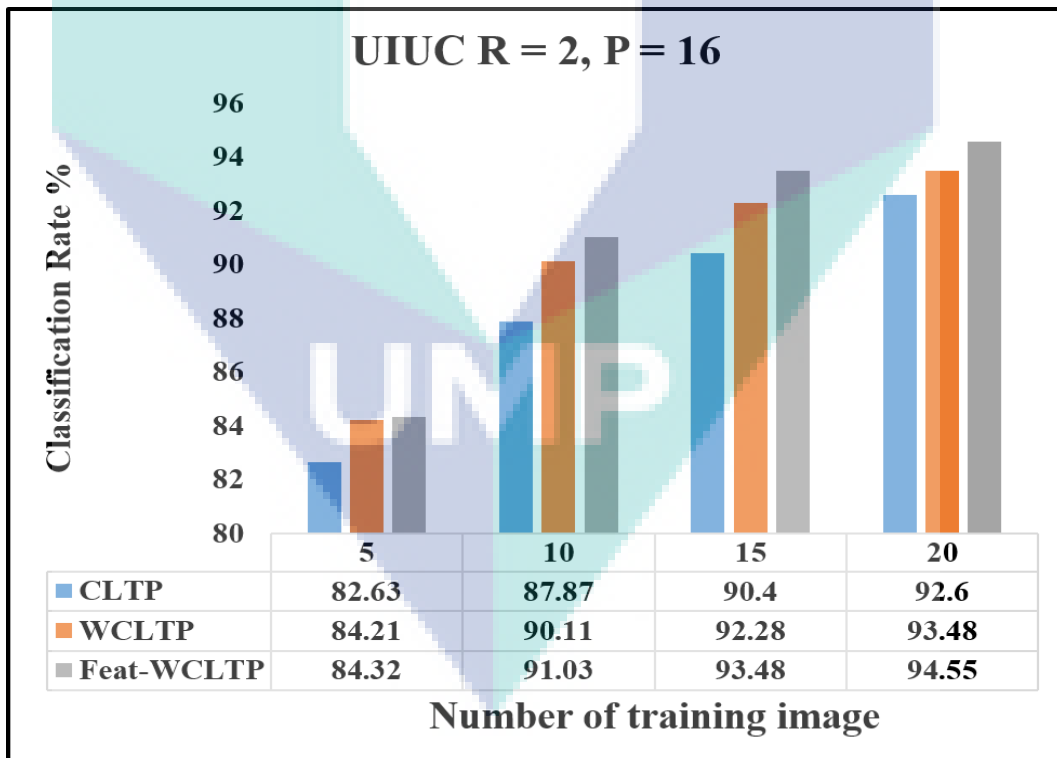
Figure 4.7 shows that the performance increases significantly with a large radius because the small radius may not be well reflected in the pattern structure. In (a) when using the TC12 Horizon dataset, the Feat-WCLTP outperforms the others in all experiments. The results of Feat-WCLTP and WCLTP when $R = 2$ were almost the same. However, the results of Feat-WCLTP were higher than those of WCLTP at an increased rate above 3%. Similar observations were found when using TC12(t), where the Feat-WCLTP outperformed the WCLTP with a significant accuracy rate difference. In (c), when using the TC10 dataset, the Feat-WCLTP is proved to be superior in all experiments where its results were above 99% under the three radius values ($R = 1, 2$ and 3).

4.4.1.3 Experimental Results on the UIUC Dataset.

Figure 4.8 illustrates the accuracy results of the proposed WCLTP, Feat-WCLTP and original CLTP using the UIUC dataset under different texture pattern sizes (i.e. $[P = 8, R = 1]$, $[P = 16, R = 2]$ and $[P = 24, R = 3]$) with different numbers of training images (i.e. 5, 10, 15, 20)

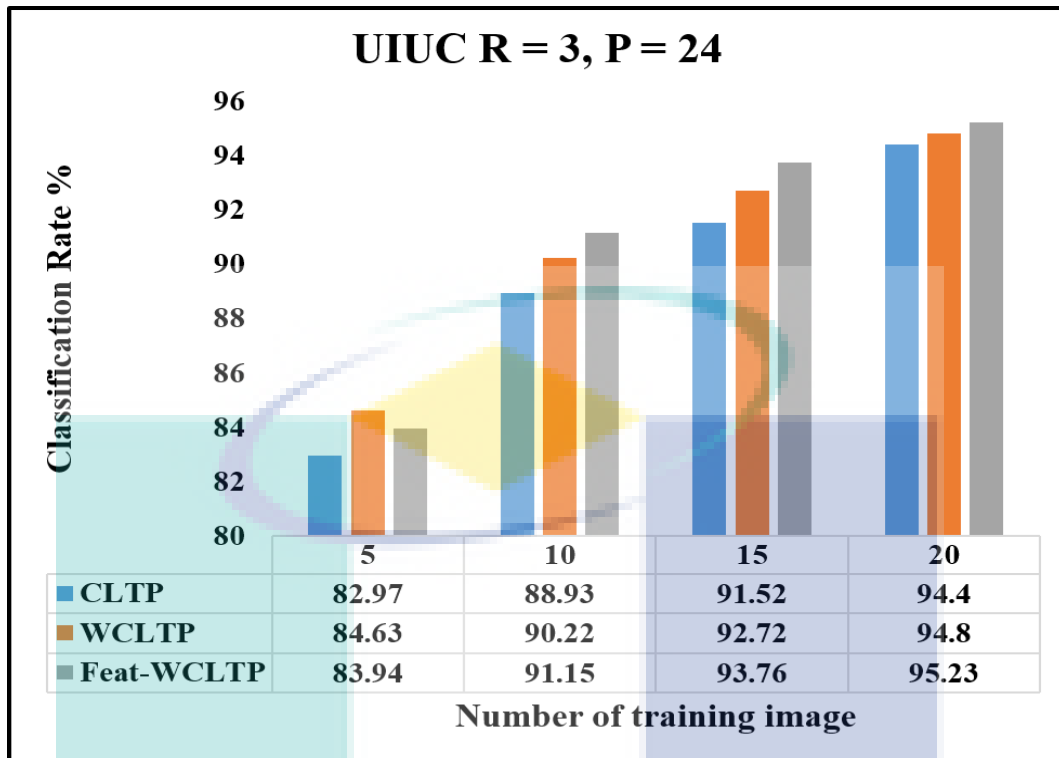


(a)



(b)

Figure 4.7 Performance comparison of proposed descriptors with CLTP using UIUC dataset. (a) with pattern size (R=1,P=8). (b) with pattern size (R=2,P=16). (c) with pattern size (R=3, P=24).



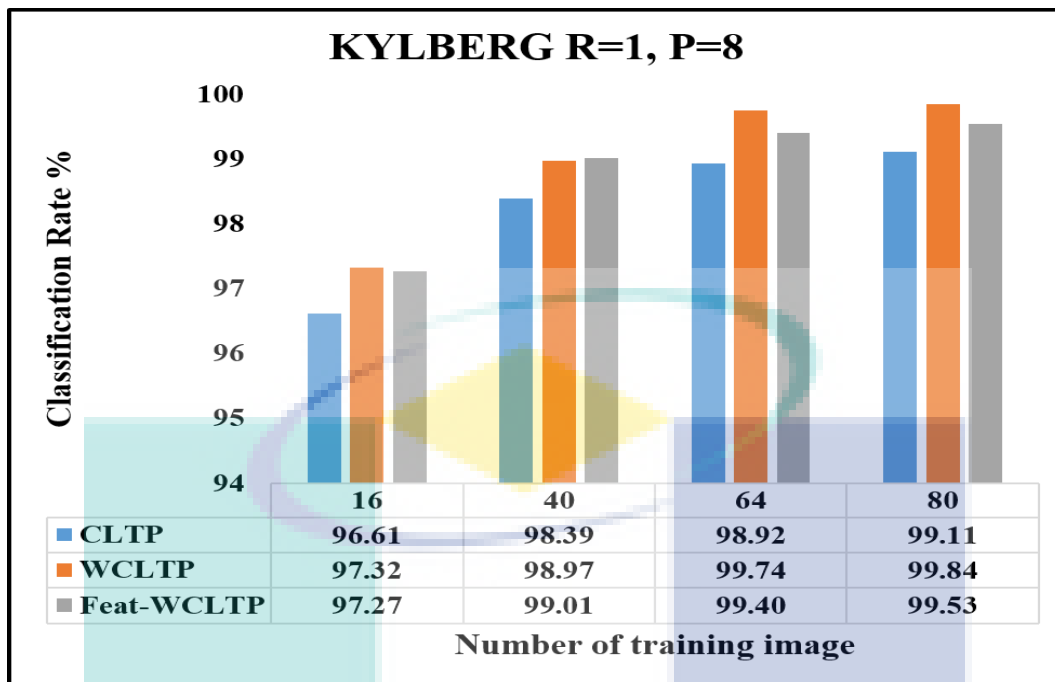
(c)

Figure 4.7 Continued

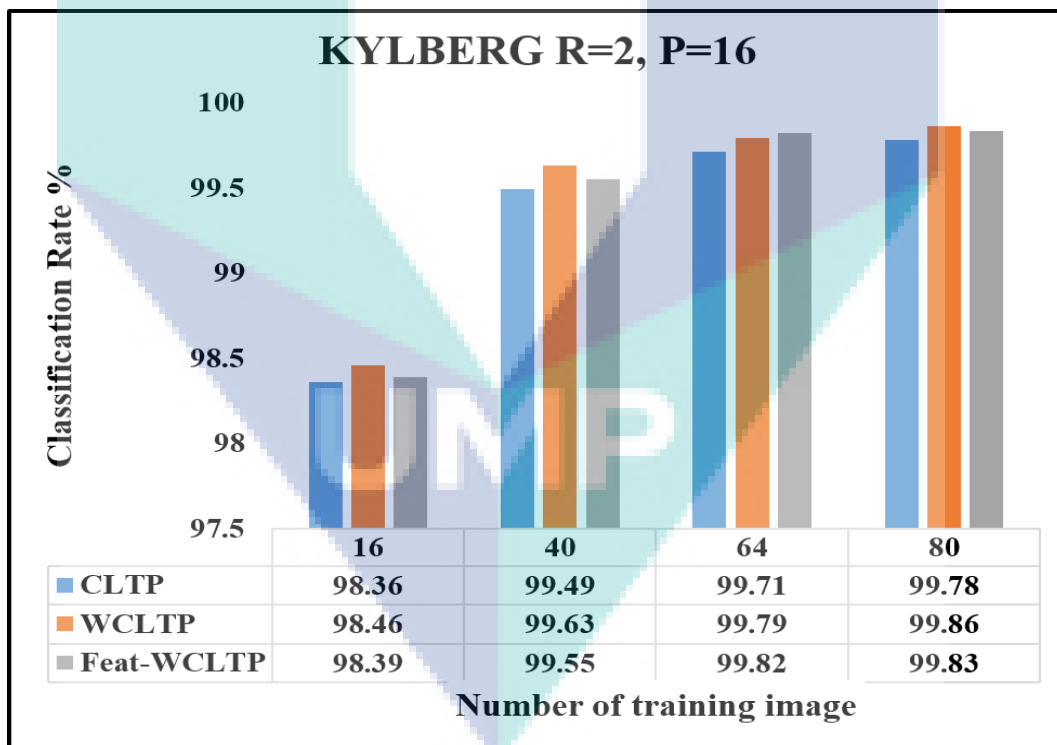
From Figure 4.7, increasing the number of training images and using a large pattern size helps achieve the highest classification accuracy. The results show the clear superiority of the proposed Feat-WCLTP especially with patterns ($P = 8, R = 1$), where it achieved a considerable improvement rate of about 3% over the WCLTP accuracy rate. In pattern ($P = 16, R = 2$) the Feat-WCLTP achieved the highest classification accuracy, reaching 94.55%, while WCLTP achieved 93.48% and CLTP achieved 92.6%. Overall, the Feat-WCLTP enhanced the performance of WCLTP in all experiments using the UIUC dataset. Generally, the Feat-WCLTP achieved the highest classification accuracy of 95.23%, while WCLTP achieved 94.80% and CLTP achieved 94.40%.

4.4.1.4 Experimental Results on the Kylberg Dataset.

Figure 4.8 illustrates the accuracy results of the proposed WCLTP, Feat-WCLTP and original CLTP using the Kylberg dataset under different texture pattern sizes (i.e. [$P = 8, R = 1$], [$P = 16, R = 2$] and [$P = 24, R = 3$]) with different numbers of training images (i.e. 16, 40, 64, 80)

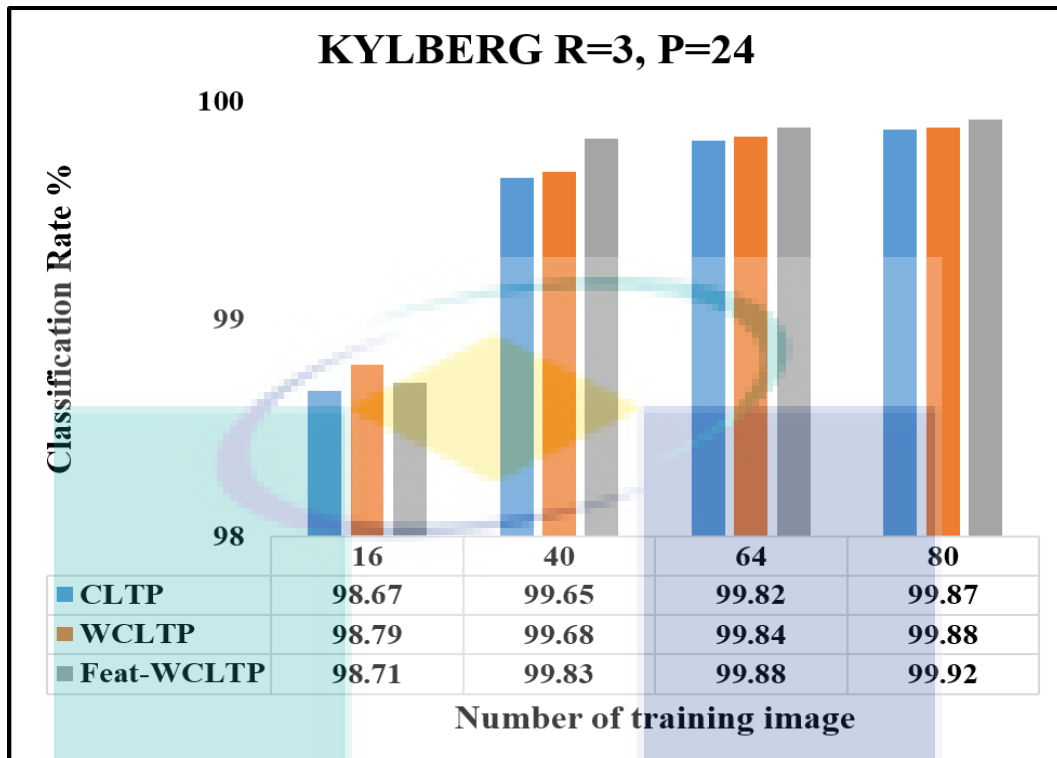


(a)



(b)

Figure 4.8 Performance comparison of proposed descriptors with CLTP using Kylberg dataset. (a) with pattern size (R=1,P=8). (b) with pattern size (R=2,P=16). (c) with pattern size (R=3, P=24).



(c)

Figure 4.8 Continued

From Figure 4.8, the following can be noted: In Figure (a), the Feat-WCLTP achieves comparable results to WCLTP with 64 and 80 training images. However, the WCLTP achieved a better result of 99.01% with 40 training images. In Figure (b), the WCLTP obtained better accuracy rates. However, Feat-WCLTP ranks second. In Figure (c), Feat-WCLTP outperforms others in all experiments with a slight difference of less than 1%.

In general, the best result was achieved by Feat-WCLTP with an accuracy of 99.92%, followed by WCLTP (99.88%) and CLTP (99.87%) for pattern size ($R = 3$, $P = 24$) when 80 images were used for training.

4.4.2 Experimental Results of Feat-WCLTP Using Medical Dataset.

In these experiments, the proposed Feat-WCLTP was evaluated using two medical datasets. These experiments follow the same data setup in Section 4.3.3.

4.4.2.1 Experimental Results on the HeLa Dataset.

Figure 4.10 shows the experimental results of Feat-WCLTP, WCLTP and CLTP using the 2D HeLa dataset under different texture pattern sizes. Similar to Section 4.3.3.1, the images of each class are randomly split into five parts using 5-fold cross-validation technique. Four parts are used for training, while the one part is used for testing.

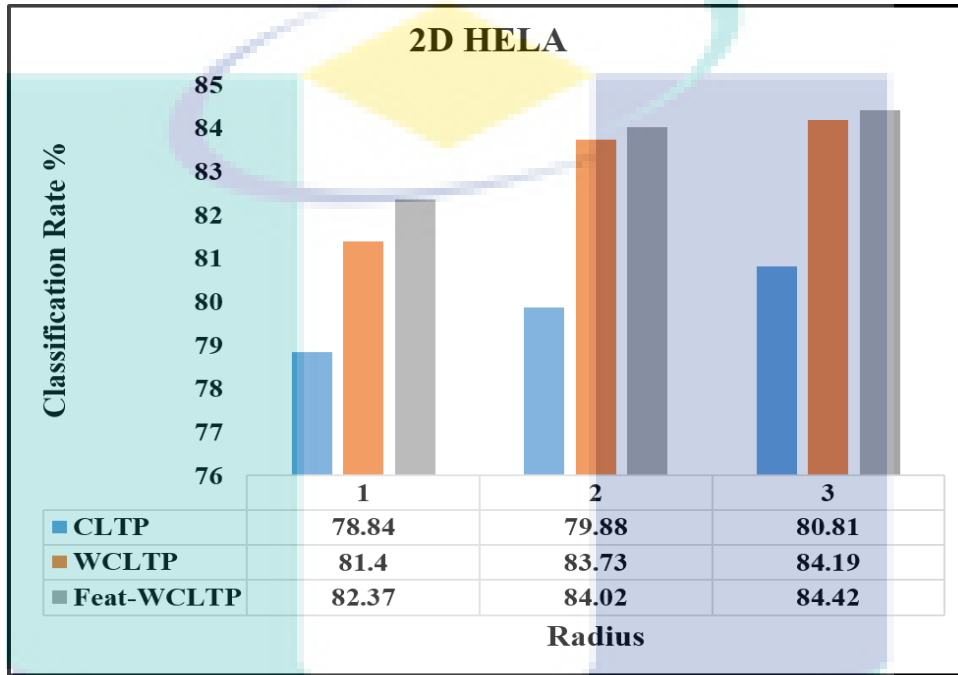


Figure 4.7 Performance comparison of proposed descriptors and CLTP using 2D HeLa dataset.

The figure shows that Feat-WCLTP performed the best in all experiments. Feat-WCLTP achieved the best classification accuracy of 84.42% with the pattern ($P = 24$, $R = 3$), while the WCLTP and CLTP achieved 84.19% and 80.81%, respectively.

4.4.2.2 Experimental Results on the Breast Cancer Dataset.

Figure 4.10 shows the experimental results for evaluating Feat-WCLTP in comparison with WCLTP and CLTP using the Breast Cancer dataset.

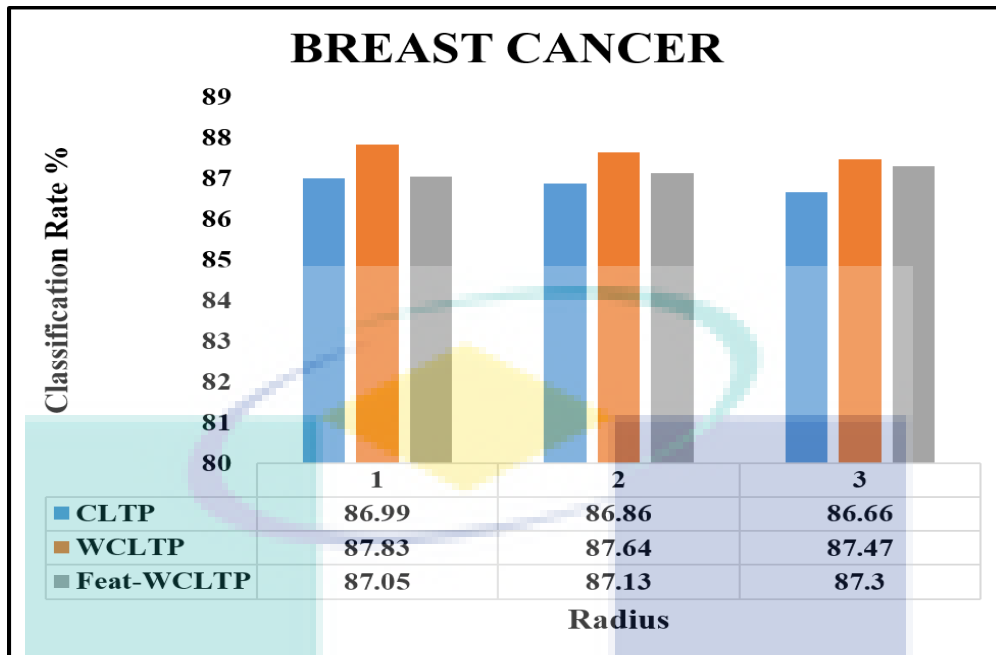


Figure 4.8 Performance comparison of proposed descriptors with CLTP using Breast Cancer dataset.

The WCLTP outperforms Feat-WCLTP and CLTP, obtaining the highest accuracy rate in all experiments. The proposed Feat-WCLTP and original CLTP are close. Feat-WCLTP uses only 1184 feature vectors compared with 26928 feature vectors for both WCLTP and CLTP. Therefore, Feat-WCLTP is the best because it achieved the balance between reducing dimensionality without degrading the accuracy of the original descriptor.

4.4.3 Dimensionality Comparison

The previous experimental results indicate the effectiveness of the proposed descriptors in improving the classification accuracy of the CLTP descriptor. These results achieved the first objective of this thesis, which is to enhance CLTP's classification accuracy. As illustrated in Chapter 3, the proposed Feat-WCLTP mainly aims to reduce the high dimensionality and maintain enhanced performance. The high dimensionality increases the computational complexity and slows down the classification process. The term 'dimensionality' denotes the number of extracted features, which is the size of the histogram that represents the image features. Figure 4.11 shows a dimensionality comparison between the proposed WCLTP, Feat-WCLTP and CLTP.

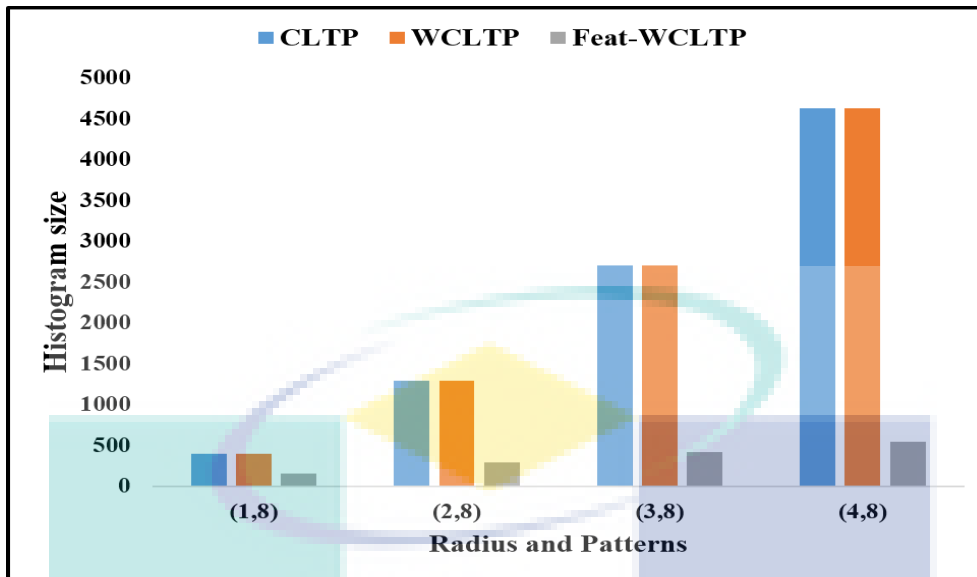
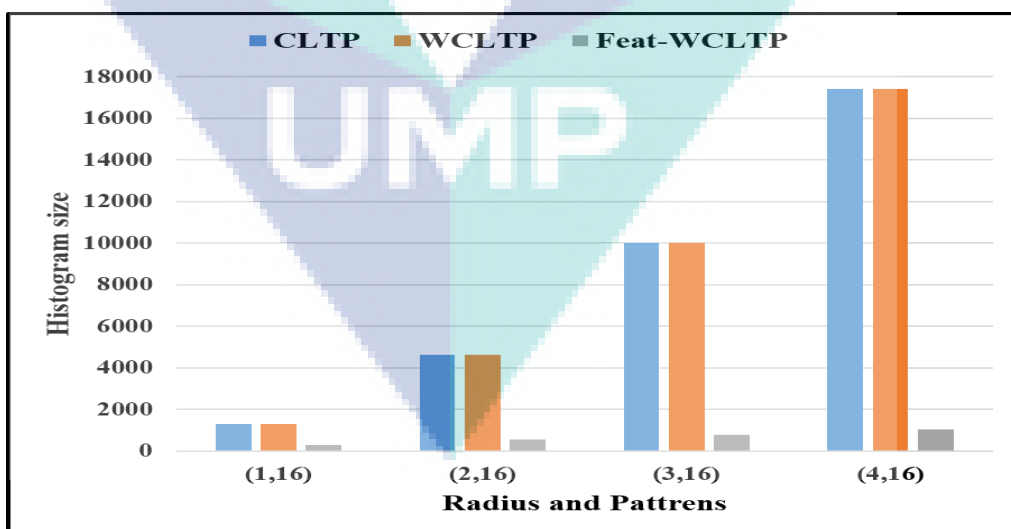


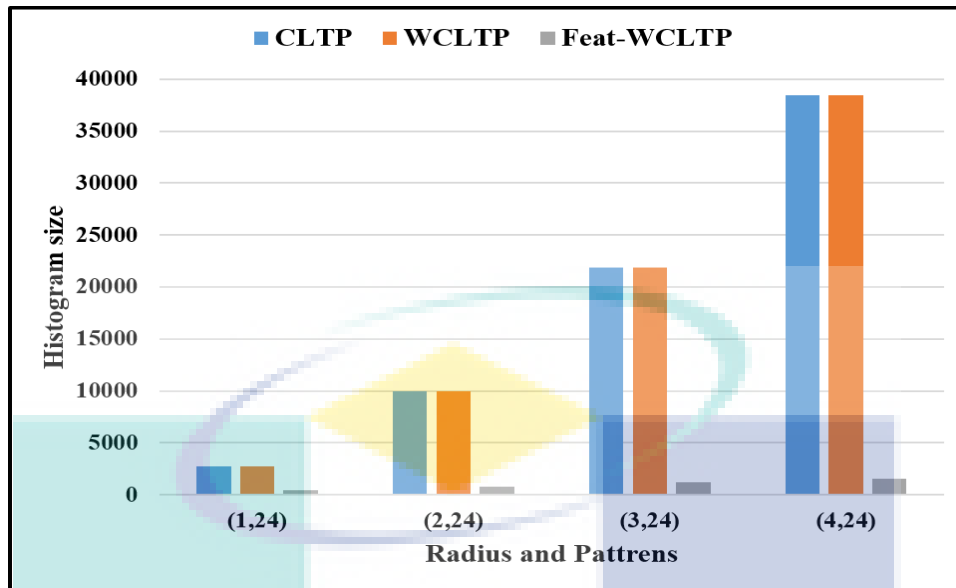
Figure 4.9 Dimensionality comparison of proposed descriptors with CLTP using P=8 and R= 1,2,3 and 4.

When using a multi-scale of R. The histogram size increased sharply when the radius increased. At R = 1 and P = 8, both CLTP and WCLTP have the same size of 400 bins, while the Feat-WCLTP has a size of 160 bins. When the R increased to = 4, the histogram size of the proposed WCLTP exceeded 4500, while the size of Feat-WCLTP was less than 550 bins. Thus, Feat-WCLTP successfully reduced the dimensionality even when a multi-scale of radii was used, and it achieved higher accuracy classification rates in many cases or maintained the same performance of WCLTP in a few cases. A large number of bins is needed in terms of P =16 or 24 as shown in Figure 4.12.



(a)

Figure 4.10 Dimensionality comparison of proposed descriptors with CLTP using P=16,24 and R= 1,2,3 and 4



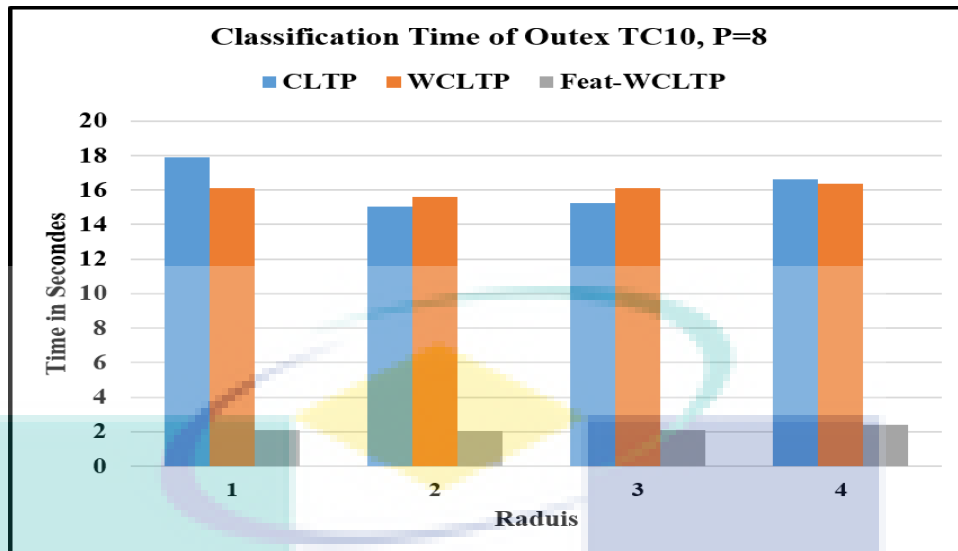
(b)

Figure 4.12 Continued

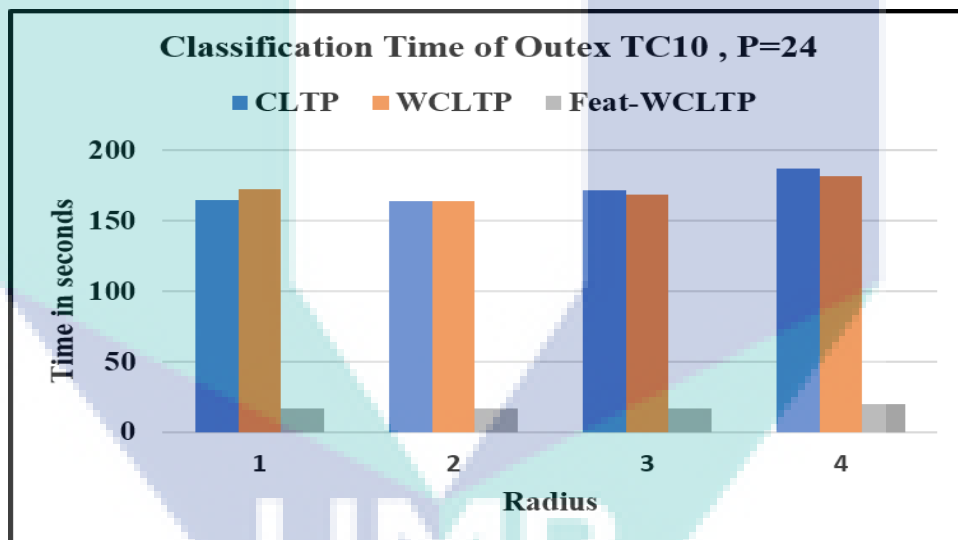
As observed in Figure 4.13, increasing the value of P increased the histogram size considerably. For example, in the pattern ($R = 4$ and $P = 24$), the WCLTP histogram size exceeded 38000 bins, while the histogram size for Feat-WCLTP was only around 1000 bins. This significant difference proved the efficiency of Feat-WCLTP in reducing the high dimensionality of WCLTP. Increasing the number of bins and size of the descriptor will reflect on its performance, as shown with CLBP and CLTP in the texture and medical datasets. Moreover, this will affect the computation complexity and storage space. To confirm the priority of the Feat-WCLTP, the experiments in the next section compare the computational complexity of the proposed descriptors and of CLTP.

4.4.4 Computation Complexity

Generally, the computation complexity for any descriptor can be determined using two key factors: computation time and dimensionality (Liu et al., 2017). In this section, the classification time of the proposed descriptors and CLTP is computed using two datasets (i.e. OuTex TC_10 and 2D HeLa) with different pattern sizes. All experiments were performed using MATLAB 2017a on a PC with 3.40 GHz Intel® Core™ i7-2600 CPU and 4 GB RAM. Figure 4.13 shows a classification time comparison between the proposed WCLTP, Feat-WCLTP and CLTP using the OuTex dataset.



(a)



(b)

Figure 4.13 Classification time comparison of proposed descriptors and CLTP using OuTex dataset with different radius (i.e. R=1,2,3,4) (a) using P =8 (b) using P=24

Figure 4.13 shows that the Feat-WCLTP is faster than WCLTP and CLTP in all experiments. In Figure 4.14(a), the time cost for both CLTP and WCLTP for texture classification is around four times that of Feat-WCLTP. The minimum classification time consumed by Feat-WCLTP was around 2.1 seconds, while the maximum of around 16.37 seconds was consumed by WCLTP. Figure 4.14 (b) shows that increasing the number of neighbouring pixels results in additional classification time. The classification time for CLTP and WCLTP using P = 24 is about 10 times that for Feat-WCLTP because of the

number of extracted features fed to the classifier. The maximum classification time is around 187 seconds for CLTP and around 182 seconds for WCLTP, whereas it is only about 20 seconds for Feat-WCLTP when $P = 24$ and $R = 4$.

Figure 4.14 shows a classification time comparison between CLTP, WCLTP and Feat-WCLTP using the 2D HeLa dataset. The differences in classification time are significant.

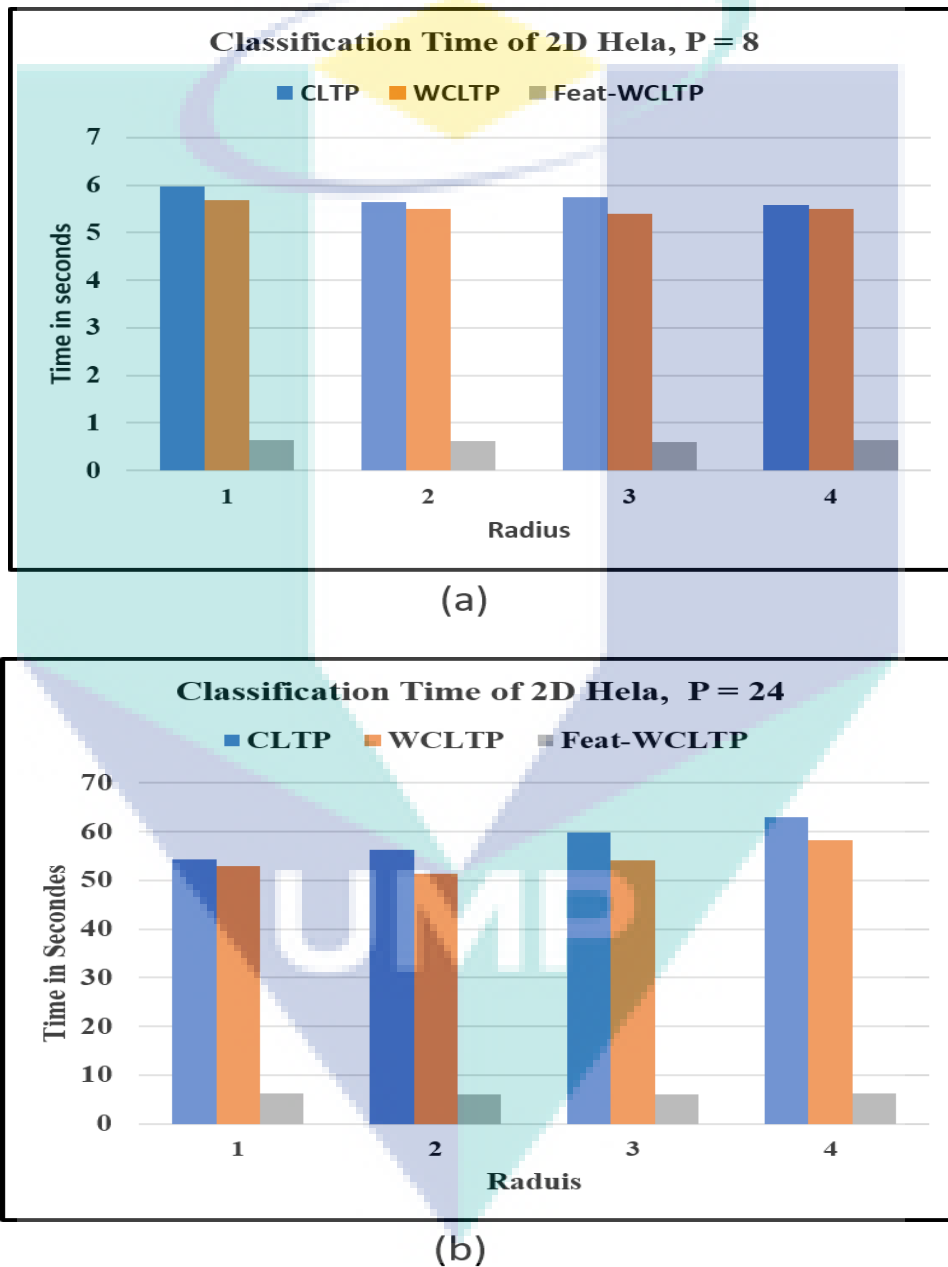


Figure 4.14 Classification time comparison of proposed descriptors using 2D HeLa dataset with different radius (i.e. $R=1,2,3,4$) (a) using $P=8$ (b) using $P=24$.

Feat-WCLTP obtained the shortest classification time of 0.63 seconds, with about a 5-second difference with both CLTP and WCLTP using pattern (P = 8, R = 1). The maximum time was obtained by CLTP (63.05) seconds using pattern (P = 24, R = 4), followed by WCLTP (58.29 seconds). Feat-WCLTP took only 6.31 seconds for the same pattern. The following table shows the best classification results on all used benchmark datasets.

Table 4.9 The best classification accuracy on benchmark datasets.

Number	Dataset	Classes	CLBP	CLTP	WCLTP	Feat-WCLTP
1	OuTex	24	99.32%	99.17%	99.35%	99.66%
3	CURET	61	94.74%	96.11%	96.57%	96.89%
4	UIUC	25	91.07%	94.40%	94.80%	95.23%
5	Kylberg	28	99.83%	99.87%	99.88%	99.92%
5	2D HeLa	10	70.93%	80.81%	84.19%	84.42%
6	Breast Cancer	3	86.69%	90.86%	92.14%	89.12%

Table 4.9 shows that Feat-WCLTP performs best in all datasets except in the Breast Cancer dataset, where the WCLTP achieved the best classification rate of 92.14%. Feat-WCLTP achieved the highest classification rate of 99.92% in all datasets, particularly in the Kylberg dataset. The following table shows a comparison of the computational complexity of the proposed descriptors, CLTP and CLBP.

Table 4.10 The number of bins and classification time using OuTex TC10 dataset

Pattern size	Dimensionality / Time	CLBP	CLTP	WCLTP	Feat-WCLTP
R=1, P=8	No. of bins	200	400	400	160
	Classification Time.	2.14	17.89	16.125	2.1
R=2, P=16	No. of bins	2,312	4,624	4,624	544
	Classification Time.	30.24	72.12	71.35	10.4
R=3, P=24	No. of bins	10,952	21,904	21,904	1,184
	Classification Time.	82.37	172	169	16.8

Table 4.10 shows the superiority of Feat-WCLTP in reducing the dimensionality, which minimises the classification time. The Feat-WCLTP obtained the minimum classification time (2.1 seconds) and the minimum number of bins (160) with pattern (R

= 1, P = 8). While CLTP obtained the maximum classification time (172 seconds) and 21,904 bins with the pattern (R = 3, P = 24).

Generally, the experimental evaluation results showed that Feat-WCLTP achieves the best classification results and considerably enhance the classification accuracy of CLTP. That's due to many reasons: first, using wavelet transform will help to increase the classification accuracy due to the shift invariant property of RDWT, second, using only mean and variance features help to diminish the impact of noise, rotation and illumination. Moreover, when using these two features, all non-uniform patterns do not need to be integrated into a single bin as in CLBP_M and CLTP_M, which means better complementary information will be provided to the sign component thereby better classification performance. Third, dividing the images into blocks helps to further enhancement on classification accuracy because the correlation between pixels in each sub-image is stronger than the correlation between pixels in the whole image.

4.5 Summary

In this chapter, the performance of the proposed WCLTP and Feat-WCLTP was evaluated using four texture (i.e. OuTex, CURET, UIUC and Kylberg) and two medical (i.e. 2D HeLa and Breast Cancer) benchmark datasets and compared with some well-known descriptors. The WCLTP outperformed the other descriptors in terms of classification accuracy and exhibited significant resistance to noise and illumination variations. Feat-WCLTP not only overcame the dimensionality problem but also significantly improved in classification accuracy.

In conclusion, the proposed WCLTP and Feat-WCLTP showed improved accuracy and dimensionality as compared with the original CLTP.

CHAPTER 5

CONCLUSION AND FUTURE WORK

5.1 Introduction

This chapter summarises the outcomes of this research, highlights the contributions of this study and provides some recommendations for future work.

5.2 Conclusions

This thesis focuses on texture classification, particularly on the feature extraction task. Feature extraction is considered the most significant task in the texture classification process. LBP is one of the simplest yet most powerful feature extraction descriptors. Hence, different variants of LBP are presented in the literature. CLTP is one of the important LBP variants that was proposed to overcome the drawbacks of LBP. However, despite the impressive performance of CLTP, it suffers from some limitations, such as high dimensionality, which mainly increases the computation time and may affect the classification accuracy.

This thesis presented a new descriptor called WCLTP, which uses RDWT to decompose an input image into four sub-bands (LL, LH, HL, HH). The LL sub-band was selected because it contains considerable information of the original image. Next, CLTP was extracted based on the LL's wavelet coefficients. Using RDWT helps increase the classification accuracy due to its shift invariant property. The proposed WCLTP demonstrated good performance using four texture (i.e. OuTex, CURET, UIUC and Kylberg) and two medical (i.e. 2D HeLa and Breast Cancer) benchmark datasets. The

results showed the superiority of the WCLTP over other descriptors in the literature. Also, the descriptor's performance may vary based on the dataset and the extraction conditions, such as texture pattern size and the number of training images. Furthermore, the CURET texture dataset was used to evaluate the robustness of the WCLTP descriptor against noise. All the CURET dataset images were corrupted by additive Gaussian noise with specific SNR values (SNR= 60, 40, 50 and 30). In these experiments, the WCLTP successfully outperformed other well-known descriptors in the literature. However, despite its impressive performance and resistance to noise and illumination variations, WCLTP still suffers from the dimensionality problem.

This thesis also presented a new texture descriptor called Feat-WCLTP, which reduced dimensionality by using two features (i.e. mean and variance) instead of P features that described the magnitude operator, where P denotes all neighbours around the pattern centre pixel. The proposed Feat-WCLTP showed impressive performance using four texture (i.e. OuTex, CURET, UIUC and Kylberg) and two medical (i.e. 2D HeLa and Breast Cancer) benchmark datasets. The experimental results showed that the Feat-WCLTP not only overcomes the dimensionality problem but also further improves the classification accuracy. Moreover, the OuTex TC_10 texture dataset and 2D HeLa medical dataset were used to evaluate the time complexity of the proposed WCLTP and Feat-WCLTP. The experimental results showed the effectiveness of the proposed Feat-WCLTP and its ability to reduce the classification time significantly compared with several previous descriptors.

This study achieves its objectives by developing, implementing and evaluating the WCLTP and Feat-WCLTP descriptors. The objectives of this research are outlined in Table 5.1 along with the chapters where these objectives are addressed.

Table 5.1 The research objectives achievement

Number	Objectives	Chapter achievement
1	To improve the classification accuracy of the CLTP.	Chapter 3
2	To propose a new Feature-based texture descriptor by overcome the computational limitation of the wavelet CLTP.	Chapter 3
3	To evaluate the performance of the new texture descriptor in medical and texture image classification.	Chapter 4

5.3 Contributions of the Study

This study contributes to texture classification research by identifying the limitations in several texture classification descriptors, including the CLTP descriptor, given that it is the backbone texture descriptor of this research. To address these limitations, this research introduces two main contributions:

The first contribution is the proposal of a new descriptor (WCLTP) by integrating RDWT with the original CLTP. This descriptor considerably improved the classification accuracy rate.

The second contribution is related to the proposed Feat-WCLTP, which reduced the dimensions of the WCLTP descriptor by addressing the high dimensionality problem in feature extraction of the WCLTP descriptor, in which the feature-based technique was used.

These contributions considerably improved the performance of the descriptors and reduced the complexity of the original CLTP. Reducing the number of extracted features positively affected the computational time of the descriptor and the dimensionality of the resultant histogram.

5.4 Suggestions for Future Research

This section presents several perspectives on directions for future research to improve the contributions of this study in particular and to enhance the performance of image classification in general.

The Feat-WCLTP and WCLTP descriptors can be enhanced with colour features. This improvement of Feat-WCLTP and WCLTP will add new value in terms of giving the proposed descriptors the capability of working with colour image datasets by handling some colour models such as RGB.

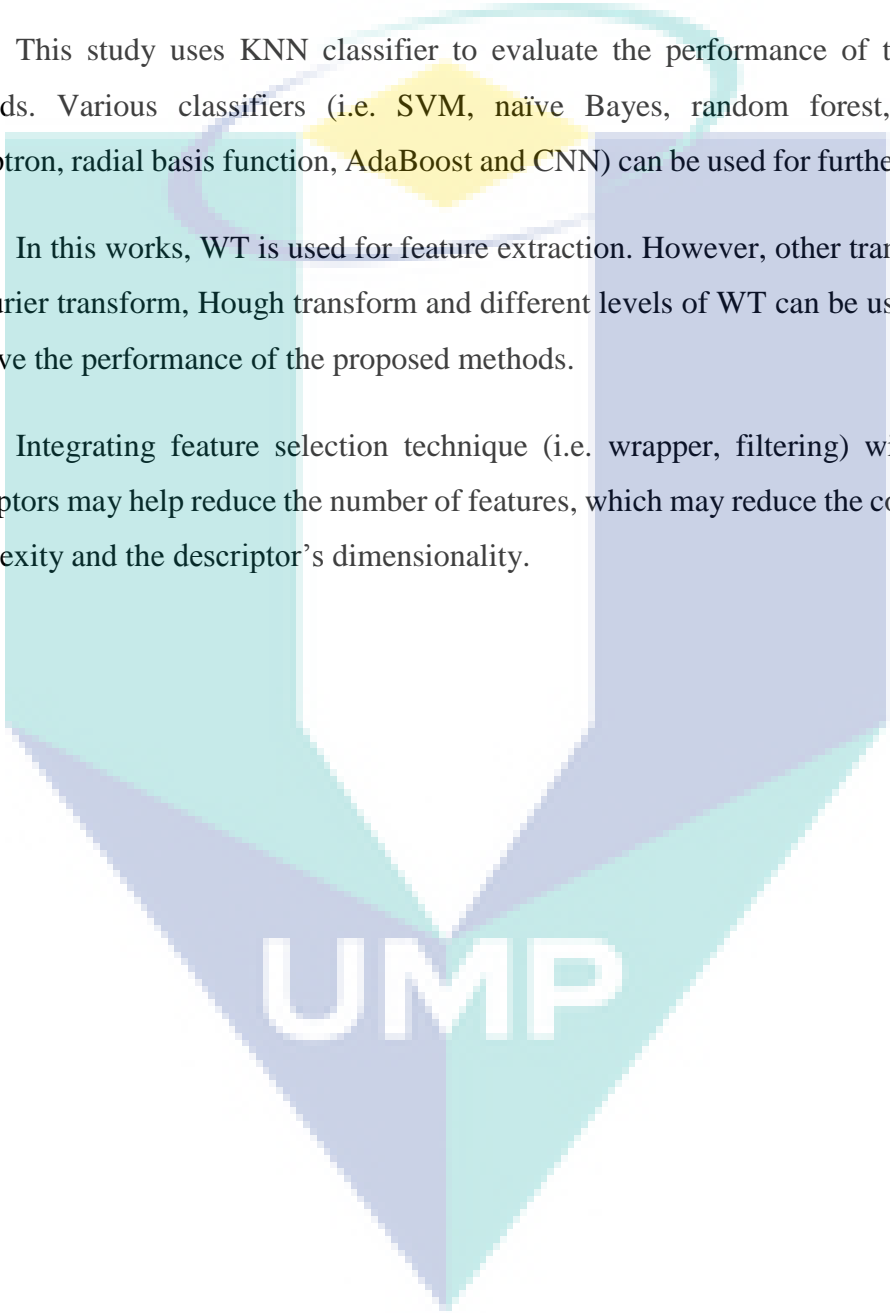
Although the Feat-WCLTP and WCLTP descriptors achieved good classification performance and outperformed the previous descriptors using the threshold value that was successfully tested and selected in previous research, this fixed value might not be appropriate in different cases. To address this limitation, optimisation algorithms can be used to select the best threshold value for each dataset.

The proposed Feat-WCLTP descriptor was evaluated using different texture and medical benchmark datasets. In this work, both descriptors were evaluated by using two types of datasets, i.e. medical and texture. In the future, these descriptors can be implemented in different domains, such as face recognition datasets and remote sensing, after considering the speciality of these different fields.

This study uses KNN classifier to evaluate the performance of the proposed methods. Various classifiers (i.e. SVM, naïve Bayes, random forest, multi-layer perceptron, radial basis function, AdaBoost and CNN) can be used for further evaluation.

In this works, WT is used for feature extraction. However, other transforms such as Fourier transform, Hough transform and different levels of WT can be used to further improve the performance of the proposed methods.

Integrating feature selection technique (i.e. wrapper, filtering) with proposed descriptors may help reduce the number of features, which may reduce the computational complexity and the descriptor's dimensionality.



UMP

REFERENCES

- Al-Kadi, O.S. (2015). A multiresolution clinical decision support system based on fractal model design for classification of histological brain tumours. *Computerized Medical Imaging and Graphics* 41: 67–79.
- Amin, S., Gupta, R. & Mehrotra, D. (2018). Analytical review on image compression using fractal image coding BT. *Soft Computing: Theories and Applications*, 584: 309–321.
- Anwer, R.M., Khan, F.S., van de Weijer, J., Molinier, M. & Laaksonen, J. (2018). Binary patterns encoded convolutional neural networks for texture recognition and remote sensing scene classification. *Journal of Photogrammetry and Remote Sensing* 138: 74–85.
- Ashour, M.W., Khalid, F., Halin, A.A. & Darwish, S.H. (2016). Multi-class support vector machines for texture classification using gray-level histogram and edge. *International Journal of Advances in Electronics and Computer Science* 3: 1–5.
- Aziz, M.N., Purboyo, T.W. & Prasasti, A.L. (2017). A survey on the implementation of image enhancement. *International Journal of Applied Engineering Research* 12: 11451–11459.
- Bala, R. & Scholar, R. (2017). Survey on texture feature extraction methods. *International Journal of Engineering Science and Computing* 7: 10375–10377.
- Boland, M. V & Murphy, R.F. (2001). A neural network classifier capable of recognizing the patterns of all major subcellular structures in fluorescence microscope images of HeLa cells. *Bioinformatics* 17: 1213–1223.
- Cataldo, S. Di & Ficarra, E. (2017). Mining textural knowledge in biological images: Applications , methods and trends. *Computational and Structural Biotechnology Journal* 15: 56–67.
- Chen, J., Kellokumpu, V., Zhao, G. & Pietikäinen, M. (2013). RLBP: Robust Local Binary Pattern. *2013 British Machine Vision Conference*, hlm. 1–10.
- Chowriappa, P., Dua, S., Rajendra Acharya, U. & Muthu Rama Krishnan, M. (2013). Ensemble selection for feature-based classification of diabetic maculopathy images. *Computers in Biology and Medicine* 43: 2156–2162.
- Colombo, C., Comanducci, D. & Del Bimbo, A. (2011). Shape reconstruction and texture sampling by active rectification and virtual view synthesis. *Computer Vision and Image Understanding* 115: 161–176.
- Cover, T. & Hart, P. (1967). Nearest neighbor pattern classification. *IEEE Transactions on Information Theory* 13: 21–27.
- Dana, K.J., Van Ginneken, B., Nayar, S.K. & Koenderink, J.J. (1999). Reflectance and texture of real-world surfaces. *ACM Transactions On Graphics* 18: 1–34.

- Davarzani, R., Mozaffari, S. & Yaghmaie, K. (2015). Scale- and rotation-invariant texture description with improved local binary pattern features. *Signal Processing* 111: 274–293.
- Davies, E.R. (2018). Handbook of texture analysis. in *Computer Vision (Fifth Edition)*, 185–200.
- Deepa, S.N. & Devi, B.A. (2011). A survey on artificial intelligence approaches for medical image classification. *Indian Journal of Science and Technology* 4: 1583–1595.
- Depeursinge, A., Fageot, J. & Al-Kadi, O.S.(2017). Chapter 1 - Fundamentals of Texture Processing for Biomedical Image Analysis: A General Definition and Problem Formulation BT - *Biomedical Texture Analysis. Biomedical texture analysis fundamentals, tools and challenges*, hlm. 1–27.
- Depeursinge, A., Foncubierta-Rodriguez, A., Van De Ville, D. & Müller, H. (2014). Three-dimensional solid texture analysis in biomedical imaging: review and opportunities. *Medical image analysis* : 176–196.
- Eskenazi, S., Gomez-Krämer, P. & Ogier, J.M. (2017). A comprehensive survey of mostly textual document segmentation algorithms since 2008. *Pattern Recognition* 64: 1–14.
- Fowler, J.E. (2005). The redundant discrete wavelet transform and additive noise. *IEEE Signal Processing Letters* 12: 629–632.
- Gu, W., Lv, Z. & Hao, M. (2017). Change detection method for remote sensing images based on an improved Markov random field. *Multimedia Tools and Applications* 76: 17719–17734.
- Guo, Y., Zhao, G. & Pietikäinen, M. (2012). Discriminative features for texture description. *Pattern Recognition* 45: 3834–3843.
- Guo, Z., Zhang, L. & Zhang, D. (2010). A completed modeling of local binary pattern operator for texture classification. *IEEE Transactions on Image Processing* 19: 1657–1663.
- Han, Y., Kim, J., Lee, K., Han, Y., Kim, J. & Lee, K. (2017). Deep convolutional neural networks for predominant instrument recognition in polyphonic music. *IEEE Transactions on Audio, Speech and Language Processing* 25: 208–221.
- Hien, T.D., Nakao, Z. & Chen, Y.-W. (2006). Robust multi-logo watermarking by RDWT and ICA. *Signal Processing* 86: 2981–2993.
- Irani Mehr, M., Riahi, M.A. & Goudarzi, A. (2013). Innovative RDWT: a new DWT-based method with applications for seismic ground roll attenuation. *Journal of Geophysics and Engineering* 10: 1–11.

- Jarholiya, S.N. (2016). Medical image fusion methods- a comparative analysis. *International Journal of Scientific & Engineering Research* 7: 1379–1387.
- Jasiewicz, J. & Stepinski, T.F. (2013). Geomorphons a pattern recognition approach to classification and mapping of landforms. *Geomorphology* 182: 147–156.
- Jha, M.K., Roy, S.D. & Lall, B. (2017). New context of compression problem and approach to solution: a survey of the literature. *International Journal of Signal and Imaging Systems Engineering* 10: 204–222.
- Jia, S., Hu, J., Xie, Y., Shen, L., Jia, X. & Li, Q. (2016). Gabor cube selection based multitask joint sparse representation for hyperspectral image classification. *IEEE Transactions on Geoscience and Remote Sensing* 54: 3174–3187.
- Joshi, S. & Karule, P.T. (2018). Review of preprocessing techniques for fundus image analysis. *AMSE-IIETA Journals-2017-Series: Advances B* 60: 593–612.
- Jović, A., Brkić, K. & Bogunović, N. (2015). A review of feature selection methods with applications. *International Convention on Information and Communication Technology, Electronics and Microelectronics*, hlm. 1200–1205.
- Junior, G.B., de Paiva, A.C., Silva, A.C. & de Oliveira, A.C.M. (2009). Classification of breast tissues using Moran's index and Geary's coefficient as texture signatures and SVM. *Computers in Biology and Medicine* 39: 1063–1072.
- Kovac, O., Lukacs, P. & Gladisova, I. (2018). Textures classification based on DWT. *International Conference Radioelektronika*, hlm. 1–5.
- Kylberg, G. (2011). Kylberg Texture Dataset v. 1.0. Centre for Image Analysis, Swedish University of Agricultural Sciences
- Lazebnik, S., Schmid, C. & Ponce, J. (2005). A sparse texture representation using local affine regions. *IEEE Transactions on Pattern Analysis and Machine Intelligence* 27: 1265–1278.
- Li, W., Pan, H., Li, P., Xie, X. & Zhang, Z. (2017). A medical image retrieval method based on texture block coding tree. *Signal Processing: Image Communication* 59: 131–139.
- Lisin, D.A., Mattar, M.A., Blaschko, M.B., Benfield, M.C. & Learned-miller, E.G. (2005). Combining local and global image features for object class recognition. *IEEE Computer Society Conference on Computer Vision and Pattern Recognition*, hlm. 47–47.
- Liu, L., Chen, J., Fieguth, P., Zhao, G., Chellappa, R. & Pietikäinen, M. (2019). From BoW to CNN : Two Decades of Texture Representation for Texture Classification. *International Journal of Computer Vision* 127: 74–109.
- Liu, L., Fieguth, P., Guo, Y., Wang, X. & Pietikäinen, M. (2017a). Local binary features for texture classification: Taxonomy and experimental study. *Pattern Recognition*

62: 135–160.

- Liu, L., Fieguth, P., Guo, Y., Wang, X. & Pietikäinen, M. (2017b). Local binary features for texture classification: Taxonomy and experimental study. *Pattern Recognition* 62: 135–160.
- Liu, L., Long, Y., Fieguth, P.W., Lao, S. & Zhao, G. (2014). BRINT : binary rotation invariant and noise tolerant texture classification. *IEEE Transactions on Image Processing* 23: 3071–3084.
- Liu, S., Pan, X., Liu, R., Zheng, H., Chen, L., Guan, W., Wang, H., Sun, Y., Tang, L. & Guan, Y. (2018). Texture analysis of CT images in predicting malignancy risk of gastrointestinal stromal tumours. *Clinical radiology* 73: 266–274.
- Mallat, S.G. (1989). A theory for multiresolution signal decomposition: the wavelet representation. *IEEE Transactions on Pattern Analysis and Machine Intelligence* 11: 674–693.
- Mehta, R. & Egiazarian, K. (2016). Dominant rotated local binary patterns (DRLBP) for texture classification. *Pattern Recognition Letters* 71: 16–22.
- Nair, A.S. & Jacob, R. (2017). A survey on feature descriptors for texture image classification. *International Research Journal of Engineering and Technology* 4: 782–784.
- Nanni, L., Lumini, A. & Brahnam, S. (2010). Local binary patterns variants as texture descriptors for medical image analysis. *Artificial Intelligence in Medicine* 49: 117–125.
- Nanni, L., Lumini, A. & Brahnam, S. (2017). Ensemble of texture descriptors for face recognition obtained by varying feature transforms and preprocessing approaches. *Applied Soft Computing* 61: 8–16.
- Nayak, D.R., Dash, R. & Majhi, B. (2016). Brain MR image classification using two-dimensional discrete wavelet transform and AdaBoost with random forests. *Neurocomputing* 177: 188–197.
- Ojala, T., Pietikäinen, M. & Harwood, D. (1996). A comparative study of texture measures with classification based on featured distributions. *Pattern recognition* 29: 51–59.
- Ojala, T., Pietikäinen, M. & Mäenpää, T. (2002). Multiresolution gray-scale and rotation invariant texture classification with local binary patterns. *IEEE Transactions on Pattern Analysis and Machine Intelligence* 24: 971–987.
- Pan, Z., Li, Z., Fan, H. & Wu, X. (2017). Feature based local binary pattern for rotation invariant texture classification. *Expert Systems with Applications* 88: 238–248.
- Pham, M.-T., Aptoula, E. & Lefèvre, S. (2018). Feature Profiles from Attribute Filtering for Classification of Remote Sensing Images. *IEEE Journal of Selected Topics in Applied Earth Observations and Remote Sensing* 11: 249–256.

- Pietikäinen, M. & Zhao, G. (2015). Chapter 9 - Two decades of local binary patterns: A survey BT - Advances in Independent Component Analysis and Learning Machines. hlm. 175–210.
- Polat, K. & Kayaalp, F. (2019). Classification of R, G and B values from face images using weighted k-nearest neighbor classifier to predict the skin or non-skin. *International Congress on Fundamental and Applied Sciences*, hlm. 1–5.
- Prakash, S. & Chaudhury, N.K. (2017). Dientric chromosome image classification using fourier domain based shape descriptors and support vector machine. *Proceedings of International Conference on Computer Vision and Image Processing*, hlm. 221–227.
- Rahimi, M. & Moghaddam, M.E. (2015). A content-based image retrieval system based on Color Ton Distribution descriptors. *Signal, Image and Video Processing* 9: 691–704.
- Rassem, T.H. & Khoo, B.E. (2014). Completed local ternary pattern for rotation invariant texture classification. *The Scientific World Journal*, hlm. 1–10.
- Rassem, T.H., Khoo, B.E., Mohammed, M.F. & Makbol, N.M. (2017). Medical, scene and event image category recognition using completed local ternary patterns (CLTP). *Malaysian Journal of Computer Science* 30: 200–218.
- Rassem, T.H., Mohammed, M.F., Khoo, B.E. & Makbol, N.M. (2015). Performance evaluation of Completed Local Ternary Patterns (CLTP) for medical, scene and event image categorisation. *International Conference on Software Engineering and Computer Systems*, hlm. 33–38.
- Ren, J., Member, S., Jiang, X., Member, S. & Yuan, J. (2013). Noise-resistant local binary pattern with an embedded error-correction mechanism. *IEEE Transactions on Image Processing* 22: 4049–4060.
- Rioul, O. & Vetterli, M. (1991). Wavelets and signal processing. *IEEE signal processing magazine* 8: 14–38.
- Ruiz, M., Mujica, L.E., Alférez, S., Acho, L., Tutivén, C., Vidal, Y., Rodellar, J. & Pozo, F. (2018). Wind turbine fault detection and classification by means of image texture analysis. *Mechanical Systems and Signal Processing* 107: 149–167.
- Sahu, O., Anand, V., Kanhangad, V. & Pachori, R.B. (2015). Classification of magnetic resonance brain images using bi-dimensional empirical mode decomposition and autoregressive model. *Biomedical Engineering Letters* 5: 311–320.
- Singh, C., Walia, E. & Kaur, K.P. (2018). Color texture description with novel local binary patterns for effective image retrieval. *Pattern Recognition* 76: 50–68.
- Smistad, E., Falch, T., Bozorgi, M., Elster, A.C. & Lindseth, F. (2015). Medical image segmentation on GPUs – A comprehensive review. *Medical Image Analysis* 20: 1–18.
- Sree, C.S. (2015). Survey on extraction of texture based features using local binary

- pattern. *International Journal of Engineering Research & Technology* 4: 334–338.
- Sree, C.S. & Rao, M. (2017). Adjacent evaluation of completed local ternary count for texture classification. *IEEE International Advanced Computing Conference*, hlm. 690–696.
- Subhedar, M.S. & Mankar, V.H. (2016). Image steganography using redundant discrete wavelet transform and QR factorization. *Computers and Electrical Engineering* 54: 406–422.
- Suresha, M. & Naik, T.H. (2017). A survey on image analysis based on texture. *International Journal of Advanced Research in Computer Science and Software Engineering* 7: 686–695.
- Tan, X. & Triggs, B. (2010). Enhanced local texture feature sets for face recognition under difficult lighting conditions. *IEEE Transactions on Image Processing* 19: 1635–1650.
- Tang, Q., Liu, Y. & Liu, H. (2017). Medical image classification via multiscale representation learning. *Artificial intelligence in medicine* 79: 71–78.
- Tang, Z., Su, Y., Er, M.J., Qi, F., Zhang, L. & Zhou, J. (2015). A local binary pattern based texture descriptors for classification of tea leaves. *Neurocomputing* 168: 1011–1023.
- Taouche, C., Batouche, M.C., Chemachema, M., Taleb-Ahmed, A. & Berkane, M. (2014). New face recognition method based on local binary pattern histogram. *International Conference on Sciences and Techniques of Automatic Control and Computer Engineering*, hlm. 508–513.
- Tech, M. & Somwanshi, D.K. (2017). Medical images texture analysis: a review. *International Conference on Computer, Communications and Electronics*, hlm. 436–441.
- Velasco-Forero, S. & Angulo, J. (2013). Classification of hyperspectral images by tensor modeling and additive morphological decomposition. *Pattern Recognition* 46: 566–577.
- Wan, C.H., Lee, L.H., Rajkumar, R. & Isa, D. (2012). A hybrid text classification approach with low dependency on parameter by integrating K-nearest neighbor and support vector machine. *Expert Systems with Applications* 39: 11880–11888.
- Weese, J. & Lorenz, C. (2016). Four challenges in medical image analysis from an industrial perspective. *Medical image analysis* 33: 44–49.
- Xu, Y., Quan, Y., Ling, H. & Ji, H. (2011). Dynamic texture classification using dynamic fractal analysis. *IEEE International Conference on Computer Vision*, hlm. 1219–1226.
- Yadav, A.R., Anand, R.S., Dewal, M.L. & Gupta, S. (2017). Binary wavelet transform-

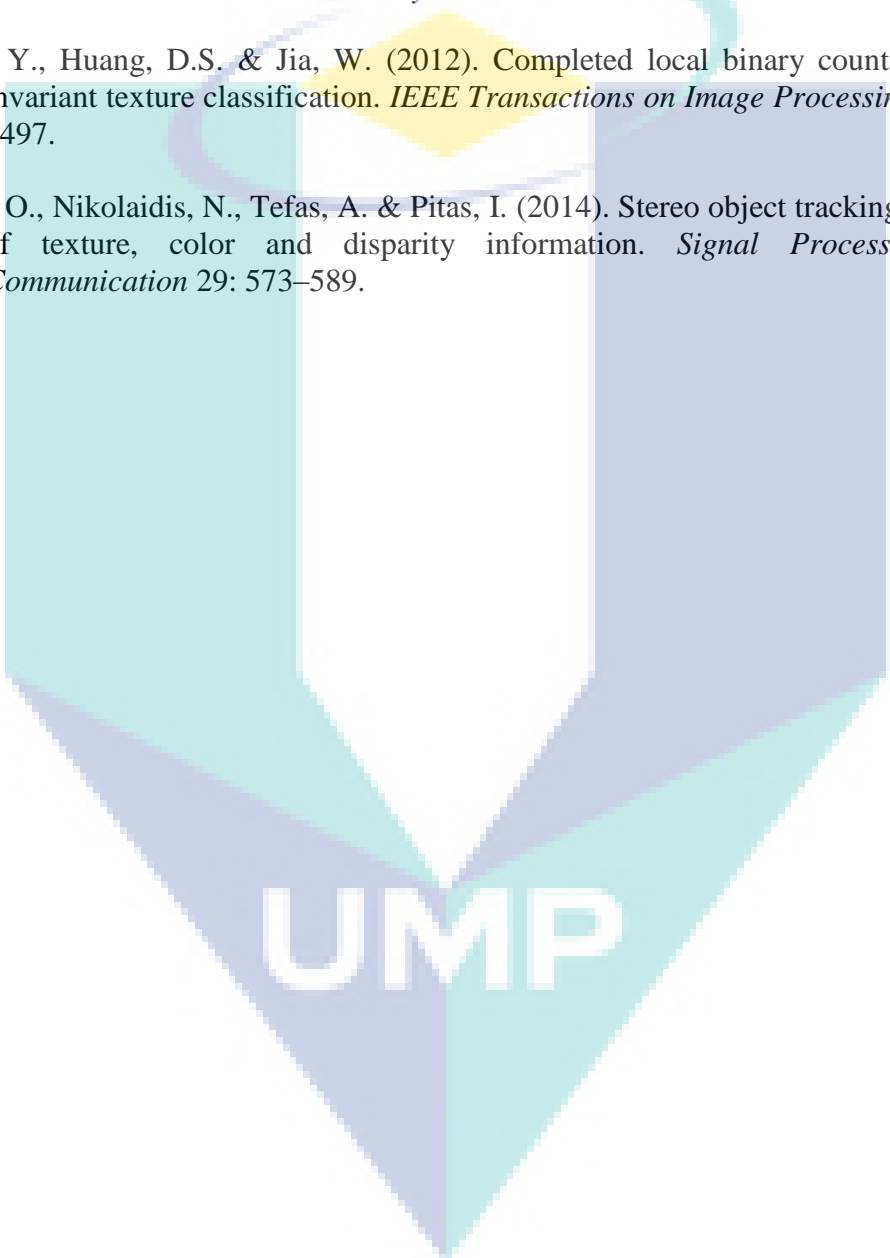
based completed local binary pattern texture descriptors for classification of microscopic images of hardwood species. *Wood Science and Technology* 51: 909–927.

Yoo, S.B., Choi, K., Jeon, Y.W. & Ra, J.B. (2016). Texture enhancement for improving single-image super-resolution performance. *Signal Processing: Image Communication* 46: 29–39.

Yu, Z., Chen, H., Liu, J., You, J., Leung, H. & Han, G. (2016). Hybrid k-nearest neighbor classifier. *IEEE transactions on cybernetics* 46: 1263–1275.

Zhao, Y., Huang, D.S. & Jia, W. (2012). Completed local binary count for rotation invariant texture classification. *IEEE Transactions on Image Processing* 21: 4492–4497.

Zoidi, O., Nikolaidis, N., Tefas, A. & Pitas, I. (2014). Stereo object tracking with fusion of texture, color and disparity information. *Signal Processing: Image Communication* 29: 573–589.



UMP